SINGLE-WALLED CARBON NANOTUBES AS SUPPORTING STRUCTURES AND STIMULATING MATERIALS FOR NG108-15 NEUROBLASTOMA-GLIOMA HYBRID CULTURE CELLS

By

MUHAMMED KHAMEIS GHEITH

Bachelor of Science
The University of Jordan
Amman-Jordan
1997

Master of Science
Middle East Technical University
Ankara-Turkey
1999

Submitted to the Faculty of the Graduate College of
Oklahoma State University in Partial Fulfillment of
the Requirements for the Degree of
DOCTOR OF PHILOSOPHY
December, 2004

SINGLE-WALLED CARBON NANOTUBES AS SUPPORTING STRUCTURES AND STIMULATING MATERIALS FOR NG108-15 NEUROBLASTOMA-GLIOMA HYBRID CULTURE CELLS

Dissertation Approved:

_____

Thesis Advisor

_____

Thesis Co-Advisor

_____

_____

_____

_____

Dean of the Graduate College

To

My Father Mr. Khameis Gheith,

My Mother Ms. Laila Gheith,

&

My Family

ACKNOWLEDGMENTS

I express my sincere thanks and appreciation to Dr. James P. Wicksted (Physics Department, Oklahoma State University, Stillwater, OK) for his supervision, continuous support, and valuable insights during my degree pursuit.

I extend my sincere thanks and appreciation also to Dr. Nicholas A. Kotov (Department of Chemical Engineering, University of Michigan, Ann Arbor, MI) for his supervision, insights, and valuable discussions throughout my study.

My endless love and loyalty to my parents, my sisters, and my brother whom I will forever be indebted to for their ever-extending love, support, trust, and willingness to endure with me the challenges of my endeavors.

I forward my thanks to Dr. Robert Matts (Department of Biochemistry and Molecular Biology, Oklahoma State University, Stillwater, OK) for his supervision and permission to use his cell culture facility to conduct most of the work presented here.

I extend my thanks to Dr. Todd Pappas, Dr. Masoud Motamedi, and Dr. Anton Liopo (Center for Biomedical Engineering, University of Texas Medical Branch, Galveston, TX) for their support and hospitality during my visit to UTMB to conduct part of the work presented in this thesis.

I also forward my sincere thanks to all members in my research committee for their input and valuable comments.

I am grateful to Dr. Warren Ford (Department of Chemistry, Oklahoma State University, Stillwater, OK) and the Oklahoma EPSCoR Nanonet for all the support.

I forward my thanks to Dr. Vladimir Sinani, and Mr. Bong Sup Shim (Department of Chemical Engineering, University of Michigan, Ann Arbor, MI), and Mr. Maxim Tchoul (Department of Chemistry, Oklahoma State University, Stillwater, OK) for their contribution and valuable discussions during my study.

My sincere appreciation to Ms. Evguenia Vorochilova for her valuable support and unshakable faith in me.

Finally, I extend my sincere thanks to all my friends and colleagues for the continuous motivation and support.

TABLE OF CONTENTS

Chapter **Page**

Chapter **Page**

LIST OF TABLES

Table **Page**

LIST OF FIGURES

Figure **Page**

Figure **Page**

Figure **Page**

CHAPTER I

INTRODUCTION

Carbon in Nature

The way carbon covalently bonds with itself to form many unique structures has made it a remarkable element that no other element existing in the periodic table is like. Carbon exists inside living organisms as a building block of amino acids, nucleic acids, and membranes, bio-macromolecules that are essential for the organization and survival of living creatures. As a free material in nature, carbon exists mainly as graphite, diamond, and as amorphous carbon such as charcoal and carbon black. Both graphite and diamond are carbon based materials however they differ in structure and, consequently, in the properties both have. In graphite, carbon atoms form sheets of hexagons layered on top of each other and held together by weak van-der Waals forces whereas in diamond carbon atoms covalently bond to form isometric crystals (cubes and octahedrons). Graphite is one of the softest materials known, and is a very good electrical conductor. Diamond is ultimately the hardest material known, and is a near perfect insulator. Recently, a new form of carbon, fullerene C_{60} or buckyball, has been discovered [1]. Fullerene is considered as the carbon quantum dot where unlike graphite and diamond it

exists as a discrete molecule with a distinct structure wherein 60 carbon atoms bond in rings of 5- and 6- atoms to form a ball of spherical shape. Seventy carbon atoms can also arrange in a similar way forming C_{70} structure which is also another known fullerene structure. Shortly after the discovery of fullerenes, a new structure of carbon was fabricated in the form of nanotubes [2-4]. Carbon nanotubes are the quantum wires of the fullerene family. They possess long cylindrical shapes and come in two main forms: single-walled nanotubes (SWNTs) [3-4] and multi-walled nanotubes (MWNTs) [2]. Single-walled carbon nanotubes posses distinct properties over multi-walled carbon nanotubes and have found more interest mainly due to their smaller diameter size (~ 1 nm compared to 20-30 nm diameter MWNTs).

Bonding in Carbon Structures

The electron configuration of the ground state of carbon atom follows $(1s)^2(2s)^2(2p)^2$ with four valence electrons available for covalent bonding with other carbon atoms. Because the energy difference between the upper 2p energy level and the lower 2s energy level is small compared to the binding energy of chemical bonds, the electronic wavefunctions of the valence electrons get mixed to enhance the binding energy of carbon atoms with each other [5]. When one of the 2s electrons gets promoted to a 2p orbital ($2p_x$), mixing of the s-orbital and p-orbital takes place forming a linear sp^1 hybridization. This is the case in acetylene C_2H_2 where the sp hybrids in the two neighboring C-atoms bond together forming a strong σ–bond whereas the remaining 2p electrons on each atom form a weak π–bond resulting in a total of triple bonds in the

acetylene (HC≡CH). In the second case, the 2s electron hybridizes with two 2p ($2p_x$ and $2p_y$) electrons forming sp^2 hybridized orbital. This is the case in graphite where each carbon atom has three sp^2 hybrids as shown in Figure 1-1, each of which contributes to the formation of σ–bonding with other hybrids in neighboring C-atoms. The remaining π–electron of $2p_z$ forms weak π–bonding with other neighboring π–electrons. The movement of electrons in these π–bonds from one atom to the other explains the ability of graphite to conduct electricity. When the 2s electron hybridizes with all three 2p electrons, an sp^3 hybridization results forming the structure of diamond. In this structure, all four sp^3 hybrids formed in each carbon atom participate in the formation of strong σ–bonds with the other four hybrids in neighboring atoms which explains the ultra hardness and resilience of diamond. In carbon nanotubes, the bonding of carbon atoms is the same as that in graphite which is namely sp^2. Sigma bonding takes place between hybrids of each carbon atom in neighboring hexagons. Some sp^3 hybridization might also exist in the structure of nanotubes especially near the end caps of the nanotubes or near curvatures and kinks along the surface [5].

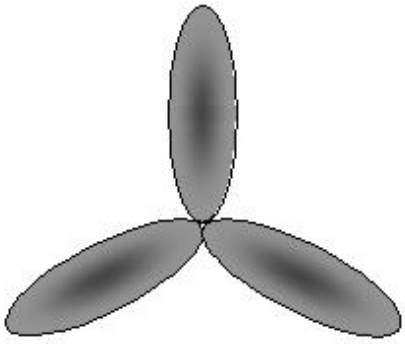

Figure 1-1. Schematic representation of sp^2 hybridization.

Structural Definition and Electronic Properties of Single-Walled Carbon Nanotubes

A single-walled carbon nanotube is a graphite sheet rolled up into a tubular shape with half a spherical fullerene structure at both ends. Depending on their method of synthesis, SWNTs can usually have a diameter of less than a nanometer and a length of several micrometers. Figure 1-2 illustrates a honeycomb lattice structure of a two-dimensional graphite sheet of an unrolled SWNT. Rolling up this sheet so that points O and A, and B and B' coincide would result in the formation of a single-walled carbon nanotube structure. Chirality (spiral property) of SWNTs is the major property that determines the symmetry and thus the structural form of the nanotubes. This chirality is represented by the chiral vector C_h which can be defined in terms of the space vectors $\bar{a}_1$ and $\bar{a}_2$ as:

$$\mathbf{C_h = n\,\bar{a}_1 + m\,\bar{a}_2 = (n,m), \quad (0 \le |m| \le n)} \qquad \text{... 1-1}$$

The space vectors can be defined in terms of the Cartesian coordinates as follows:

$$\mathbf{\bar{a}_1 = a\,[(\sqrt{3})/2\,\hat{i} + 1/2\,\hat{j}\,], \quad \bar{a}_2 = a\,[(\sqrt{3})/2\,\hat{i} - 1/2\,\hat{j}\,]} \qquad \text{... 1-2}$$

where **a** is the lattice constant given by 1.44 Å x √3 = 2.49 Å. In Figure 1-2, the carbon nanotube axis extends perpendicular to the chiral vector C_h, which represents the circumference of the nanotube. Thus, the diameter of the nanotube can be calculated via:

$$\mathbf{D = |C_h|/\pi = (a/\pi)\,(n^2 + m^2 + nm)^{1/2}} \qquad \text{... 1-3}$$

and the chiral angle "θ" can also be calculated as:

$$\mathbf{\cos(\theta) = (2n + m) / (2(n^2 + m^2 + nm)^{1/2})} \qquad \text{... 1-4}$$

Because of the symmetry of carbon hexagons, SWNTs can assume many structural forms depending on the arrangement of the hexagon rings with respect to the nanotube

axis. Different nanotube structures have different (n,m) integers and thus different conformational symmetry as implied by equation 1-1. Figure 1-3 shows the three well-known structures of SWNTs characterized by the arrangement of carbon atoms at the end of a cross-sectional ring across the nanotube axis. Each one of these structures belongs to a set of (n,m) integers. Armchair nanotubes (Fig. 1-3A), for example, belong to C_h=(n,n) group, zigzag nanotubes (Fig. 1-3B) are members of the C_h=(n,0) group, and chiral (spiral) nanotubes, which are the most abundant of all, (Fig. 1-3C) belong to C_h=(n,m) group where $0 < |m| < n$. By knowing (n,m), the symmetry and structure of SWNTs can be identified, as well as the diameter and the chiral angle [6].

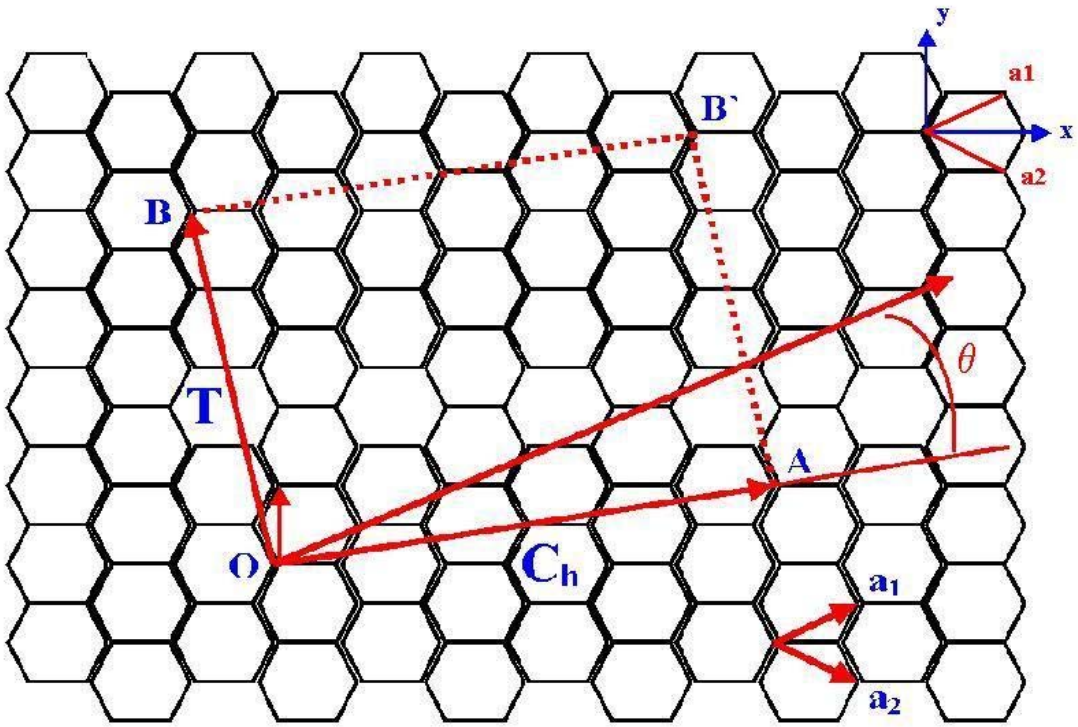

Figure 1-2. Honeycomb structure of two dimensional graphite sheet, where the chirality of the nanotube is determined by the chiral vector C_h which is perpendicular to the nanotube axis that extends along the translational vector T [modified from reference 6].

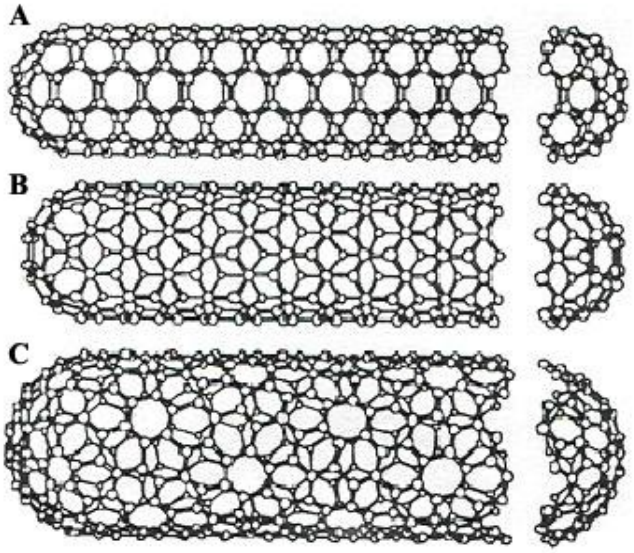

Figure 1-3. The three well-known single-walled carbon nanotubes armchair (A), zigzag (B), and chiral (C) structures [6].

One of the unique properties of single-walled carbon nanotubes is the fact that these materials can come in two types mainly semiconducting, and metallic with some semi-metallic ones as well. The electronic identity of nanotubes can be predicted by theoretical calculations starting with the 2D-graphene structural model [6-9]. Rolling up the graphene sheet into a 1D nanotube structure imposes boundary conditions along the circumferential direction as follows:

$$\mathbf{C_h \,.\, k = 2\pi q} \qquad \textbf{… 1-5}$$

where C_h is the chiral vector, k is the wavevector, and q is an integer. This boundary condition gives k a number of allowed values that when introduced into the energy dispersion relation of 2D- graphene sheet, the energy dispersions of a nanotube result. So for each k value, there exists one and only one constant energy value. In other words, the energy change with respect to the k vector is zero at that particular E-value. This is

reflected in the observation of single lines in the density of states (DOS) plot called van Hove singularities, which do not appear in the plot of 2D graphite as shown in Figure 1-4 [6].

As a consequence of equation 1-4, the electronic identity of nanotubes has been predicted theoretically [10-12] and experimentally [13] to greatly depend on their diameter and chiral angle. So, each nanotube belonging to a particular (n,m) pair of integers has the uniqueness to be either metallic, semiconducting, or in-between as semi-metallic as shown in Figure 1-5. For example, calculations predicted that all armchair nanotubes with (n,n) are metallic whereas zigzag and chiral nanotubes are metallic only if the condition n-m=3x(integer) applies. Other nanotubes with n-m≠3x(integer) are semiconducting with ~0.5 eV energy gap value. This bandgap energy in semiconducting nanotubes is inversely proportional to the diameter of the nanotubes (detailed reviews of the electronic properties of carbon nanotubes can be found in reference 6).

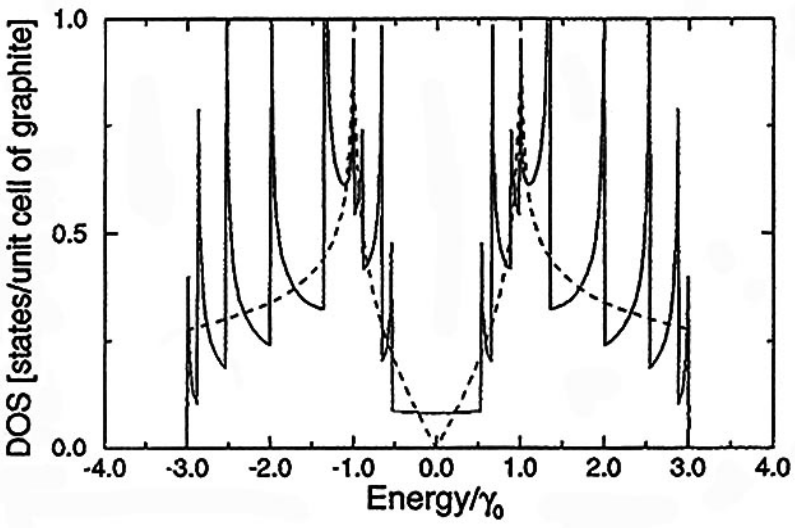

Figure 1-4. Calculated density of states for a metallic (9,0) zigzag nanotube illustrating the sharp van Hove singularities which are absent in 2D graphite (dotted line) [10].

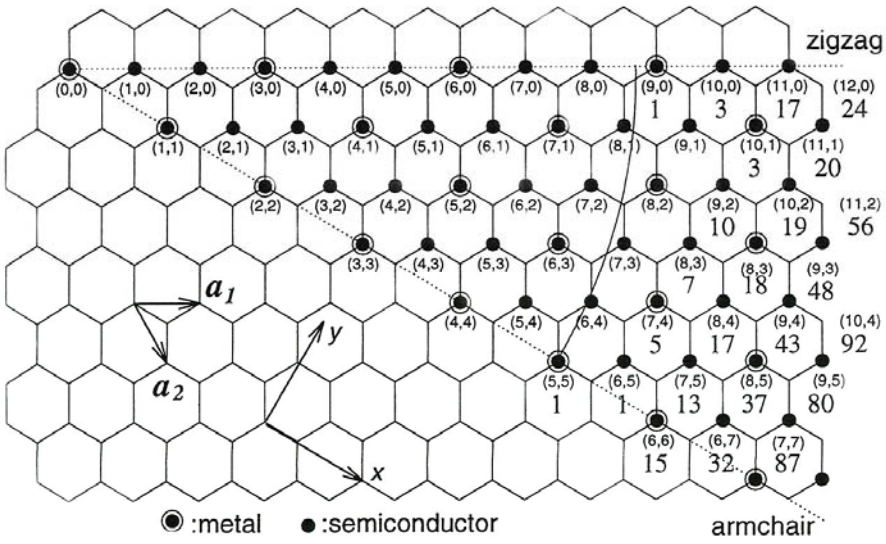

Figure 1-5. The 2D graphene sheet illustrating the (n,m) integers for all armchair, zigzag, and chiral nanotube structures with those that are metallic (dotted circles) and those that are semiconducting (small dots). The numbers below the (n,m) integers indicate the number of caps that can be joined to form that particular (n,m) nanotube structure [14, 15].

Synthesis Methods of Single-Walled Carbon Nanotubes

The structural properties of single walled carbon nanotubes including their diameter and chirality depend mainly on the method of synthesizing these materials and the conditions under which they are synthesized. For this, a brief description of the different methods developed to synthesis SWNTs is presented in this section.

A number of techniques have been developed to produce carbon nanotubes in large gram quantities. These include the method of laser vaporization [16], carbon arc synthesis [17], carbon vapor deposition [18], and high-pressure carbon monoxide (HiPCO) method [19]. Metal catalysts such as Fe, Co, and Ni are usually essential elements used to aid the synthesis of single walled carbon nanotubes but not multi-walled carbon nanotubes.

In the laser vaporization method, an intense pulsed laser beam (typically an Nd-YAG laser) is focused on a target of metal/graphite composite. The intense laser beam evaporates the graphite target forming the nanotubes in a furnace operating at ~ 1200^{o}C. The formed nanotubes are then swept into a water-cooled Cu finger with a strong Ar gas. This technique is known to produce bundles of nanotubes with narrow diameter distributions of 1.38±0.02 nm and 100 μm length [16].

Single-walled carbon nanotubes can also be produced by striking an electrical arc between two graphite rod electrodes of 5-20 mm diameter that are usually separated by 1 mm distance as in the arc discharge method. A potential difference of 20-25 V is maintained between the two electrodes with a current of 50-120 A flowing between them. The process takes place in a closed chamber under high temperature of >3000^{o}C and 500 Torr with a continuous He gas flow. During the operation, carbon vaporizes from the positive graphite electrode which contains metal catalysts and a carbon deposit containing carbon nanotubes is formed on the negative electrode [17]. This arc process usually yields a narrow size distribution of single-walled nanotubes with average diameter less than 1.5 nm.

The production of single-walled carbon nanotubes from the vapor phase via carbon phase growth method has also been reported as a potentially efficient way to produce single-walled carbon nanotubes providing the suitable synthesis conditions [20]. In this approach, gaseous hydrocarbons such as CH_4, CO, and C_6H_6 in addition to H_2 gas are reacted in a chamber under high temperature of 1100 ^{o}C. Formation of carbon nanotubes takes place on the surface of metal nanoparticles that serve as catalysts.

All of the above described nanotubes synthesis methods were known to produce both single-walled and multi-walled carbon nanotubes and in small quantities until the

development of the high pressure carbon monoxide decomposition (HiPCO) method where via this method only single-walled carbon nanotubes are produced and in large amounts [19]. This HiPCO method is a continuous flow method of single-walled carbon nanotubes production where typically a mixture of CO and $Fe(CO)_5$ gas is continuously passed through a heated furnace. Thermal decomposition of $Fe(CO)_5$ produces Fe clusters on which SWNTs nucleate and form. Controlling the furnace temperature and pressure roughly controls the size and diameter of the resulting nanotubes. Small SWNTs of 0.7 nm diameter can be produced at high temperature of 1200 ^{o}C and 10 atm pressure [19]. This HiPCO method, compared to other synthesis methods [19], has the advantage of producing relatively large quantities of SWNTs with no production of MWNTs and with no amorphous carbon resulting from the synthesis process.

Purification and Functionalization of SWNTs

Due to the nature of single-walled carbon nanotubes synthesis conditions, the production of SWNTs is usually combined with the production of other undesired impurities including catalysts, carbon nanoparticles, fullerenes, and amorphous carbon. Additionally, the strong intrinsic van der Waals attractions between nanotubes results in the existence of nanotubes as bundles of multi-number of individual nanotubes which makes it difficult to disperse these materials in commonly used solvents. This has long been a hurdle facing the fast progress in the nanotubes technology and research and has been an obstacle in the way of utilizing nanotubes for various applications. To fully realize the importance of single-walled nanotubes, highly pure nanotube samples must be obtained. A strong surface functionalization of the nanotubes is also required in order to

overcome the van der Walls forces. This has stimulated a tremendous research effort to develop various approaches to purify and solubilize single walled carbon nanotubes as we briefly review in this section.

The most commonly adopted approach to purify nanotubes from metal catalysts and other undesired impurities is the refluxing nitric acid treatment [21-23]. The nanotubes are usually suspended in high concentration of nitric acid, refluxed at high temperature and then washed with deionized water. This process usually oxidizes the metal catalysts into their ions due to the strong oxidization nature of nitric acid, which makes it easy for the ions to be washed out of the sample. It, in addition, opens the end caps of the nanotubes and introduces carboxylic acid groups into the ends and on the structural defect sites of the nanotubes where they are most reactive [24-26]. Although this process of purification is known for its effectiveness in eliminating metal catalysts it is, however, crucial that this process be carried out under controlled temperatures and exposure times. Extensive exposure to nitric acid can destroy the walls of the nanotubes and even cause digestion of the tubes themselves [27]. Prolonged sonication of nanotubes in concentrated nitric acid and sulfuric acid can cut the nanotubes into small pieces. This treatment has been adopted as a process for cutting long tangled ropes of nanotubes into shorter segments, opened ends tubes of 100-300 nm length called fullerene pipes [28]. Other purification procedures have also been reported before including thermal annealing, hydrochloric acid treatment, and gas-phase purification [29-32]. Controlled optimal conditions of thermal annealing combined with hydrochloric acid treatment have been reported before to produce high nanotubes yield and optimal high purity with less destroyed nanotubes as compared to nitric acid treatment [30].

Acid treatment of single-walled carbon nanotubes is usually considered as the

primary first step to functionalize nanotubes by covalently attaching carboxylic acid groups to their surface which helps the debundling and dissolution of the nanotubes in solvents [33]. However, the fact that nanotubes have high surface area adds as an advantage for the surface functionalization of nanotubes via a variety of other covalent surface functionalities. Covalent functionalization of nanotubes surface via fluorination [34], aryl diazonium reactions [35-36], *in-situ* radical polymerization of sodium 4-styrenesulfonate [37], addition of dichlorocarbene [38], and via many other chemical functionalities have all been reported before (For good review on the chemistry and covalent chemistry of single-walled carbon nanotubes, the reader should consult references 39 and 40).

Attributed with the covalent functionalization of nanotubes is the formation of new bonds in the graphene sheet. Although this process is undesirable as it disturbs the electronic symmetry of graphene, it offers the advantages of both dispersing the nanotubes in common solvent and providing functional groups such as carboxyl and hydroxyl groups on the surface of the nanotubes that facilitate the attachment of different chemical moieties to the nanotubes surface [34].

Non-covalent functionalization of nanotubes has also been widely reported as an alternative approach to both modify the nanotubes surface and facilitate their dispersion. This approach is more preferable than covalent functionalization since it preserves the electronic makeup of nanotubes as no covalent bonding is involved. Well-dispersed nanotubes have been obtained using ionic surfactants such as sodium dodecylbenzene before [41] as well as high molecular weight non-ionic surfactants [42]. Non-covalent functionalization via adsorption and wrapping of different polymers such as poly(aryleneethynylene), poly(phenylenevinylene), polyvinyl pyrrolidone, and others is

also a widely applied approach for nanotubes dissolution [42-52].

Depending on the type of application required, the choice of functionalities to disperse nanotubes could be determined [53]. Functionalization of nanotubes with biological macromolecules such as DNA and peptides is desirable since these molecules could impart the biocompatibility property to nanotubes as shall be reviewed later in this chapter. For applications involving the utilization of nanotubes in electronic devices and sensing purposes, non-covalent functionalization is not desirable as it blocks the accessibility to the nanotubes surface via the polymer or surfactants wrapping.

In the present study, the non-covalent functionalization approach is adopted. An amphiphilic poly(N-cetyl-4-vinylpyridinium bromide-*co*-N-ethyl-4-vinylpyridinium bromide-*co*-4-vinylpyridine) polymer that has been engineered in our laboratory is employed [54]. With its dual hydrophobic and hydrophilic nature, this polymer represents a good dispersing agent of the nanotubes as it attaches to the nanotube surfaces via its hydrophobic moieties whereas the charged hydrophilic groups contribute to the dispersion of the nanotubes. Adding to this is the fact that these hydrophilic groups provide a good positively charged coating of the nanotube surface that is essential for strong electrostatic interactions with the negatively charged phosphate groups of the cells membrane.

Characterization of Single-Walled Carbon Nanotubes

Many spectroscopic and microscopic techniques can be utilized to characterize and identify the structural properties of single-walled carbon nanotubes. Raman spectroscopy represents one of the most powerful and versatile techniques that can provide valuable

insights about the structural properties of SWNTs such as their diameter, chirality, and electronic classification whether semiconducting or metallic [55-59]. The strong coupling between electrons and the phonons in the nanotube structure gives rise to a strong Raman signature under resonance conditions between the incident photon and the electronic transitions between van Hove singularities [60-61]. By monitoring changes in the intensity, shape, and position of nanotubes Raman bands, one can gain valuable information about the surface modification of nanotubes upon purification and functionalization of SWNTs [62-64].

Figure 1-6 shows the Raman spectrum of HiPCO single-walled carbon nanotubes. The motion of the carbon atoms in the radial direction across the nanotube gives rise to what is called the radial breathing modes (RBM) in the 100-400 cm^{-1} range. The position of each RBM peak is inversely proportional to the diameter of the nanotubes existing in the sample according to the relation:

$$\nu_{RBM}\,(cm^{-1}) = (223.5\,(cm^{-1}.nm)/d(nm)) + 12.5\,(cm^{-1}) \qquad \ldots 1\text{-}6$$

where ν_{RBM} is the Raman frequency of the RBM's and d is the diameter of the nanotubes [65]. Probing the sample with a laser spot size of almost a micron (almost one thousand times larger than the diameter of a single nanotube) allows the excitation of a multiple number of nanotubes at the same time. These different excited nanotubes with different diameters come in resonance with the excitation frequency that gives rise to the various RBM peaks observed in Figure 1-6 [66-67]. The diameter of the nanotubes in resonance with the main observed RBM bands can be calculated from equation 1-6.

The band seen in the 1500-1600 cm^{-1} region is the well-known G-band of SWNTs resulting from the tangential C-C stretching vibrations both longitudinally and transversally on the nanotube axis [57, 60]. This G-band is similar to that appearing in

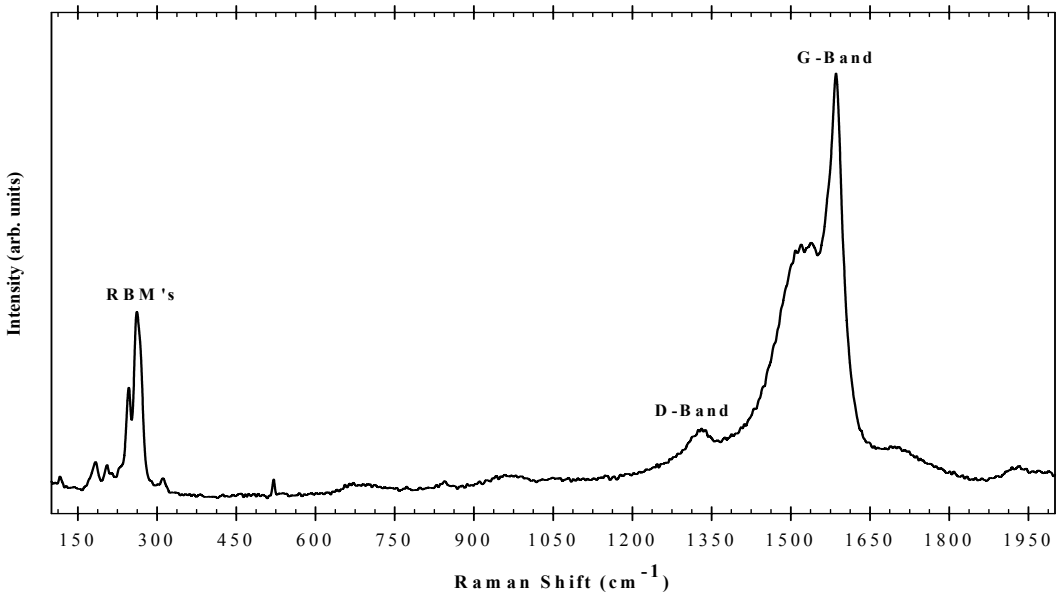

Figure 1-6. Raman spectrum of HiPCO single-walled carbon nanotubes showing the RBM in the 100-400 cm^{-1} range, the D-band at around 1350 cm^{-1} and the G-band in the 1400-1650 cm^{-1}.

the Raman spectrum of graphite thus it is called sometimes 'the graphitic band'. Because carbon atoms arrange differently with respect to the roll-up axis of the tube in different nanotube structures, their stretching modes will differ with their chirality and this reflects on the shape of this G-band that varies for those metallic and semiconducting [60].

The depressive disorder peak, known as the D-band, is seen in the 1300-1400 cm^{-1} range. This peak is attributed to scattering from sp^2 carbons containing defects and is an indication of disordered graphite [60, 68]. This Raman D-band is usually a spectral indicative of strong covalent functionalization imposed on the nanotube surface. Strong covalent bonding to the carbon atoms breaks the sp^2 symmetry of the nanotubes transforming it to sp^3 symmetry. This creates a structural defect within the nanotube at the bonding site which causes more enhanced scattering of phonons [69]. This can be

observed from the Raman spectrum of functionalized nanotubes as the intensity of the D-band increases drastically with respect to that of the G-band [33-40]. Evidence of non-covalent functionalization of nanotubes can also be obtained from Raman spectroscopy. Polymers adsorption or wrapping around the nanotubes surface has been observed to cause an up-shift in the Raman frequencies of both radial breathing modes and G-tangential modes bands as well as narrowing in the bandwidth of the G-band [48, 52].

UV/vis/NIR absorption spectroscopy is another powerful technique that offers valuable insights regarding the electronic structure of carbon nanotubes. Whether carried out in solution-phase or solid-phase samples, the absorption bands from van-Hove singularities is always a clear spectral signature of the electronic state of nanotubes. Disruption of the electronic structure of the nanotubes via covalent functionalization of nanotubes surface can be evidenced using absorption spectroscopy as the different transition bands from van-Hove singularities disappear after the functionalization [35-40]. Determination of the effects of chemical modification on the band gaps of single-walled carbon nanotubes has been reported before using NIR spectroscopy [24]. Detailed electronic structural characterization of functionalized nanotubes and investigation of selective reactions of functional groups with nanotubes can also be studied using absorption spectroscopy [70].

Thermo gravimetric analysis (TGA) gives insightful information about the purity of nanotubes and provides quantitative information about the content of nanotubes in a sample. The percent weight ratios of carbon content in terms of the ratios of amorphous carbon, single-walled nanotubes, and other carbon residues within a sample can be easily obtained using TGA. After the modification of the nanotubes, TGA can provide the ratios of the amorphous carbon and residue to that of the nanotube sample. Thus, the

TGA method is a good way to provide information about the effectiveness of a purification method. In addition, it provides information about the ratio of SWNTs present and polymers or surfactants if used in the purification process [34-35].

Microscopic techniques particularly high-resolution transmission electron microscopy (HRTEM) provide relatively accurate measurements of the diameter and size of SWNTs and their aggregation status as bundles or individual tubes. Upon the purification of nanotubes, microscopy can provide evidence on the presence and absence of catalysts and impurities within a sample. HRTEM can provide accurate quantitative information of an individual nanotube size and the size of a surfactant or polymer coating on the nanotube surface upon functionalization as will be seen in the present study. Other microscopic techniques including scanning electron microscopy and atomic force microscopy can also provide valuable structural information on functionalized carbon nanotubes.

All the spectroscopic and microscopic techniques can be combined to provide structural identification and characterization of single-walled carbon nanotubes and their surface functionalization that would help in understanding their properties and help advance the research in this field.

Importance and Applications of Single-Walled Carbon Nanotubes

While graphite lacks the high strength diamond has and while diamond lacks the electrical conductivity graphite has, single-walled carbon nanotubes have both. Owing to the nature and strength of the single covalent bonding between carbon atoms and the structural symmetry of their structure, single-walled carbon nanotubes possess

remarkable properties that made them very popular in both the scientific and the industrial societies with high potential for many applications [71]. Their importance is being better recognized specially in the view of the aforementioned purification and dispersion approaches which have facilitated the better utilization of nanotubes in many applications.

One very important property of single-walled carbon nanotubes is their remarkable mechanical properties as predicted by theoretical and experimental observations [72-73]. Individual single-walled carbon nanotubes are known to have a very high Young's modulus of up to 1000 GPa or more, which is almost equal to that of the graphite in-plane modulus (~ 1000 GPa) and almost five times that of steel (~ 200 GPa [74]) [75]. Nanotubes are also extremely tough materials because of their ability to sustain high strain and high loads where they exhibit large breaking strength of up to 30 GPa which is close to that of Silicon Carbide (~ 53 GPa) [72]. These remarkable mechanical properties make nanotubes great candidates as reinforcing materials that can be incorporated with plastics, ceramics, and polymer composites to yield lightweight, high strength structures. Efforts have been directed towards incorporating single-walled carbon nanotubes into structural composites such as layer-by-layer thin films [76] and carbon fibers [77-78] that can lead to a better mechanical properties of high strength and high Young's modulus.

The ability of π–bond electrons to move from one atom to another in nanotubes gives these materials their unique electrical properties of high conductivity. Due to this interesting property, single-walled carbon nanotubes have been introduced as base materials for many nanoelectronic devices [79-82], actuators [83], and super-capacitors [84]. Nowadays single-walled carbon nanotubes form the infrastructure of field-effect transistors (NT-FET) [85-86]. Their combined properties of high surface area (1580

m^2/g), good conductivity, and high sensitivity to gases [87-89] have allowed SWNTs to be used as sensing materials for gasses and chemical vapors [90-92]. Nanotube-based field effect transistors have been utilized to monitor changes in the conductivity of nanotubes upon adsorption of some harmful gases such as nitrogen oxides, ammonia, and methane [93-96]. Operating at room temperature with high efficiency, high sensitivity, good conductivity, and small size as compared to other existing sensors, makes these SWNTs based sensors a very useful part for our everyday life.

In addition to the many applications mentioned above, single-walled carbon nanotubes have been used in many other applications. Due to their long fibrous structure and small diameter tips, carbon nanotubes can be used as field emission electron sources [97-98]. Single-walled carbon nanotube-coated surfaces have been used in manufacturing flat panel displays where an applied electrical potential between the SWNTs-coated surface and a phosphor-coated surface anode causes the emission of electrons from the nanotubes into the anode where the phosphor-coated surface illuminates [99]. Based on their electron emission capability, a stable, intense luminescent, and long life lighting elements have been prepared before based on carbon nanotubes [100]. In addition, carbon nanotubes have also been used as base materials for making scanning probe tips [101] with high strength, flexibility, and long life which offer higher resolution and better characterization of materials at the nanoscale.

Carbon Nanotubes in Biological and Biomedical Applications

High purity and water dispersion are crucial requirements when considering single-walled carbon nanotubes in biological and biomedical applications. For efficient

biological and biomedical applications of nanotubes, their functionalization with bioactive groups is usually favorable. Modification of the nanotube surface via covalent [102] and non-covalent attachment of peptides [103] has been reported to both render the nanotubes soluble and even control the assembly of peptide-nanotubes based macromolecular structures [104-105]. Protein attachment to nanotube surface has also been reported to render the nanotubes water soluble as in the case of bovine serum albumin coated nanotubes [106]. It has also been seen to render the nanotubes biocompatible, and to impart some binding sites on the nanotube surface for specific binding of different biological systems [107-108]. Dispersion of nanotubes in water has also been reported via the interaction of single-stranded DNA (ssDNA) molecules that wrap around the nanotubes in a helical fashion [109]. The interaction of DNA molecules with the nanotubes was seen to be dependent on the sequence of the DNA [110], which was employed to separate the nanotubes based on their diameter and electronic identity whether metallic or semiconducting [109, 111].

With a better understanding of the mode of interaction between nanotubes and biological molecules, a full appreciation of the potential importance of nanotubes in biological and biomedical application can soon be recognized [112]. So far, carbon nanotubes have been mainly utilized as sensing materials of various biological molecules such as DNA [113-114], and glucose [115-118]. Nanotubes were also used as conducting channels in nanotubes based field effect transistor devices where the electrical conductivity of, mainly, semiconducting nanotubes was utilized to sense proteins [119-122]. Nanotubes were also used as molecular tips functioning as probes in chemistry and biology [123].

Biocompatibility of Nanomaterials with Focus on Single-Walled Carbon Nanotubes

Biocompatibility of nanomaterials in general and carbon nanotubes in particular represents one of the most important and sensitive issues determining the real utilization of these materials in biomedical applications. Only a limited number of studies addressing the biocompatibility issue of carbon nano-materials, especially carbon nanotubes and their interfacing with animal cells, have been reported so far. It is only recently that the subject of the impact of carbon nanotubes on health and the environment has been raised. It was reported before that when nanocrystals of buckyballs (C_{60}) were dissolved in water they kill one-half of the E-Coli bacteria existing in water, which makes these buckyballs materials powerful antibiotics [124-125]. On the other hand, because C_{60} molecules have a powerful capability to attract electrons from any nearby molecules, they have the potential to convert oxygen and molecules into strong radicals that can be harmful to living tissues. This was previously observed before where the membrane of human dermal fibroblast (HDF) and human liver carcinoma (HepG2) cells was seen to become degraded when exposed to C_{60} molecules at 20 ppb amounts [126], which makes C_{60} molecules quite lethal to living tissues.

Single-walled carbon nanotubes have the potential to be used as drug and vaccine delivering agents [127]. However, their effect on the target living cells and tissues where they are interfacing is a very important issue to be investigated. In a study applied on human 3T6 and murine 3T3 fibroblasts cells, it was seen that fluorescently labeled single-walled carbon nanotubes were able to internalize into the membrane of these cells and accumulate in the cytoplasm or the nucleus without inducing any toxicity effects within

the cells [128]. In addition, single-walled carbon nanotubes and single-walled carbon nanotubes-protein conjugates were demonstrated to act as molecular transporters that internalize mammalian cells without introducing any toxicity effects [129]. However, more careful *in-vivo* toxicity investigations of the possible health risks associated with single-walled carbon nanotubes reported recently from two separate studies have shown that single-walled carbon nanotubes can induce pulmonary granulomas and pulmonary inflammation in rat lungs [130-131]. In these studies, it was suggested that single-walled carbon nanotubes exhibit a new mechanism in inducing the observed lung lesions in rats which differs from those induced by other toxic materials such as carbon black, quartz, and silica particles [131]. A more lethal health effect of single-walled carbon nanotubes was observed before where it was reported that when nanotubes were included inside the lung tissue of rats, they were seen to agglomerate causing tissue damage, and respiratory problems leading, consequently, to the death of rats [124].

Obviously, the biocompatibility of carbon nanotubes and their impact on health remain to be clarified [132-133]. Additional studies are required in order to further explore the biocompatibility, cytoxicity, and health impacts of these man-made materials on living systems. It is premature to judge these issues at this point with such a limited number of studies reported so far [134]. To a large extend the biocompatibility and toxicity of nanomaterials can depend mainly on their surface properties such as their surface chemistry which controls the general properties of these materials [126, 135-140]. The experimental conditions, the type of biological system investigated, and the dose amount can also determine the response of the biological system to these nanomaterials [129].

Goal of the Present Study

In biomedical applications, good mechanical and electrical properties are major and essential requirements of materials that are used in the fabrication of devices utilized as external implants and prostheses for treatments of neuronal and bone injuries. The current most widely used materials for extracellular implants are titanium and gold, which are mainly used for treatments of bone-related injuries, and silicon electrodes, which are widely used for treatments of neuronal related injuries. Both titanium and gold exhibit good mechanical properties (Young's modulus of 110 MPa and 80 MPa for titanium and gold, respectively) and are conductive, particularly, gold. However, these materials lack the flexibility which can also be essential property for efficient use of special implants utilized to treat joint injuries like hip and knee injuries. Silicon, on the other hand, has good electrical conductivity (10^{-2}-10^{4} $S.cm^{-1}$), however it does not offer the same high strength that both titanium and gold offer. An ideal material to be used as base material of implants, prostheses, and orthopedic devices, must offer all combined properties of high strength, good electrical conductivity, and at the same time flexibility. All these essential properties are possessed by single-walled carbon nanotubes and that is why these materials were utilized in the present study. Such materials can be great candidates, with tremendous promise, for many biomedical applications. In the present study, we intend to present a scientific illustration of such applications of these man-made materials single-walled carbon nanotubes. Investigation of the biocompatibility of single-walled carbon nanotube-based structural composites, their long-term impact on the viability, growth, and differentiation of NG108-15 neuroblastoma x glioma hybrid culture neuronal cells, and the illustration of the possible use of such composites as external

supporting implants and as stimulating materials of neuronal growth, all represent the objectives compromised of the research work presented in this thesis.

In order to achieve the intended objectives of this study, the need for a pure and a well-dispersed nanotube suspension is essential. Stable dispersions of nanotubes were first prepared by the modification of nanotube surface using poly(N-cetyl-4-vinylpyridinium bromide-*co*-N-ethyl-4-vinylpyridinium bromide-*co*-4-vinylpyridine) amphiphilic polymer following the procedure we have recently reported [54]. Microscopic and spectroscopic evidence of the surface modification and mode of interaction of the used polymer with nanotube surfaces are first presented. Following the preparation of nanotubes dispersion, layer-by-layer assembly was employed to construct single-walled carbon nanotube-based thin film composites. Driven by electrostatic interactions, this method offers the possibility of preparing thin films and freestanding structures of nanotubes that can sustain the long-term exposure to cell culture medium. Additionally, the layer-by-layer can also provide an efficient way to control the mechanical and the electrical properties of the resulting films. These nanotube films can be used to interface with neuronal cells. Such interface is characterized in the present study by studying the growth and differentiation of NG108-15 cells on the surface of the prepared nanotube structures.

Being non-degradable, the possibility of using single-walled carbon nanotubes as reinforcing structures -utilizing their high strength- for external implants is also illustrated. Scanning electron microscopy was used to characterize the outgrowth of neurites from differentiated cells on the surface of freestanding structures of nanotubes and to demonstrate how the neurites extension varies with the surface morphology of the freestanding structures.

In the final part of the thesis, the potential use of single-walled carbon nanotubes as stimulating materials for neuronal cells is illustrated. The good electrical conductivity of nanotubes is utilized where thin LBL films of nanotubes were used as stimulating substrates of NG108-15 cells. Changes in the membrane electrical activities resulting from such stimulation were recorded via the whole cell patch clamping method. This demonstrates, for the first time, the possibility of making a contact between these inorganic materials carbon nanotubes and living cells and opens the door for future applications of nanotubes as sensing materials of neuronal networking and signaling.

CHAPTER II

EXPERIMENTAL SECTION

Materials

Single-walled carbon nanotubes closed-ended, as prepared "AP-grade" (without any chemical treatments), produced via the carbon discharge method, were purchased from Carbolex (USA). The hydrophobic polymer poly(N-cetyl-4-vinylpyridinium bromide-*co*-N-ethyl-4-vinylpyridinium bromide-*co*-4-vinylpyridine) (molecular structure shown in Figure 2-1) was courtesy of *Dr. Alexander A. Yaroslavov* (Department of Chemistry, Lomonosov Moscow State University). Polyelectrolytes poly(dimethyldiallylammonium) (PDDA; M_w ~ 400,000-500,000) and poly(acrylic acid) (PAA; M_w ~ 450,000) were purchased from Sigma-Aldrich and used without any purification. High purity water (>18.2 MΩ.cm) was used for the preparation of all solutions and for washing purposes. Fresh phosphate buffer saline PBS (Dulbecco PBS ATCC no. 30-2200) was used for cells washing and dispersion, unless otherwise indicated. The pH of the solutions was adjusted with 0.1 M HCl or 0.1 M NaOH. All uncoated glass and silica wafers were thoroughly cleaned in freshly prepared "piranha" solution (1:3 H_2O_2 (30%)/H_2SO_4 (98%); DANGEROUS when in contact with organic materials) for 30-min and then

extensively rinsed with Di-H_2O multiple times and dried with a gentle N_2-gas flow.

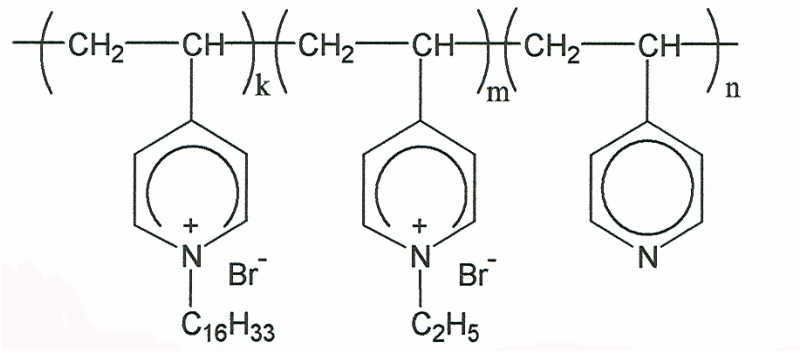

Figure 2-1. Chemical structure of poly(N-cetyl-4-vinylpyridinium bromide-co-N-ethyl-4-vinylpyridinium bromide-co-4-vinylpyridine) polymer used for the surface functionalization of carbon nanotubes in the present study.

Purification of Single-Walled Carbon Nanotubes

In order to obtain high yield, pure nanotube sample, hydrochloric acid treatment was followed [30]. Briefly, 0.089 g of as received single-walled carbon nanotubes were suspended in 20 ml of concentrated hydrochloric acid and the mixture was sonicated at room temperature for 1-hour. The treated nanotubes were then washed and filtered using a Fluoropore FGLP filter membrane with 0.2 μm pore size and then dried at room temperature.

Preparation of NTs/Polymer Suspension

Modified nanotube suspension was prepared as reported before [54]. Briefly, aqueous solution of poly(N-cetyl-4-vinylpyridinium bromide-*co*-N-ethyl-4-

vinylpyridinium bromide-*co*-4-vinylpyridine) polymer was prepared by dissolving 25 mg of the polymer in 5 ml of deionized water in a glass vial. The sample was left for two days to allow polymer swelling. A 2 ml of dimethylformamide (DMF) was then added for the complete dissolution of the polymer. To prepare the suspension of NTs/polymer mixtures, 27 mg of nanotubes were suspended in 90 ml of water/DMF (5/2 v/v) solvent mixture and then 2.25 ml of the prepared polymer solution was added. The pH of the mixture was adjusted to pH 9 and sonicated for 5-min until a visually homogeneous suspension was formed.

Preparation of LBL Films of SWNTs

Figure 2-2 represents a schematic illustration of the layer-by-layer assembly procedure followed in this study. A glass substrate was first dipped in a 1% positively charged polydimethyldiallylammonium (PDDA; M_w ~ 400,000-500,000) solution (pH 6) for 10 min. This initial PDDA layer reverses the negative surface charge due to the oxide layer present on the glass substrate surface and at the same time, it ensures good coverage of the substrate surface with a positively charged layer that will enhance the deposition of the consequent negatively charged layer. After dipping in the PDDA solution, the substrate was rinsed with Di-H_2O for 1 min. The rinsing was repeated three times to ensure the removal of excess PDDA. The substrate was then dipped in 1% negatively charged poly(acrylic acid) (PAA; M_w ~ 450,000) solution (pH 6) for 10 min to assemble a negatively charged layer. Following that, the substrate was rinsed with Di-H_2O for 3-min and the rinsing was repeated three times to ensure the removal of excess PAA.

Afterwards, the substrate was dipped in the positively charged nanotubes solution for 1-hr and then removed and washed three times with Di-H_2O for 1 min each time and then dried with a gentle nitrogen flow. The whole cycle of dipping into the PAA and nanotubes solutions was then repeated as many times as required. The final layers sequence is identified as $(PDDA)_1(PAA/NTs)_n$, where 1 indicates the one time dipping in the PDDA solution and n indicates the number of dipping cycles in the PAA and nanotube solutions.

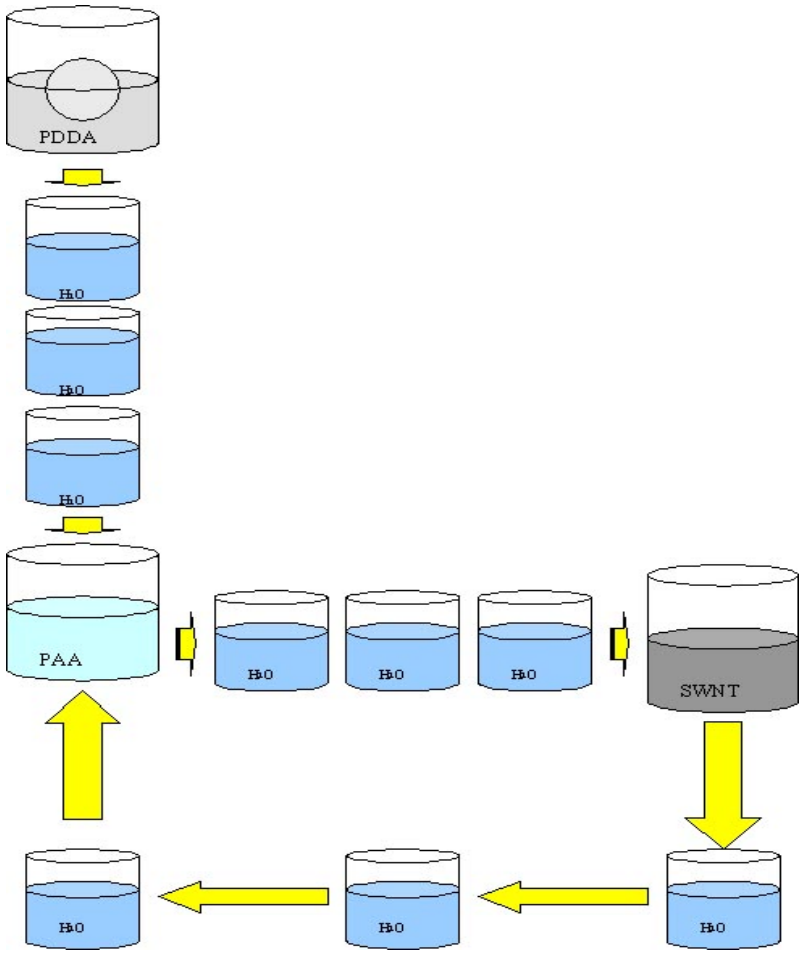

Figure 2-2. Schematic illustration of the layer-by-layer assembly process adopted in this study to prepare thin films of modified single-walled carbon nanotubes. The arrangement is demonstrated in the shape of the letters L, b, and L illustrating layer-by-layer.

Conductivity Measurements of Nanotube Layer-by-Layer Films

Resistance of nanotube LBL films was measured using two-point probe configuration employing a digital multimeter (Fluke 45 dual multimeter display). In this configuration, the nanotube substrate is connected in series to a DC voltage source that is also connected to reference resistor. The current passing through the sample and the reference resistor is the same and is used to measure the resistance of the sample by calculating the ratio between the voltage drop across the reference resistor and the sample.

Culturing and Seeding of NG108-15 Hybrid Cells

The NG108-15 neuroblastoma x glioma hybrid culture cells (ATCC-American Type Culture Collection no HB-12317) were generally cultured at 37 ^{o}C in humidified 95% air and 5% CO_2 environment in T-75 (cm^2) tissue culture Falcon flasks. The culture medium consisted of 90% DMEM (Dulbecco-Vogt modification of Eagle's minimum essential medium, GIBCO no. 11965-092) [141] and 10% FBS (Fetal Bovine Serum, ATCC no. 30-2020) supplemented with 0.1 mM Hypoxanthine, 400 nM Aminopterin, and 0.016 mM Thymidine (HAT) [142-143] and 0.5% (v/v) of 10000 I.U./ml Penicillin-10000 μg/ml Streptomycin solution. The HAT supplement is used to prohibit the growth of non-hybrid cells in the culture. Culture medium was replaced every 24-48 hrs and subculturing of cells (cells harvesting) was performed every 4-5 days. Cells were used in experiments after more than 20 subculturing passes at a density of more than 10^6 cells/ml.

Following the LBL assembly of nanotube films on the cover slips, the slips were placed in the bottom of a 60 mm Falcon cell culture dishes and were sterilized by first washing briefly with %70 ethanol followed by two times rinsing with phosphate buffer saline. The substrates were then exposed to UV-light for 5-min and then washed with a full culture medium. Fresh medium was then added in the dishes containing nanotube substrates at 5 ml volume and incubated at 37^{o}C for at least 30-minutes prior to cells seeding. Cells were cultivated from the bottom of the culture flask using 0.25% Trypsin/0.53mM EDTA (ATCC no. 30-2101) solution and then were seeded on the NT substrates at 250-500 x10^{3} cells/ml density and incubated at 37 ^{o}C. For cells differentiation experiments cells were first centrifuged at 65xg for 5-minutes and re-suspended in fresh culture medium containing %0 serum and then seeded on top of the nanotube substrates. Medium used for cells differentiation was all serum-free medium following previous protocols of serum starvation induced cells differentiation [144]. Other protocols reported the use of %1 FBS serum and a 5 μM Forskolin supplement containing medium for cells differentiation but this was not followed here [145-147].

Electrophysiological Analysis

Recordings from neurons and tranfected cells were made on an Olympus IX-71 inverted microscope. Measurements were carried out in electrophysiological solution consisting of (in mM) 130 NaCl, 2.0 $CaCl_2$, 3.0 KCl, 1.2 $MgCl_2$, 10 glucose, and 10 HEPES, pH 7.4 and at room temperature. Cells were voltage clamped using single patch electrode in the whole-cell configuration and held at -70 mV using an SEC-05LX

amplifier (NPI Electronics GmbH, Tamm, Germany) interfaced to a computer using an ITC-18 interface (Instrutech Corp.). Patch pipettes were made from 1.5 mm OD 8515 glass (Warner Instruments) and pulled to a resistance of 2-5 MΩ using a Sutter Instruments P 87 puller. Patch electrode solutions contained (in mM) 140 K-gluconate, 2.0 $MgCl_2$, 0.2 mM $CaCl_2$, 2.0 1,2-bis (2-aminophenoxy) ethane- N,N,N',N'-tetraacetic acid (BAPTA), and 1.0 HEPES (pH 7.4). K-gluconate was substituted with KCl in some experiments. Voltage clamp protocols were controlled using HEKA Pulse (v. 8.54, HEKA Instruments Inc.).

Preparation of Substrates for Electrophysiological Measurements

Two different types of substrates were used for electrophysiological measurements. Figure 2-3 illustrates the electrical cell setup used for stimulating the neurons via the nanotubes LBL film. A highly conductive (4-8 Ω) Indium Tin Oxide (ITO)-coated glass substrates 25x50x1.1 mm (Delta Technologies, Limited USA) were used as conductive substrates for the assembly of LBL nanotube films. A 15x25 mm^2 area on the surface of the ITO-coated glass was etched by drop coating this area with concentrated HCl (%36) for 1-hour followed by intense 3-times washing with De-H_2O for 10-min each time. Thirty layer-by-layer films of nanotubes were then assembled on the treated non-conductive area of the substrates bridging the two untreated conductive ITO-coated parts of the substrate as illustrated in Figure 2-3. The same procedures outlined before for assembling LBL-films were followed. At the end of the LBL assembly, the films were annealed at 100 ^oC for 1-hour.

In order to illustrate that cells can be stimulated via the nanotube film only, a second substrate was used for control experiments to stimulate cells grown on naked glass surface and at the same time in contact with the conductive nanotubes film via the conductive physiological medium. Figure 2-4 illustrates such design where the same treated ITO substrates mentioned above (shown in Figure 2-3) were used, however an additional area (15x15 mm^2) was further treated with concentrated HCl to etch the ITO coating as shown in Figure 2-4. Thirty layer-by-layer films of nanotubes were then assembled on the substrate covering the 15x25 mm^2 treated area and part of the 15x15 mm^2 treated area in such a way that the nanotube film bridges the ITO ends of the substrate surface. The substrates were then annealed at 100 ^oC for 1-hour.

Cells were only seeded and grown in a specially designed chambers. In the first substrate shown in Figure 2-3, the cell chamber was mounted on the nanotube layer-by-layer film assembled on the ITO treated glass surface as shown in the figure. In the second substrate shown in Figure 2-4, the cell chamber was mounted on the substrate in such a way that half of the chamber was resting on the nanotube layer-by-layer film and the other half was resting on the ITO treated glass surface (15x15 mm^2 area) as illustrated in Figure 3-4. Chambers were mounted on the substrates using conductive non-toxic silicone elastomer and left to dry overnight at 50 ^oC. Silver electrodes were used as conducting wires and were mounted on both sides of each substrate using conductive silver epoxy as shown in both Figures 2-3 and 2-4. All substrates were placed in 100 mm Falcon type culture dishes and incubated at 37 ^oC following cells seeding. For external stimulation, an external voltage supply (continuous mode Grass SD9 stimulator) was used and was connected to the silver electrodes.

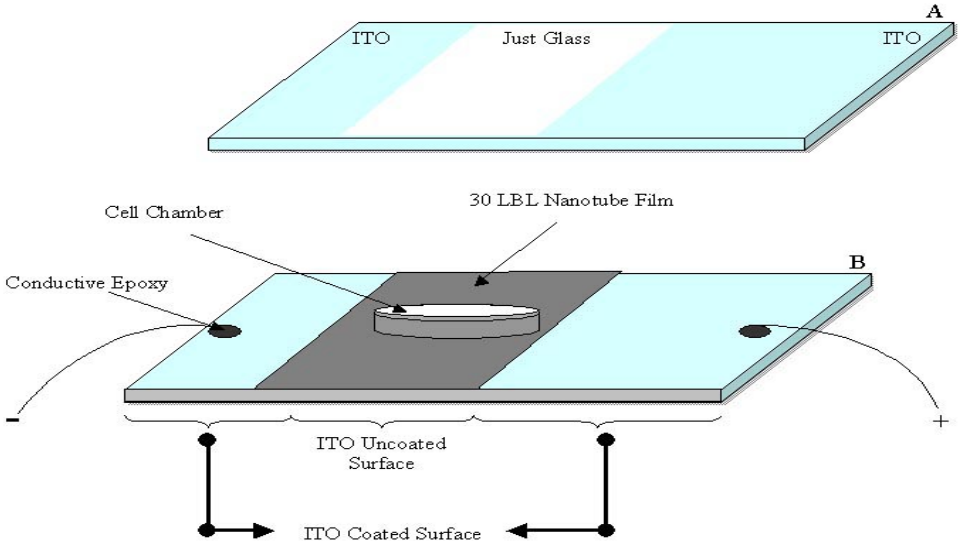

Figure 2-3. (A) Illustration of the treated ITO-substrate where the white area represents the treated surface and is glass only whereas both blue areas represent the untreated surface and are ITO coated. **(B)** Illustration of the substrate used as electrical cell for stimulating the neurons in the patch clamping experiment where nanotube LBL films used were assembled on the glass surface (dark gray area in B) and cells were grown only in the cell chamber on top of the nanotube film (B).

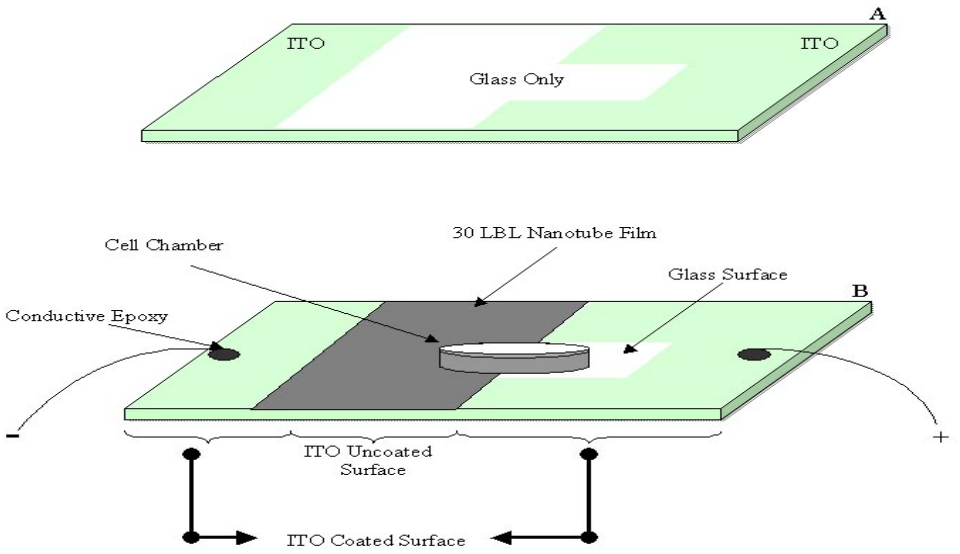

Figure 2-4. Illustration of the substrate used in the control experiments. The treated ITO-surface is represented by the white area in A and B whereas the ITO coated surface is represented by the green areas. Nanotube LBL films were assembled on the glass surface (dark gray area in B) and cells were grown only in the cell chamber on top of the nanotube film (B). As a control experiment, cell grown on glass only were stimulated.

High Resolution Transmission Electron Microscopy (HRTEM)

Samples for the HRTEM measurements were prepared by placing a drop of either pristine nanotubes in DMF or polymer modified nanotubes suspension on a copper Lacey carbon grid. Excess solution was removed using a filter paper and the samples were left to dry at room temperature one day prior to measurements. Images of pristine nanotubes were conducted on a high resolution JEM-2000FX JOEL microscope at accelerating voltage of 200 kV. Images of polymer modified nanotubes were conducted on a higher resolution JEOL 2010F analytical electron microscope with a field emission source at 300 kV accelerating voltage.

Scanning Electron Microscopy (SEM)

For the SEM measurements, all samples were prepared as follows: cover slips containing cultured cells layer were first washed briefly with PBS buffer and then the cells were fixed with 2% of Glutaraldehyde in buffer at room temperature for 2-hrs. The substrates were then washed with 0.1M potassium phosphate buffer three times for 20-min each time and then incubated in 1% Osmium Tetroxide for 2-hrs at room temperature. Cells were then washed with 0.1M potassium phosphate buffer three times for 20-min each time. Following that, the cells were dehydrated in ethanol solution (30%, 50%, 70%, 90%, 95%, and three times 100%) for 20-min each time and critical point dried. The slips were then mounted on aluminum stubs and coated with a layer of gold-palladium. The imaging was carried out using a JEOL JXM 6400 microscope

(maximum resolution 3.5 nm at 40 kV), Philip XL30 field emission gun microscope (maximum resolution 2 nm at 30 kV), or FEI Nova Nanolab Dualbeam FIB microscope (maximum resolution 3.5 nm at 30 kV).

Confocal Microscopy

All samples were first checked for auto-fluorescence under the confocal microscope and no auto-fluorescence was seen. To examine cells viability, a viability/cytotoxicity kit Calcein/Ethidium(EthD) dye was used (Molecular Probes L-3224). A stock solution of the dye was prepared by adding 2 μl of the supplied EthD dye into 0.5 ml phosphate buffer saline and vortexing till good mixture is obtained. The supplied Calcein was then added to the EthD/PBS mixture at 0.5 μl amount. This gives a final concentration of 4 μM EthD and 8 μM Calcein. Prior to adding the dye to cells, slips containing cultured cells layer were first washed briefly with PBS buffer, mounted on microscope slides then covered with the formed Calcein/Ethidium dye and imaged using a Leica SP2 laser scanning confocal microscope at an excitation of 488 nm of an Argon-ion laser.

To study neurons differentiation and neurites morphology, cells on substrates were labeled using a lipophilic dialkylcarbocyanines (DiI) dye (Molecular Probes V22885). Briefly, cell substrates were washed with phosphate buffer saline and then covered with 100 μl of %0.5 (v/v) DiI in culture medium and incubated at 37^{o}C for 2-hrs. Afterwards, substrates were washed with fresh culture medium 3-times by incubating in excess culture medium (%0 FBS) for 10-min at 37^{o}C and then viewed under the confocal microscope using 488 nm Argon-ion laser line excitation.

Atomic Force Microscopy

For the AFM measurements, a drop of nanotube solution was added on top of a clean silicon substrate and left for 1-hr at room temperature. The substrate was then rinsed with Di-water for 1-min and dried using a gentle nitrogen flow. Atomic force microscopic images were obtained using a Nanoscope III (Digital Instruments, Veeco Metrology Group, USA) microscope used at the tapping mode and with a standard Si/N tips.

UV/Visible Absorption Measurements

Absorption measurements of nanotube LBL films were taken from nanotube films on glass slips using a HP8453A diode array Hewlett-Packard spectrophotometer. Absorption measurements of pristine and polymer-modified nanotubes were taken from solid samples on CaF_2 windows using a CARY5/CARY500 UV/vis/NIR spectrophotometer (Varian Analytical Instruments, CA, USA).

Raman Spectroscopy Measurements

For the Raman measurements, two different samples of pristine nanotubes and polymer-modified nanotubes were prepared separately as thin films. The films were formed by drop coating a clean silicon wafer with a drop of nanotube suspensions and drying at 80 ^{o}C. This process was repeated for each sample at least 10-15 times to give a rather thick film. The Raman measurements were carried out on a Jobin Yvon micro-

Raman system (Ramanor U1000, Instruments SA, USA) using a spectra-physics Argon-ion laser at an excitation wavelength of 514.5 nm (2.41 eV). The back-scattered data were analyzed using a double-gating spectrometer and collected using a Hamamatsu photomultiplier (R 943-02, Hamamatsu, USA). All measurements were taken at room temperature and for each sample the Raman data was collected at different light spots on the sample surface. For every Raman spectrum taken, the position of the peaks was verified by calibrating the spectral positions with respect to silicon substrate peak at 521 cm^{-1}. The spectral resolution of the instrument was 2-3 cm^{-1}.

Ellipsometry Measurements

Thickness of films was determined using a commercial ellipsometer (J. A. Woollam Co., Inc., NE) at 600.59 nm and 1075.7 nm wavelengths and at 75^{o} incidence angle. The minimum thickness measurable using this ellipsometer was 5 nm and the maximum was no more than 1 μm.

CHAPTER III

RESULTS AND DISCUSSION

Surface Modification of Single-Walled Carbon Nanotubes

As we have mentioned before, because of the synthesis conditions at which SWNTs are produced, pristine nanotubes exist as bundles of multiple individual nanotubes which makes it hard to dissolve these materials in aqueous solutions. Mixing a sample of pristine nanotubes in water/DMF solution results in the formation of a non-uniform mixture of nanotubes bundles that suspend randomly in the solution as shown in Figure 3-1A. This solution soon starts to precipitate (not shown) as the nanotube bundles start to agglomerate in the absence of a force stronger than the van der Waals forces that govern their bundling. The addition of poly(N-cetyl-4-vinylpyridinium bromide-*co*-N-ethyl-4-vinylpyridinium bromide-*co*-4-vinylpyridine) polymer solution (see experimental section) into the nanotubes/water-DMF mixture and sonicating briefly results in the formation of a uniform suspension of nanotubes as shown in Figure 3-1B. The solution is quite dark black in color which indicates the separation of nanotubes aggregates and bundles and the uniform dispersion of individual nanotubes in the solution. This suspension was proven stable over months without completely aggregating

or precipitating. This procedure of obtaining stable nanotubes suspension by simply adding the polymer to the nanotubes mixture is quite straightforward and non-complicated way compared to other proposed approaches in literature [34-37,148-150], which makes quite attractive way to form dispersions of nanotubes [54].

Many polymers and surfactants have been reported in literature as surface modifying, stabilizing, and dispersing agents for single-walled carbon nanotubes as was reviewed in chapter one [41-52]. The choice of poly(N-cetyl-4-vinylpyridinium bromide-*co*-N-ethyl-4-vinylpyridinium bromide-*co*-4-vinylpyridine) polymer here serves well the objectives compromised of the work presented in this study. This polymer was engineered to a structure in such a way that its amphiphilic (hydrophobic and hydrophilic) nature contributes both to the functionalization and the formation of stable dispersions of nanotubes [54]. The resulting nanotubes dispersion is very essential for the layer-by-layer films construction. Additionally, the fact that this polymer possesses positively charged hydrophilic groups makes it attractive for biological applications. Imparting positive charges on the nanotubes surface is essential for maximum cells attachment and differentiation since surface properties and surface charge of cell culture substrates usually play an important role in cell attachment and neurites outgrowth [151-153].

Figure 3-1. Suspensions of unmodified pristine single-walled carbon nanotubes **(A)** and polymer-modified single-walled carbon nanotubes **(B)**.

Microscopic Characterization of Polymer-Modified Nanotubes

Careful inspection of the attachment of the polymer to the nanotubes was obtained using high-resolution transmission electron microscopy (HRTEM). Figure 3-2 represents a HRTEM image of pristine nanotubes as received from the source and prior to purification and polymer modification. As can be seen, all the nanotubes exist as bundles (notice the arrows) of many individual nanotubes of variable widths in the 15-20 nm range depending on the number of individual nanotubes in each bundle (can reach 50 tubes in one bundle). The dark spherically shaped objects seen in the image represent the catalyst impurities (Ni or Y) and/or amorphous carbon that exist in the sample as a result of the synthesis process.

By treating the nanotubes with hydrochloric acid (see experimental section), the metal catalysts impurities existing in the sample can be oxidized and then easily washed out of the nanotubes sample. This hydrochloric acid treatment is an established way to purify nanotubes from metal catalysts without destroying their structure [30]. Figure 3-3A shows a high-resolution TEM image of nanotubes following their purification and after surface modification with poly(N-cetyl-4-vinylpyridinium bromide-*co*-N-ethyl-4-vinylpyridinium bromide-*co*-4-vinylpyridine) polymer. No metal catalysts can be seen in this image after purifying the nanotubes. Compared to the as received pristine nanotubes (Figure 3-2), this image shows an individual single-walled carbon nanotube with almost a monolayer coating on its surface. This coating is attributed to the polymer which tends to attach to the hydrophobic surface of the nanotubes. The polymer layer is rather uniform and extends along the nanotube length. This indicates the ability of this polymer to form elongated structural arrangements around the nanotubes via most probably its

hydrophobic groups which could explain its ability to disperse and stabilize the nanotubes in solution [54]. The observed nanotube in the image has a diameter of nearly 1.21 nm as determined from the section analysis (Figure 3-3B), which agrees with the average diameter provided from the source (approximately 1.2 nm). The net diameter of the polymer-coated nanotube is 3.06 nm indicating a polymer layer of approximately 0.925 nm thickness. This value nearly matches the thickness of a polymer monolayer, which is 0.8 nm, estimated on the basis of the molecular geometry of the polymer assuming the adsorption of its backbone hydrophobic groups directly to the nanotubes surface [54].

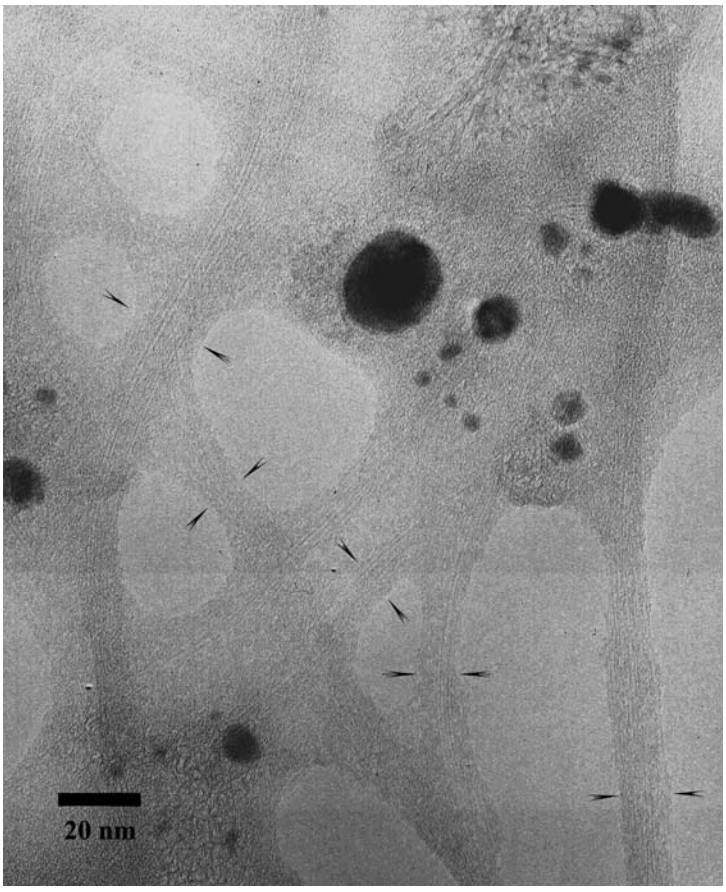

Figure 3-2. HRTEM image of as received nanotubes prior to purification and polymer modification.

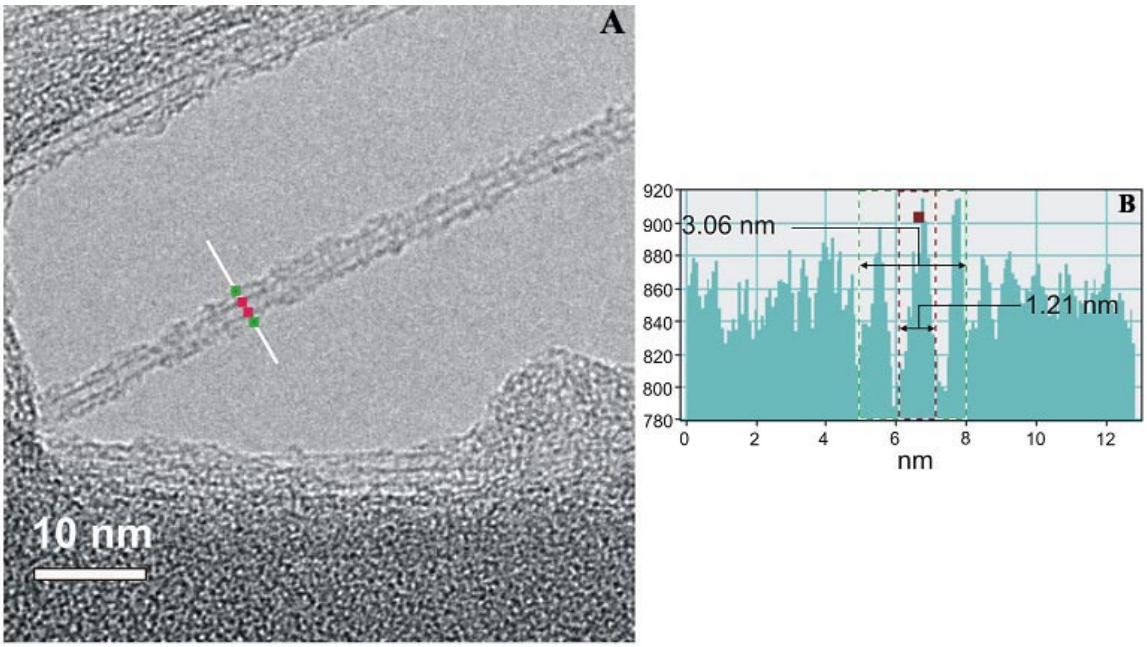

Figure 3-3. **(A)** HRTEM image of nanotubes following their purification and surface modification with poly(N-cetyl-4-vinylpyridinium bromide-co-N-ethyl-4-vinylpyridinium bromide-co-4-vinylpyridine) polymer. The red dots indicate the boundaries of an individual nanotube of diameter 1.21 nm as shown in the section analysis **(B)**, whereas the green dots indicate the boundaries of the polymer-coated nanotube with total thickness of 3.06 nm as shown in **(B)**.

Atomic force microscopy has also been assigned to provide supporting insights about the size and length of nanotubes. Figure 3-4A illustrates an AFM image taken from a sample of polymer-modified nanotubes. The image shows the presence of two individually existing single-walled nanotubes of length approximately 250-400 nm. Section analysis of one of the shown nanotubes indicates that the diameter of the nanotubes is approximately 2.506 nm as shown in Figure 3-4B. This value represents the diameter of an individual single-walled carbon nanotube coated with the polymer if to be compared with that value obtained from the HRTEM image (Figure 3-3B) which was 3.06 nm. The thickness value of the polymer-coated nanotube obtained from the AFM is less than that obtained from the HRTEM. This disagreement is mainly due to the

difference in the resolution of the two instruments. It can also be explained as a result of a difference in the two individual nanotubes captured in both images where the diameter of that nanotube observed in the AFM possibly differs from that observed in the HRTEM. The value obtained from the HRTEM image represents a more accurate value than that obtained from the AFM image due to the possibility that the AFM tip might have altered the real thickness of the polymer layer as it presses against the polymer coating when it scans across the nanotube. The tip could have also altered the structural arrangement of the polymer on the nanotube surface causing by that a shift of the polymer during the scanning process. However, the AFM image provided a second microscopic evidence of the effect of the polymer on the nanotubes breaking their bundles and dispersing them as individual nanotubes.

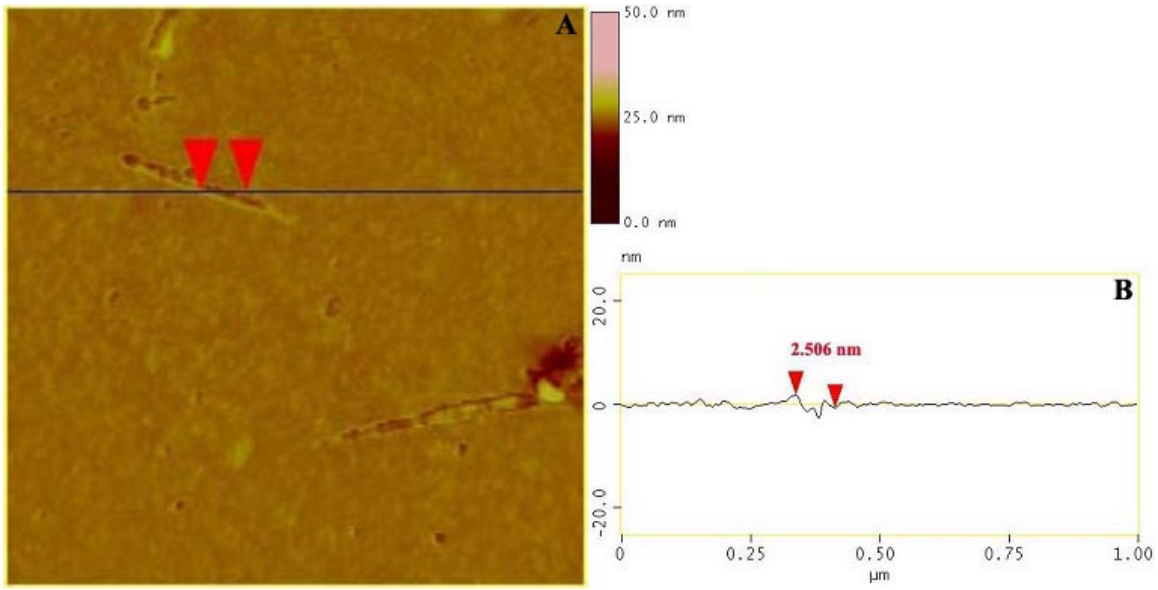

Figure 3-4. **(A)** AFM image taken from a sample of nanotubes after modification with the polymer. **(B)** Section analysis of one of the shown nanotubes indicates that the total diameter of the polymer-coated nanotube is approximately 2.506 nm.

Spectroscopic Characterization of Polymer-Modified Nanotubes

Both the HRTEM and the AFM measurements presented strong evidence on the presence of single individual nanotubes after the surface modification with the polymer. The HRTEM image showed a uniform polymer coating around the nanotubes and provided accurate quantitative information about the diameter of individual nanotubes and the thickness of the polymer layer. In order to gain insights about the mode of interaction of polymer with nanotubes, both absorption and Raman scattering spectroscopic techniques were utilized for this purpose. Both are proven techniques for probing the electronic and structural properties of single-walled carbon nanotube [55,70].

Figure 3-5 shows background corrected UV/Vis/NIR absorption spectra of unmodified pristine nanotubes (Figure 3-5, black line) and polymer-modified nanotubes (Figure 3-5, red line). By inspecting the pristine nanotubes spectrum, three broad bands are noticed. Two dominant bands are seen at namely 1058 nm and 1833 nm and one broad band is seen at 720 nm. The band at around 1833 is seen at around 0.67 eV as shown in Figure 3-5 inset. This energy value corresponds to transition energy between the first pair of van Hove singularities ($v^1_s \rightarrow c^1_s$) in semiconducting nanotubes [154]. Similarly, the band seen at 1058 nm has also been assigned to semiconducting nanotubes and is observed at around 1.2 eV (Figure 3-5 inset) energy value corresponding to transition between the second set of van Hove singularities ($v^2_s \rightarrow c^2_s$) [154]. The band seen at 720 nm appears at ca 1.7 eV in Figure 3-5 inset and corresponds to transition between the first set of van Hove singularity in the DOS of metallic nanotubes ($v^1_m \rightarrow c^1_m$) [154]. Calculated gap energies of different nanotubes as a function of tubes diameter

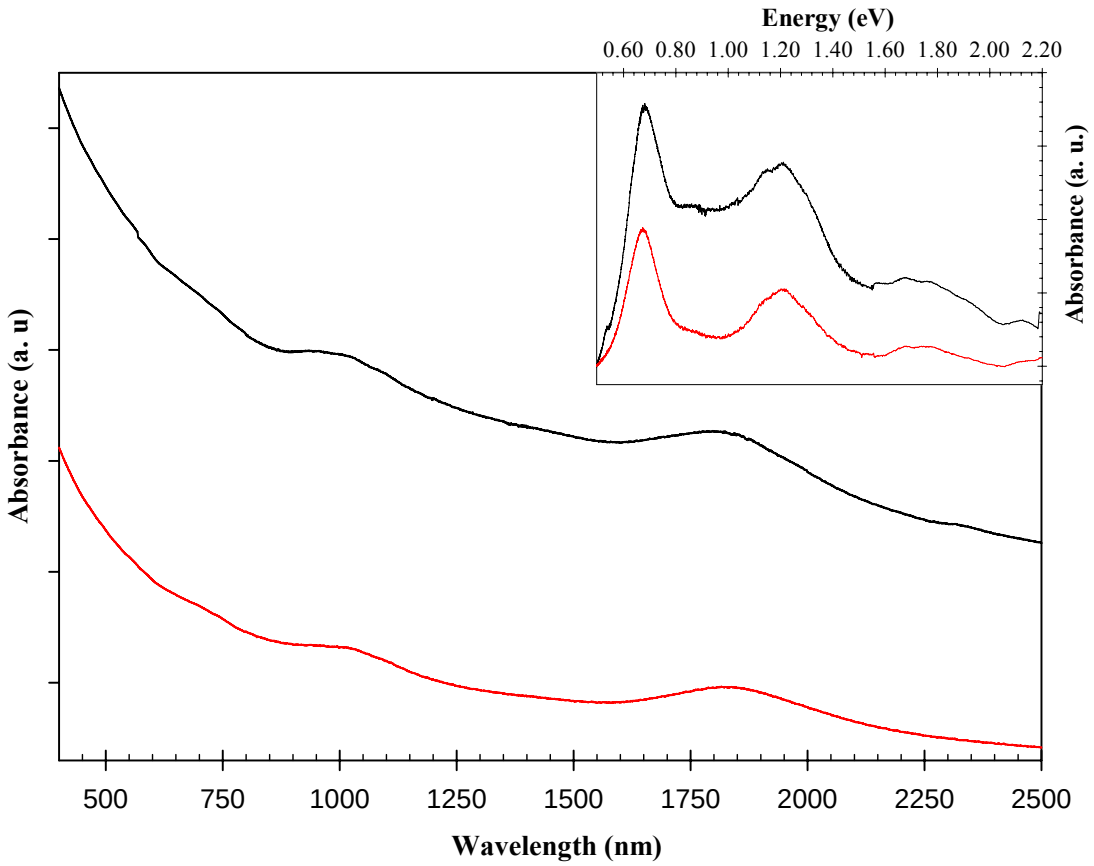

Figure 3-5. Absorption spectra of pristine nanotubes (black line) showing bands resulting from transitions between van-Hoov singularities at various positions which remain conserved at the same positions after the modification with the polymer (red line). Inset shows the same absorption spectra in eV energy units after linear baseline correction of spectra. All spectra were treated with a background subtraction.

indicated that three observed absorption bands come from three different nanotubes with almost the same diameter of 1.3-1.5 nm. The band at 1.7 eV appearing from transition in metallic nanotube is predicted to be generated from a (10,10) metallic nanotube [154].

The absorption spectral features are preserved after the polymer modification (Figure 3-5 red line). No noticeable alterations in the absorption bands were seen in the polymer-modified nanotubes spectrum where the same number of absorption bands were observed at almost the same spectral positions and same spectral bandwidth. One would expect that these van Hove transition bands would be significantly altered or even disappear if

the polymer were covalently attached to the nanotubes [35-36,39-40,70]. However, this was not the case here which indicates that there is no electronic interaction between the polymer and the nanotubes and there is no disturbance of nanotubes electronic structure as a result of polymer modification. This leads to the conclusion that the polymer is not covalently bonding to the nanotubes. This leaves two possibilities of that the polymer is either electrostatically interacting with the nanotubes surface or physically adsorbing to their surface. The former possibility of electrostatic interaction is excluded here since the surface of the nanotubes is uncharged which leaves us with the other possibility of hydrophobic interactions between the polymer and nanotubes. This is rather expected knowing the nature of the polymer chemical structure. The presence of both backbone and side chain hydrophobic groups on the polymer (see Figure 2-1) can both contribute to the hydrophobic interactions with the hydrophobic surface of the nanotubes. However, we have recently reported that it is the side chain hydrophobic groups that most probably contribute to the attachment of polymer to the tubes surface [54]. A number of similar polymers with no backbone hydrophobic groups or with short length backbone hydrophobic groups failed to interact strongly with the nanotubes and failed to disperse them in solution [54]. The argument that the polymer is hydrophobically interacting with the nanotubes surface is in agreement with the HRTEM observations where it was seen that the polymer forms a monolayer coating on the nanotubes surface (see Figures 3-3). Similar absorption observations have also been reported before with other different polymers and surfactants [48,156].

Observing no changes in the absorption spectrum of polymer-modified nanotubes excludes the possibility of nanotubes doping via polymer attachment which otherwise would reflect on the observation of major alterations in, possibly, the position of the

transition bands [155]. This is concluded from solution-phase absorption measurements conducted before, where it was seen that the absorbance linearly depends on the concentration of nanotubes in solution whereas this absorption signature remains unchanged with variations in polymer concentration in solution [54].

Valuable insights about the polymer mode of interaction with the nanotubes were further obtained utilizing Raman spectroscopy. The laser excitation energy used in the study was 2.41 eV (514.5 nm wavelength of Ar^{+}-ion laser) which falls in the energy window of semiconducting nanotubes that will be mostly in-resonance with this excitation energy. Figure 3-6 shows the Raman spectra of single-walled nanotubes both before (pristine) and after functionalization with the polymer. Two main RBM bands are observed in the pristine spectrum at namely 148.2 cm^{-1} and 165.3 cm^{-1} spectral positions (Figure 3-6 inset A). Employing equation 1-5, the diameter of the resonant nanotubes giving rise to these two RBM bands can be calculated as 1.65 nm and 1.46 nm for the first RBM band (at 148.2 cm^{-1}) and for the second (at 165.3 cm^{-1}), respectively. The dominant nanotubes diameter is 1.46 nm since the intensity of the corresponding RBM band is the highest (inset A). The diameter value falls in the range of diameters (1.3-1.5 nm) predicted from the absorption bands for probably a semiconducting nanotube [154].

By carefully inspecting the radial breathing (RBM) region after the incorporation of the polymer, it is noticed that the overall intensity of the RBM bands decreases in the polymer-modified nanotubes spectrum (Figure 3-6 inset A). A difference in the shape of the RBM pattern is also noticed where the RBM bands become less resolved and a new weak band appears at around 156.5 cm^{-1} that was not seen in the pristine spectrum (see inset A). The most evident difference noticed in the spectrum of polymer-modified nanotubes is the upshift in the RBM bands compared to those in the pristine nanotubes

spectrum. The set of RBM bands is seen to upshift by 10-15 wavenumbers after the polymer is added to the nanotubes. The observed decrease in the intensity of the RBM bands in the modified nanotubes spectrum can be attributed to the decrease in the resonance effect as those nanotubes get debundled as a result of polymer attachment to their surface [63]. The presence of the positively charged moieties of the polymer on the surface of the nanotubes causes the bundled nanotubes to break apart as a result of polymer intercalation between adjacent nanotubes powered by electrostatic repulsion. The debundling effect brings different nanotubes in resonance that were not in resonance before the polymer modification which explains the appearance of the new RBM band at 156.5 cm^{-1} in the polymer spectrum. The observed upshift in the RBM region after the modification of the nanotubes with the polymer cannot be interpreted as a consequence of the debundling of the nanotubes. According to the HRTEM image (Figure 3-3), the polymer was seen to form a layer coating extending along the nanotube length. This attachment was concluded to be via hydrophobic interactions between the polymer hydrophobic groups and the hydrophobic surface of the nanotubes according to the absorption measurements (Figure 3-5) [54]. The observed upshift in the RBM Raman bands of polymr/nanotubes sample can be thus explained as a result of increase in the stiffness of the RBM modes vibrations. This can only be the case if the polymer is actually wrapping around the nanotubes forming a monolayer as seen from the HRTEM image. This is a logical explanation as the polymer wraps around the nanotube surface, it imposes a physical strain on the carbon atoms that acquire more energy of vibration in the radial direction which causes the observed Raman shift [54]. These observations are analogous to those reported before when nanotubes are coated with organic polymers [48] and amphiphilic peptide helices [104].

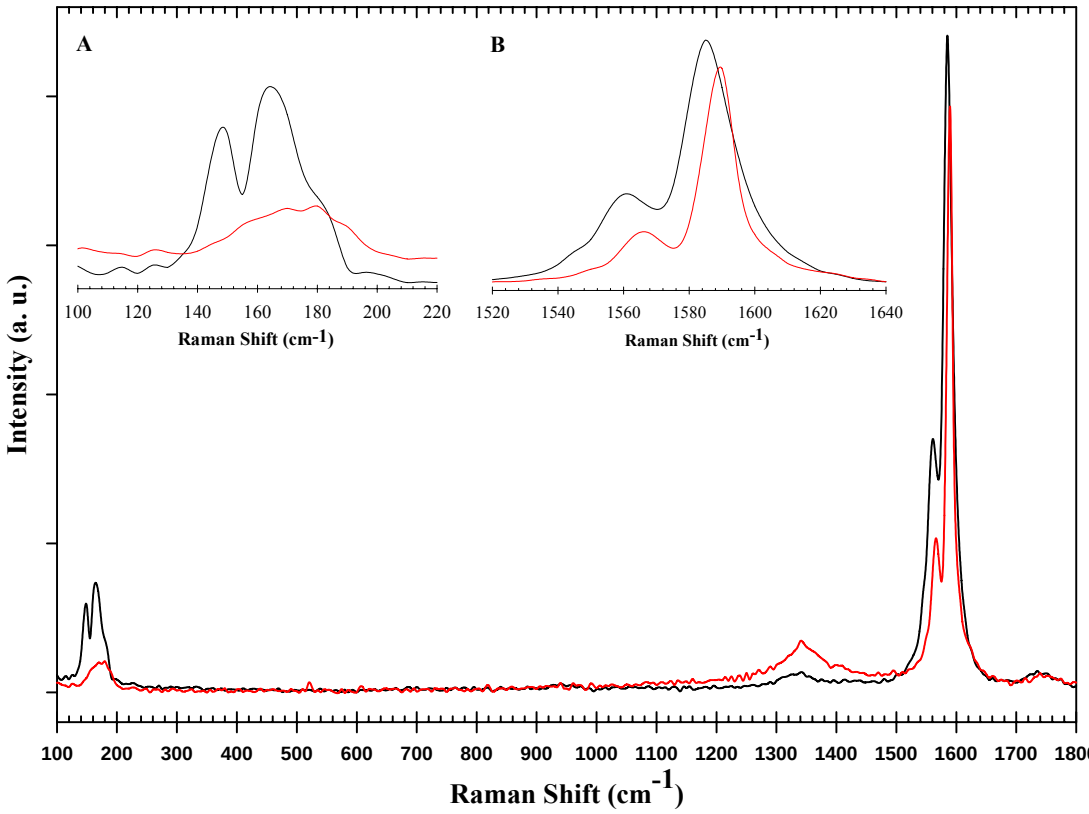

Figure 3-6. Raman spectra of pristine unmodified single-walled carbon nanotubes (black line) and polymer-modified nanotube (red line) averaged over several scans and baseline corrected. Insets show the RBM region (100-220 cm^{-1}) **(A)** and the G-band region (1520-1640 cm^{-1}) **(B)** of the spectra.

A clear trend in the spectral position of the G-band before and after the modification with the polymer can also be noticed. In both spectra, the shape of the G-band is a Lorentzian line-shape characteristic of in-resonance semiconducting nanotubes [60]. In the spectrum of pristine nanotubes, bands appearing at 1559.5 cm^{-1} and 1585.7 cm^{-1} resulting from the transverse and longitudinal C-C stretching modes, respectively, are seen to upshift to 1564.3 cm^{-1} and 1590.5 cm^{-1} after the addition of the polymer (Figure 3-6 inset B). This seen upshift in the tangential modes of the G-band is a further indicative of the polymer wrapping around the nanotubes as was also observed before

[48,52]. The strong adsorption of the hydrophobic groups of the polymer to the nanotubes surface influences the tangential vibational modes of carbon atoms on the nanotube, increasing the stiffness of such modes which explains the observed Raman upshift. This shift is smaller than the shift seen in the RBM bands which indicates further the wrapping mode of the polymer around the nanotubes as it exerts more dramatic effect on the vibration modes in the radial direction rather than the tangential direction. In addition, a narrowing of the G-band was also noticed in the polymer/nanotubes sample (Figure 3-6 inset B). The presence of the positively charged moieties of the polymer on the surface of the nanotubes causes the bundled nanotubes to break apart as a consequence of repulsive forces as the polymer interlocates between adjacent nanotubes. This reduces the interaction between adjacent nanotubes and causes their debundling which explains the band narrowing [48].

The depressive D-band appearing around 1350 cm^{-1} is widely accepted as a Raman indicative of covalent functionalization of nanotube [33-40]. By examining this Raman feature in both pristine and modified nanotubes spectra (Figure 3-6), a slight increase in the relative intensity of this D-band to the G-band is noticed in the polymer/nanotubes spectrum. This, however, is quite a small increase compared to what has been reported before from covalent functionalization [33-40]. No covalent attachment has taken place here as concluded from the absorption observations (Figure 3-5). Instead the polymer wraps around the nanotubes via attractive forces between hydrophobic groups. This wrapping is quite strong (concluded from the large shift of 10-15 cm^{-1} in the Raman RBM bands of polymer/nanotubes spectrum) and it imposes physical strain and constraint [157] on the tubes surface that might generate structural defects and might increase the degree of disruption in the graphene structure. This is used to explain the

observed slight increase in the D-band intensity of polymer-modified nanotubes sample.

Characterization of Layer-by-Layer Nanotube Films

The polymer modification of nanotubes in this study allowed the preparation of stable dispersions of nanotubes that manifested their processing into structural composites of thin films required for achieving the goals of this study. Layer-by-layer (LBL) assembly was chosen for nanotube thin films preparation. This method represents one of the most effective, simple, and universal methods of preparing thin films of oppositely charged moieties [158-159]. Driven by electrostatic attraction between oppositely charged electrolytes, the LBL can be simply applied to almost any kind of charged molecules [for good review on the LBL method, see Ref. 160].

In the present study, the LBL was chosen because of a number of advantages this method offers over other methods like Langmuir-Blodget and spin coating. The most important advantage is the fact that this LBL approach offers the formation of strong nanotube films that can sustain the long-term exposure to cell culture medium which usually contains a variety of biological compounds including serum, ions, salts, proteins…etc, which are essential nutritions for cells growth. Illustrating the use of nanotube structures for biomedical applications requires the incubation of these materials with cells in culture medium, and thus the need for a strong nanotubes film with long retention is very necessary and can be easily obtained using the layer-by-layer assembly. Additionally, with the LBL method, the dipping sequence between the oppositely charged moieties gives rather uniform nanotube films that can be easily characterized for

thickness and conductivity measurements. Depending on the number of dipping cycles (see experimental section), the thickness of the resulting film can be controlled and the structure can be engineered to yield a rather strong and a highly conductive structure of nanotubes. Such structural properties are crucial requirements for successful utilization of nanotube composites in biomedical applications, and can be manipulated using the LBL protocol.

The sequence of the LBL assembled layers can be roughly illustrated as shown in Figure 3-7. The assembly starts first with a thin layer of the positively charged PDDA polyelectrolyte that coats the negatively charged surface of glass substrate. Due to the positively charged surface of the nanotubes, a second layer of negatively charged PAA polyelectrolyte is then assembled on top of the PDDA layer forming a negatively charged coating that will allow for the deposition of the nanotubes layer. The nanotubes layer is then deposited followed by a layer of PAA polyelectrolyte and the cycle can then be repeated as desired until the required number and thickness of layers is obtained. Figure 3-8 shows two scanning electron micrographs of two different nanotube films of 1-layer (Figure 3-8A), and 10-layers (Figure 3-8B). The single 1-LBL film of nanotubes can be easily distinguished from the 10-LBL film. By depositing a single nanotubes layer, some nanotubes are seen to randomly scatter on the surface displaying some intertube contacts and forming bundles as can be seen in Figure 3-8A. As the deposition of nanotubes increases to 10 layers, the morphology of the coated surface becomes totally different as observed in Figure 3-8B. As the nanotube layers are assembled on top of each other, the tubes form dense contacts with each other displaying net-like, mats, and wound bundles morphologies. Seen in Figure 3-8B are dark gaped areas which might indicate spaces between different layers. The good intertube contacts formed between nanotubes in

elevated layers adds to the strength of the formed film and can be advantageous in preparing nanotube composites with high strength and good electrical conductivity [76].

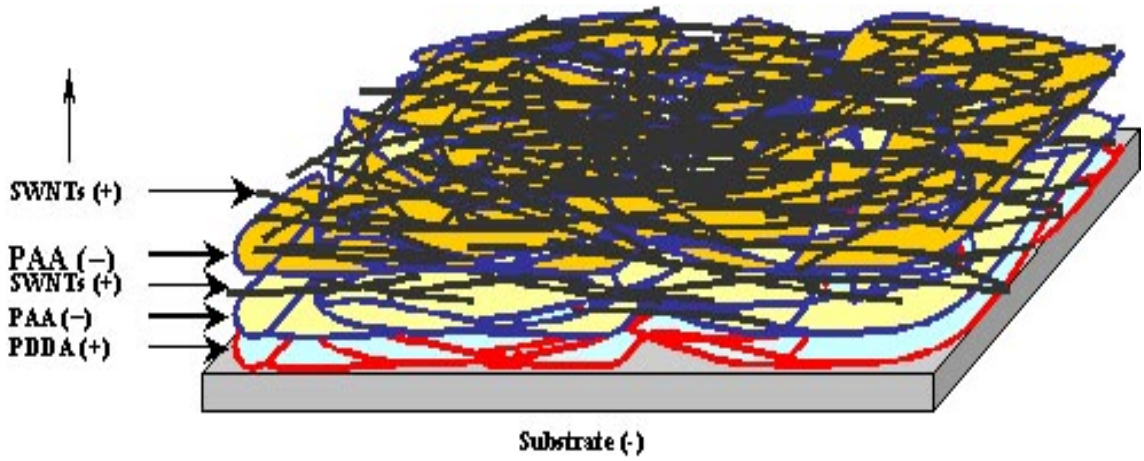

Figure 3-7. Schematic illustration of the sequence of layers deposition in the LBL approach. The blue covering indicates the initial PDDA layer followed by the PAA layer (beige covering) followed by the nanotubes layer (black lines). This sequence forms the first layer of nanotubes and the deposition cycle of a second layer can start again with a layer of PAA (orange coating) followed by the nanotubes layer (black lines) and so on.

In order to monitor the deposition of nanotube layers, UV/Vis. absorption spectroscopy was utilized. Figure 3-9 shows the change in the absorbance of nanotube films as a function of the number of deposited Layers. Measured at two different wavelengths namely 350 nm and 550 nm, the absorbance is seen to linearly increase with the number of layers assembled. This linear increase in the absorbance indicates the increase in the concentration of nanotubes loading as more layers are deposited following Beer's law [159]. The thickness of the assembled films was also noticed to increase with the number of nanotube layers as can be seen in Figure 3-10. The thickness of one

assembled layer of nanotubes is approximately 23 nm and this thickness increases as more layers are deposited. The thickness of any number of layers can be roughly estimated by multiplying the number of layers by the thickness of single layer. For instance, the thickness of 100-layers of nanotubes will be roughly 2.30 μm.

Further spectroscopic characterization of the nanotube LBL films was obtained using Raman spectroscopy. Figure 3-11 shows a Raman spectrum of 10-LBL nanotube film. As seen, the figure shows all the well-known Raman spectral features of single-walled carbon nanotubes including the radial breathing modes, the D-band, and the G-band. This adds extra advantage to the layer-by-layer process as it preserves the structure and spectral properties of the nanotubes even after their incorporation into structural composites of thin films.

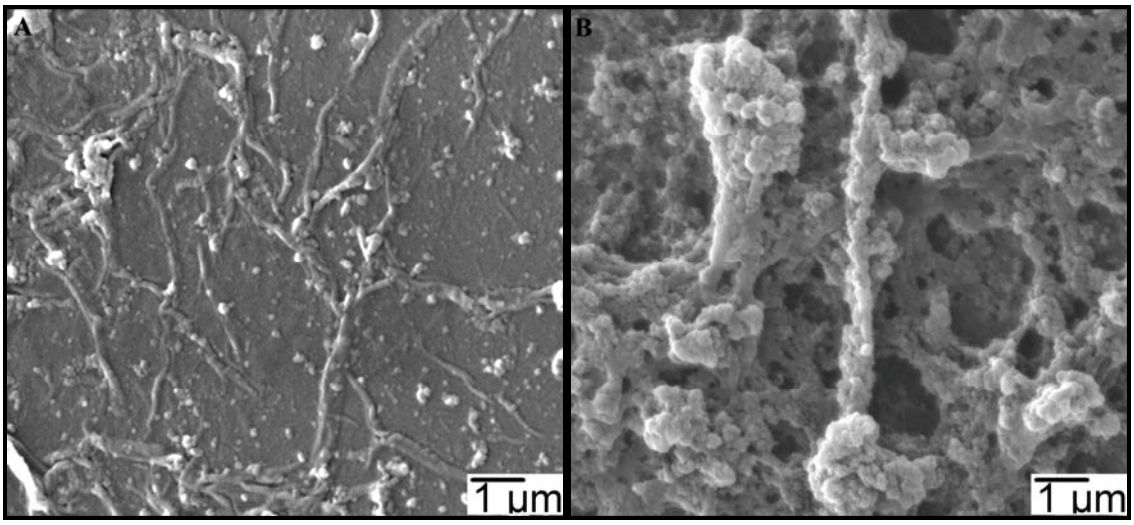

Figure 3-8. Scanning electron microscopic images of 1-LBL **(A)** and 10-LBL **(B)** assembled films of nanotubes. The nanotubes randomly exist on the surface after the deposition of a single layer (A),whereas more layers deposition increases the amount of nanotubes loading onto the surface inducing more intertube contacts as seen in (B).

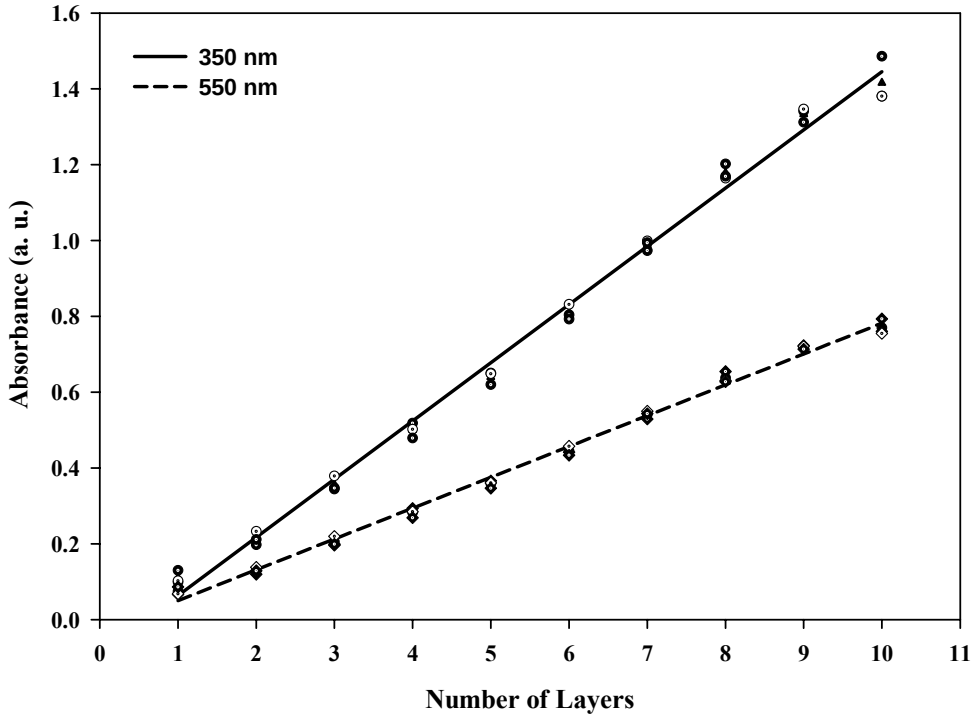

Figure 3-9. Linear increase of nanotube films absorbance with the number of deposited layers.

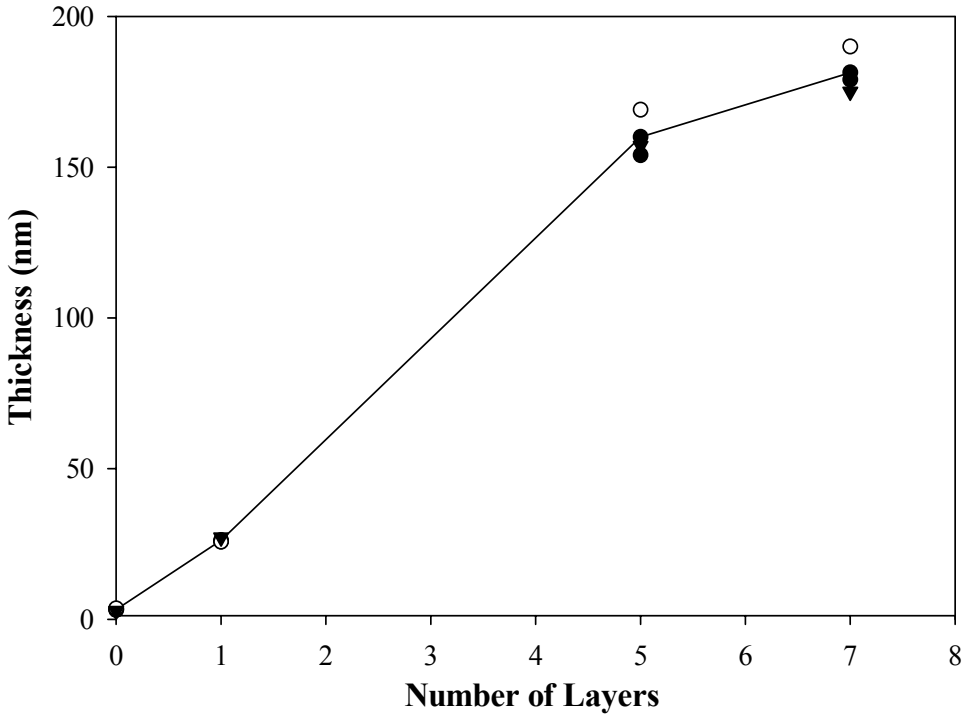

Figure 3-10. Increase of films thickness (determined from ellipsometry measurements) as the number of deposited nanotube layers increases.

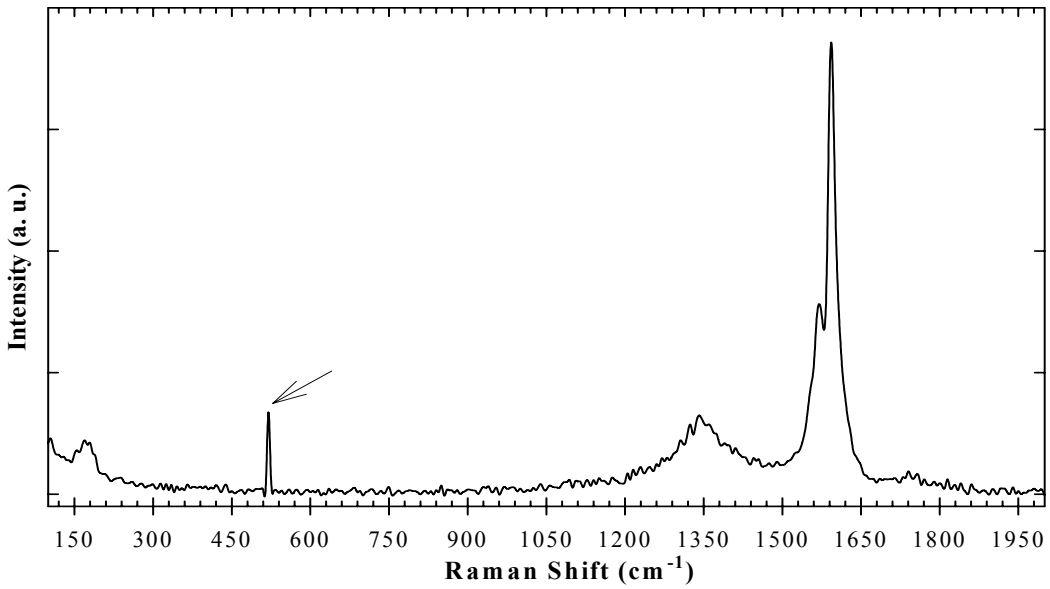

Figure 3-11. Raman spectrum of 10-LBL nanotubes film showing all the known Raman features of nanotubes. The arrow indicates the position of silicon band at around 521 cm^{-1}.

The Target NG108-15 Hybrid Culture Cells

The successful utilization of single-walled carbon nanotubes strong mechanical properties, flexibility, and good conductivity in biomedical applications depends exclusively on how biocompatible these materials, or their based structures, are and how they impact living cells. In order to address these issues, this study presents an *in-vitro* investigation of the biocompatibility of the polymer-modified single-walled carbon nanotube composite LBL films applied on the target cells NG108-15 neuroblastoma-glioma hybrid culture line. These cells were produced originally by virus generated cell fusion of mouse neuroblastoma cells N18TG2 and rat glioma cells C6-BU-1 [161-162] forming the hybrid cells NG108-15. The resulting baby cells of the hybrid shown in Figure 3-12 -which represents an SEM image of dividing small NG108-15 cells after

one-day growth in full culture medium- contain chromosomes of both parental cells and exhibit combined properties of the original cells as will be discussed in following paragraphs. For the present study, NG108-15 cells were chosen because they represent a good neuronal model system for *in-vitro* studies as they exhibit many neuronal characteristics of mammalian nerve cells [142]. They exhibit large contact areas and ability to extend long neurites that would facilitate their attachment to the nanotube substrates and would allow the characterization of their growth and differentiation on the nanotubes surface. Being a neuron-like, these cells possess voltage and ion membrane channels that make them easily excitable and capable of generating action potentials [163-167]. Using the nanotube structures as substrates, the membrane potential of these cells can be stimulated and detected which would provide a better understanding (under many physiological conditions) of the biology and chemistry of these living cells in contact with inorganic materials like carbon nanotubes.

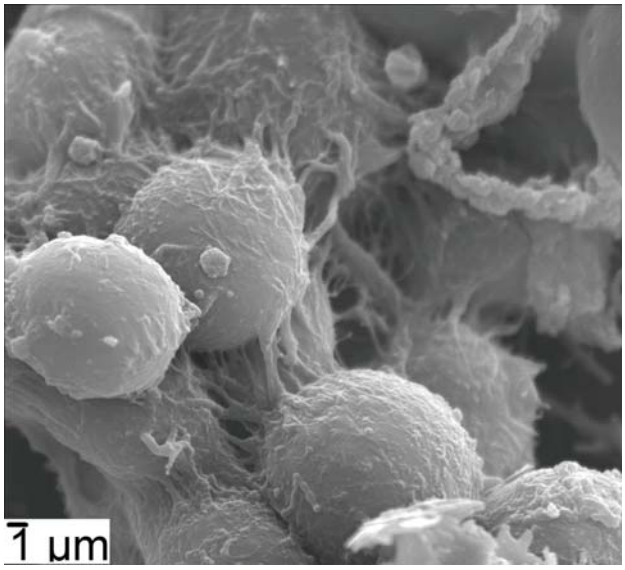

Figure 3-12. Scanning electron micrograph of dividing baby NG108-15 cells after 1-day growth in full culture medium (consisting of %90 DMEM, %10 FBS, HAT, Penicilin/Ctreptomycin).

The hybrid NG108-15 cells usually exhibit cell morphological changes during the period of their growth. Being an adherent type of cells, they tend to attach to the surface of the culture substrates and to each other. Once they are seeded on the culture substrate, they attach to it within minutes and start to divide. Figure 3-13A shows a confocal microscopic image of NG108-15 cells after 1-day growing in a full culture medium consisting of %90 DMEM, %10 FBS, HAT, Penicilin/Ctreptomycin. The image shows a low density cells number well in contact with each other. These cells, when fully grown, have a round shape with average surface area of approximately 7500 μm^2 and can even reach up to 75000 μm^2. Similar surface morphology is also noticed when these cells are dividing where they also assume circular shapes as shown in Figure 3-12. Noticed from Figure 3-13A, is the presence of neurites and branches extending out of these cells bodies. These neuronal processes, when cells are not differentiated, extend over short distances ranging from 10 μm to 100 μm or slightly longer. They represent a passageway of communication between neighboring cells and help anchor the cells to the substrate surface as they contain attaching proteins necessary for the cells attachment. After 3-4 days of culturing time, these cells are noticed to increase in number as shown in Figure 3-13B. They continuously divide and proliferate increasing their number to a confluent density that calls for subculturing, which is usually done every 4-5-days. In the subculturing process, the cells layer is detached from the bottom of the culture flask and the cells are seeded at very low density in new flasks and the growth process starts again. This is necessary in order to maintain a viable continuous cell line which otherwise would decline if the cells are kept at very high densities without subculturing.

When growing NG108-15 cells in a serum free medium, the absence of serum inhibits the proliferation of the cells and induces their differentiation [144]. When

differentiated, these cells usually undergo some morphological developments over the course of just a few hours. These include the flattening of the cell body followed by the generation of many spine-like branches from the cells membrane. The cells then start to extend neurites whose length can reach up to more than a millimeter and increases with the length of the incubation period [168]. Figure 3-14 illustrates a confocal image of differentiated NG108-15 cells after incubating them for 7-days in serum-free medium. The differentiation of these cells in the figure is characterized mainly by the existence of one or more elongated neurites extending from the cell body over an average length of 400-500 μm. From these neurites, many branches and axons emerge that can extend over long distances on the surface. The higher number of neurites and branches extending from the cells and the longer these neurites are, the better and more enhanced the cell differentiation is [168].

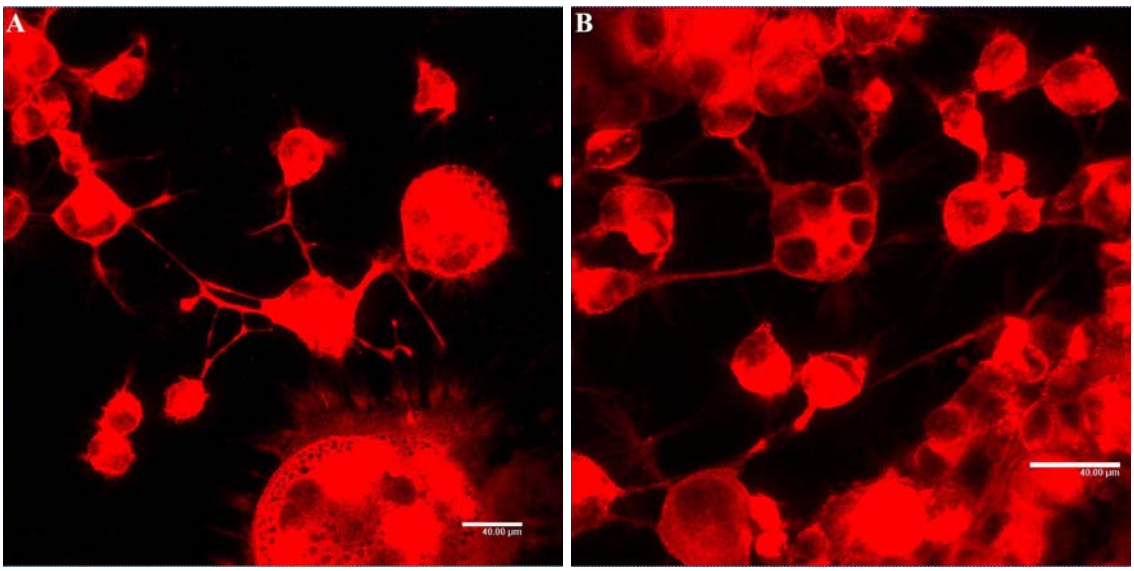

Figure 3-13. Confocal microscopy images of low density NG108-15 cells after 1-day incubation **(A)** and higher density of cells after 4-5 days incubation **(B)** in full culture medium. Scale bars are 40 μm.

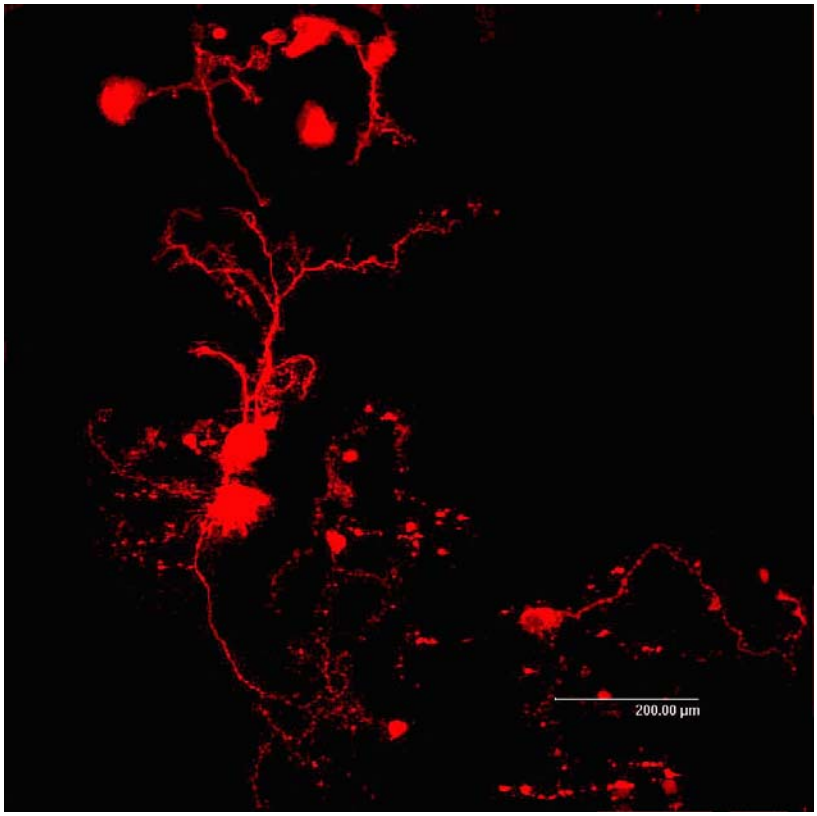

Figure 3-14. Confocal microscopy image of differentiated NG108-15 cells after 7-days incubation in serum-free medium. The image shows well-differentiated cells characterized by the presence of long neurites and many neuronal processes. Cells were dyed with a lipophilic neuron tracer Dialkylcarbocyanines DiI (Molecular Probes cat. no N22880). Scale bar: 200 µm.

Prior to using the NG108-15 cells on the surface of nanotube structures, their growth and viability were first monitored. Figure 3-15 illustrates the cell density as a function of the number of culture days. As noticed, the number of cells is seen to increase exponentially over more than 100-days in culture. The doubling time of this type of cells is usually 18-20 hours [142]. After 10-days in culture, the number of cells was seen to sharply increase reaching up to a million cells per milliliter. After reaching the 40^{th} day in culture, the cell density was seen to increase to two million cells per milliliter, and continued to increase slightly within this range. This continuous increase is an indication

of cells viability and culture line continuity, which are important for reliable in-vitro studies. Cells were used in most of our experiments in their confluent state after at least 40 culture days.

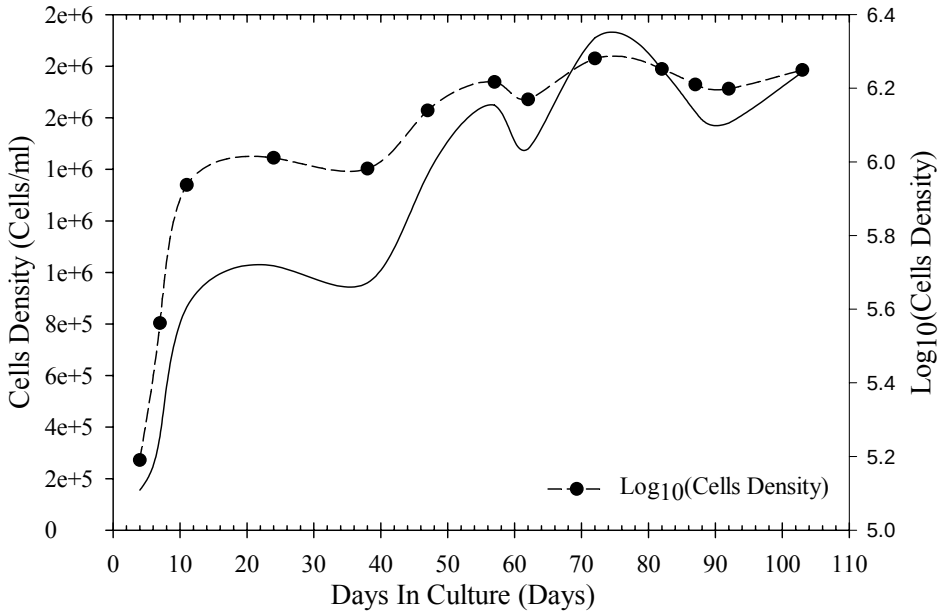

Figure 3-15. Exponential increase in cells density with the number of days in culture indicating confluent cell line. The y-axis on the right represents the logarithmic values of the cell density (dashed line).

Biocompatibility of Nanotubes Layer-by-Layer Films

To study the biocompatibility of the polymer-modified nanotube based films and long-term viability and survival of cells on their surface, cells were incubated with three-nanotube LBL films, namely 1-, 5-, and 10-layers, in full culture medium at 37 ^{o}C and were examined after 3-days, 5-days, and 10-days incubation time. Figure 3-16 shows confocal microscopy images of NG108-15 cells cultured on the surface of the three

nanotube LBL films after 3-days and 10-days incubation. Viable cells are distinguished by their continuous intracellular esterase activity. This activity is determined by the enzymatic conversion of the non-fluorescent cell-permeant calcein into a strongly fluorescent calcein that gets retained within live cells giving rise to green fluorescence (515 nm) when excited at 488 nm. Dead cells, on the other hand, are recognized by their red fluorescence produced by Ethidium Homodimer EthD-1 dye which enters cells with destroyed membrane and attaches to their nucleic acids and remains, on the other hand, excluded from those cells with intact membrane. As can be seen from Figure 3-16, a large number of the cells give green fluorescence indicating their viability on the surface of all the used nanotube films even after 10-days of incubation. Closer analysis of these images can give quantitive insights on the percentage of live cells on the different nanotube films. A histogram illustrating the percentage of live cells after 3-, 5-, and 10-days incubation with the nanotube substrates is presented in Figure 3-17. A total of two thousand random cells were counted in each sample from multiple spots on the LBL substrate surface. After 3-, and 5-days incubation of the cells, it was seen that almost 95-98% of the cells were live cells (identified by their green fluorescence in Figure 3-16) and only 2-5% of the cells were dead cells (identified by their red fluorescence in Figure 3-16) on the surface of all the films. After a longer incubation time of 10-days, more than 94% of the cells remained alive on top of the nanotube films. A 10-days period is a quite sufficient time for most of the in-vitro studies which are, usually, conducted over few days only (1-3 days). This is an important observation as it indicates that the polymer-modified nanotube based LBL films support the long-term viability, and the survival of NG108-15 hybrid cells. The ability of these cells to remain viable on the surface of nanotube-based films even after 10-days of incubation indicates their

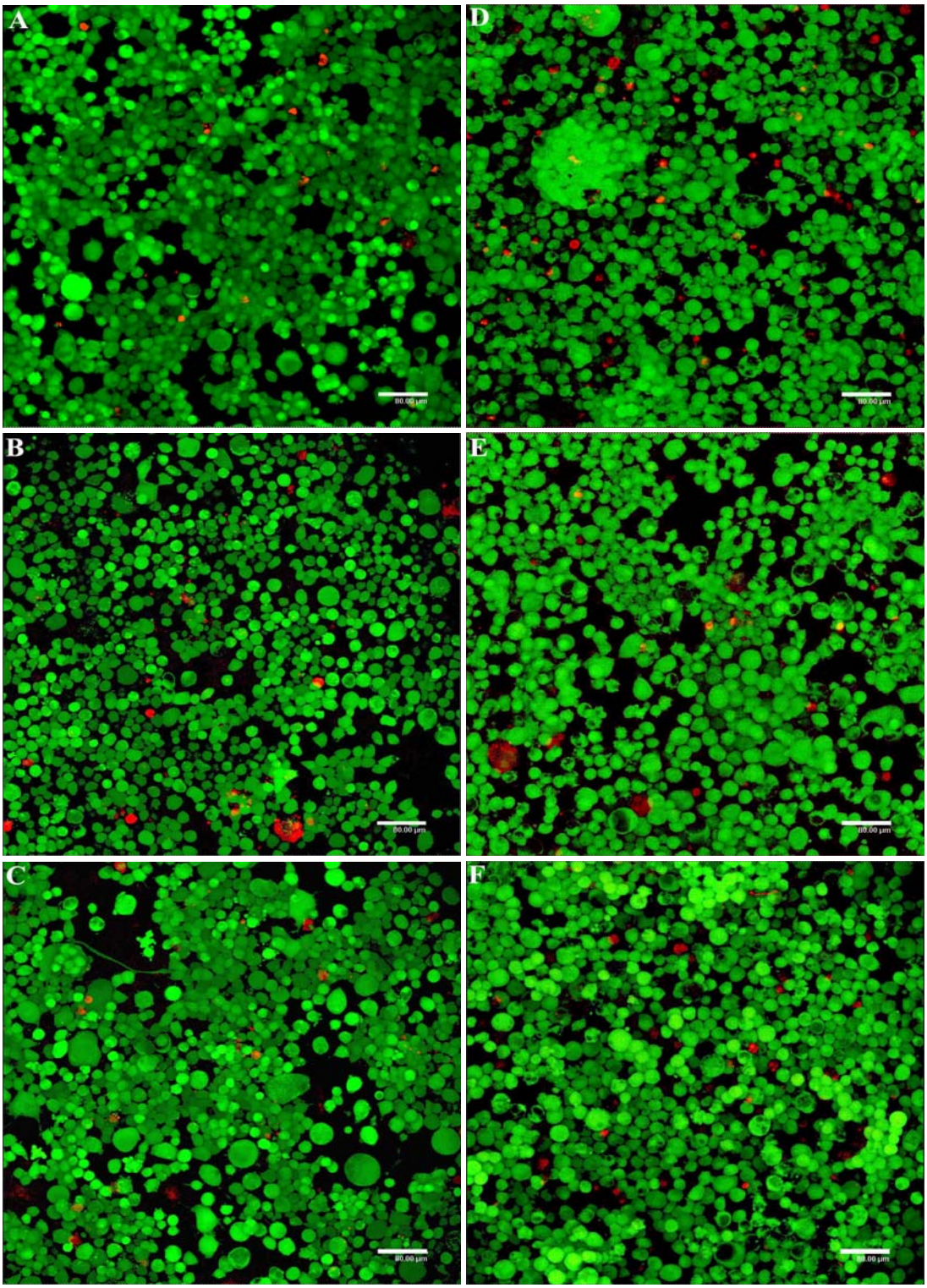

Figure 3-16. Confocal microscopy images of NG108-15 cells cultured on the surface of 1-LBL (A & D), 5-LBL (B & E), and 10-LBL (C & F) nanotube films after 3-days incubation (A, B, C) and 10-days incubation (D, E, F). Viable cells are recognized by retaining fluorescent calcein dye (Molecular Probes L3224) giving rise to green fluorescence and those dead cells are recognized by their red fluorescence produced by Ethidium Homodimer EthD-1 dye (Molecular Probes L3224). All scale bars are 80 μm.

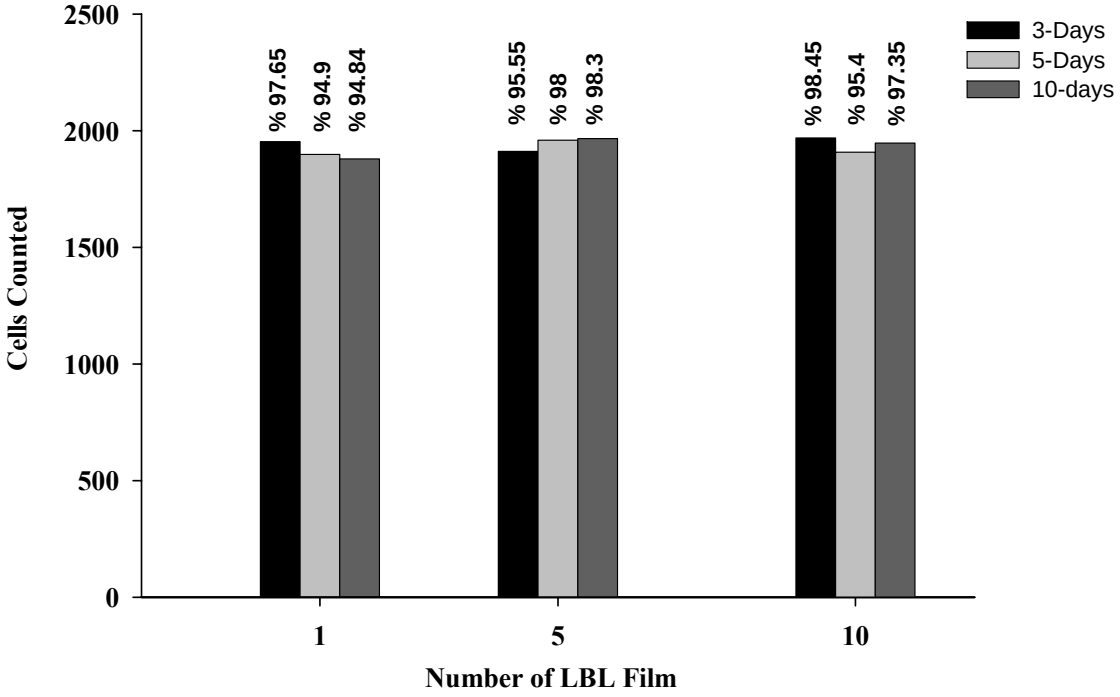

Figure 3-17. Percentage of live cells after 3-days, 5-days, and 10-days incubation with 1-LBL, 5-LBL, and 10-LBL nanotube films. A total of 2000 cells were counted randomly in each case and those cells giving green fluorescence in Figure 3-16 were counted as live cells.

attachment and growth on these nanotube-based substrates surface because of their adherent property which is a key requirement to their survival [142]. This is suggestive of the non-toxicity of the polymer-coated nanotube LBL films to this particular type of cell culture line [169]. No appreciable difference in the ratio of survived cells was noticed between the three nanotube films used, which indicates that the viability and the survival on these cells is independent on the umber of assembled nanotube layers.

In order to examine the feasibility of using nanotube LBL films as culture substrates for neuronal growth, we monitored the growth of NG108-15 cells on different nanotube films after 3-days of incubation in full culture medium. Figure 3-18 shows confocal micrographs of live NG108-15 cells on the surface of 1-, 5-, and 10-LBL films. The cells

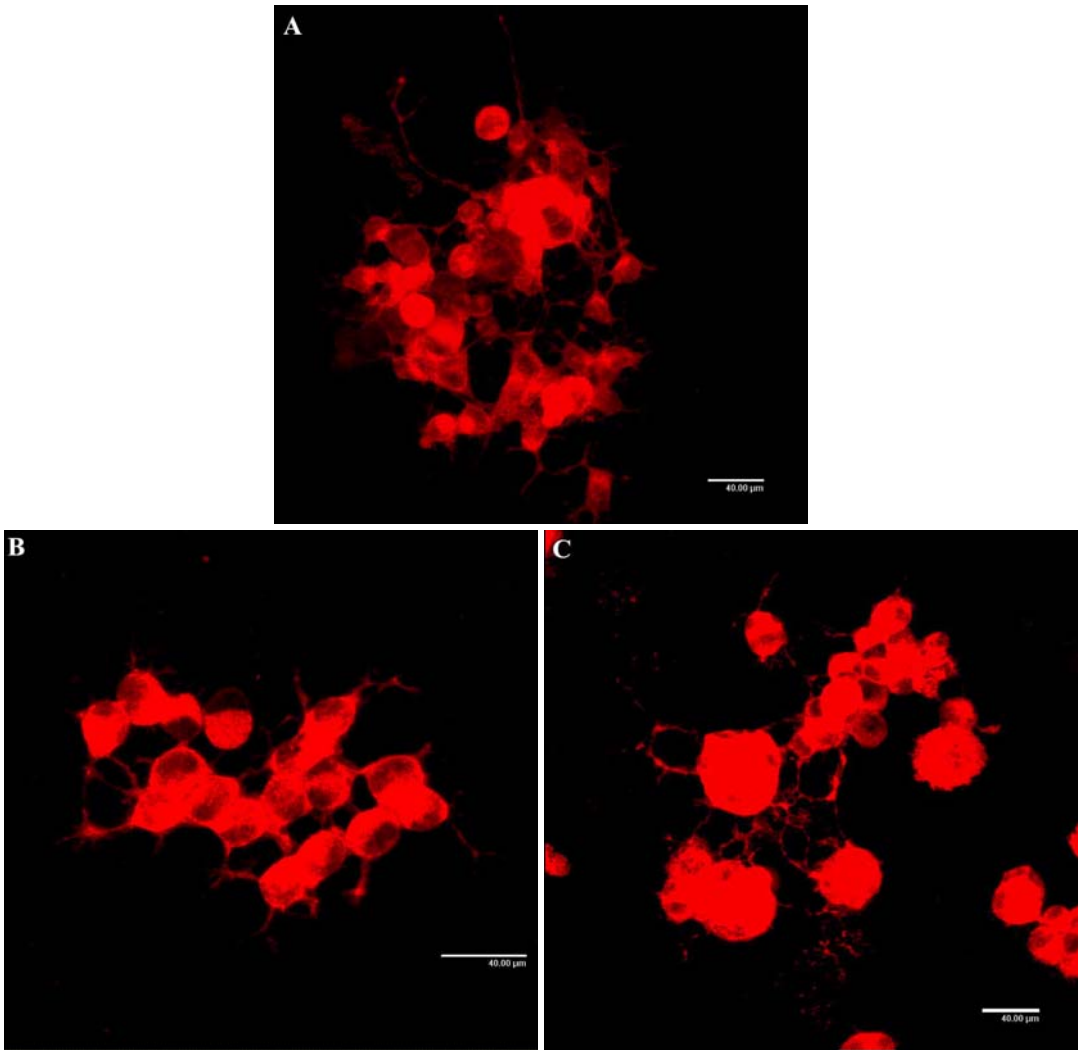

Figure 3-18. Confocal microscopy images of NG108-15 nerve cells grown on the surface of 1-LBL **(A)**, 5-LBL **(B)**, and 10-LBL **(C)** nanotube films after 3-days incubation period. Cells were dyed with a lipophilic neuron tracer Dialkylcarbocyanines DiI (Molecular Probes cat. no N22880). All scale bars are 40 µm.

were first labeled with a lipophilic Dialkylcarbocyanines (DiI) dye (Molecular Probes V22885) that emits red fluorescence when excited at 488 nm. This dye is a neuronal tracer as it has the ability to diffuse through the membrane of live cells and trace along their neurites so that their surface morphology and growth can be easily monitored. We have inspected the cells at multiple spots on the surface of each nanotube film and almost

all the cells were seen to give red fluorescence indicating their viability (since the used dye attaches to live cells only) and the surface homogeneity of the nanotube films. The cells were seen to grow in an equal fashion on the surface of 1-, 5-, and 10-LBL nanotube films without any noticeable differences (Figure 3-18). On all the nanotube substrates used, the cells were seen to have almost round shapes and were seen to extend out neurites attaching to the substrate surface. Some cells appeared more grouped next to each other than isolated. These are basically cells that are in the process of division on the surface of the nanotubes (see Figure 3-18).

To gain a better outlook at the cells growth on the surface of the nanotube films, scanning electron microscopy was employed. Shown in Figure 3-19 are SEM micrographs of NG108-15 cells on the surface of 1-, 5-, and 10-LBL assembled nanotube films. The shown cells are dead cells that were fixed directly following the third day of incubation with the nanotube films. The illustrated cells have round morphological shape characteristic of healthy, well-grown cells. Images shown in Figure 3-19 (A, C, and E) captured cells at the moment of proliferation where small immature cells are seen generating from larger ones similar to those cells growing on a typical culture dish as was shown in Figure 3-12. Figure 3-19 (B, D, and F) show higher magnification images of two cells right at or following the moment when they are dividing from each other. These images also show the tendency of these cells to extend neurites and small branches in a way to attach to the surface of the nanotube LBL films.

Both presented confocal and SEM images give strong evidence on the biocompatibility of the prepared LBL films of polymer-modified nanotubes. The ability of the cells to grow on the films surface by attaching to it, dividing, and proliferating indicates their ability to carry out some of their most important natural processes on the

surface of the assembled nanotube films. This is a very strong demonstration of the possibility of using such single-walled carbon nanotube based composites as structural substrates for neuronal growth [169].

Differentiation of NG108-15 Cells on Nanotube LBL Films

The differentiation of NG108-15 cells is quite essential for electrophysiological investigations. When differentiated, these cells usually exhibit highly excitable membranes whose potential can be easily stimulated and detected [164]. The differentiation of NG108-15 cells on the surface of nanotube structural composites is, thus, of special importance if single-walled carbon nanotube structures are to be used as stimulating materials of such neuron-like cells as will be demonstrated in a later section of this thesis.

In this section, we discuss the differentiation of NG108-15 cells on the surface of 1-, 5-, and 10-LBL nanotube films. Cells differentiation was induced by incubating the cells with the substrates in serum-free culture medium. Figure 3-20 shows confocal images of differentiated NG108-15 cells taken after 7-days incubation with 1-LBL (A-B), 5-LBL (C-D), and 10-LBL (E-F) nanotube films. Incubation for 7-days period is usually sufficient time for achieving good cells differentiation. Comparing these images with those of cells grown on nanotube films for 3-days in full medium (Figure 3-18), we notice a remarkable difference in the morphology of the cells. The cells are seen to exhibit enhanced neurites formation on the surface of all nanotube films accompanied with the formation of secondary neurites generations as can be seen from Figure 3-20.

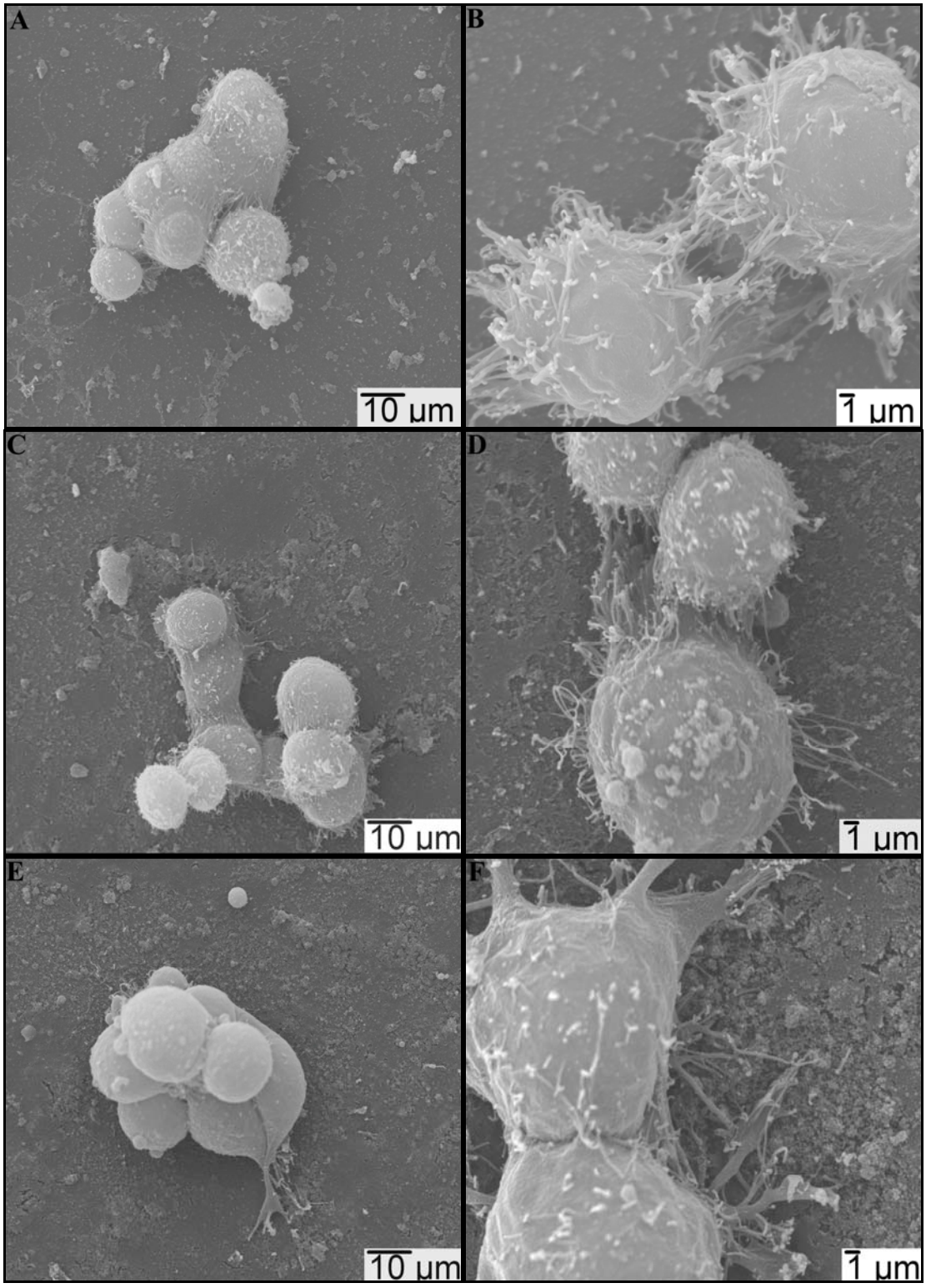

Figure 3-19. Scanning electron micrographs of NG108-15 nerve cells captured as the cells were dividing on the surface of 1-LBL **(A-B)**, 5-LBL **(C-D)**, and 10-LBL **(E-F)** nanotubes films after 3-days incubation. Images B, D, and E represent high magnification images captured at the moment of two cells dividing from each other.

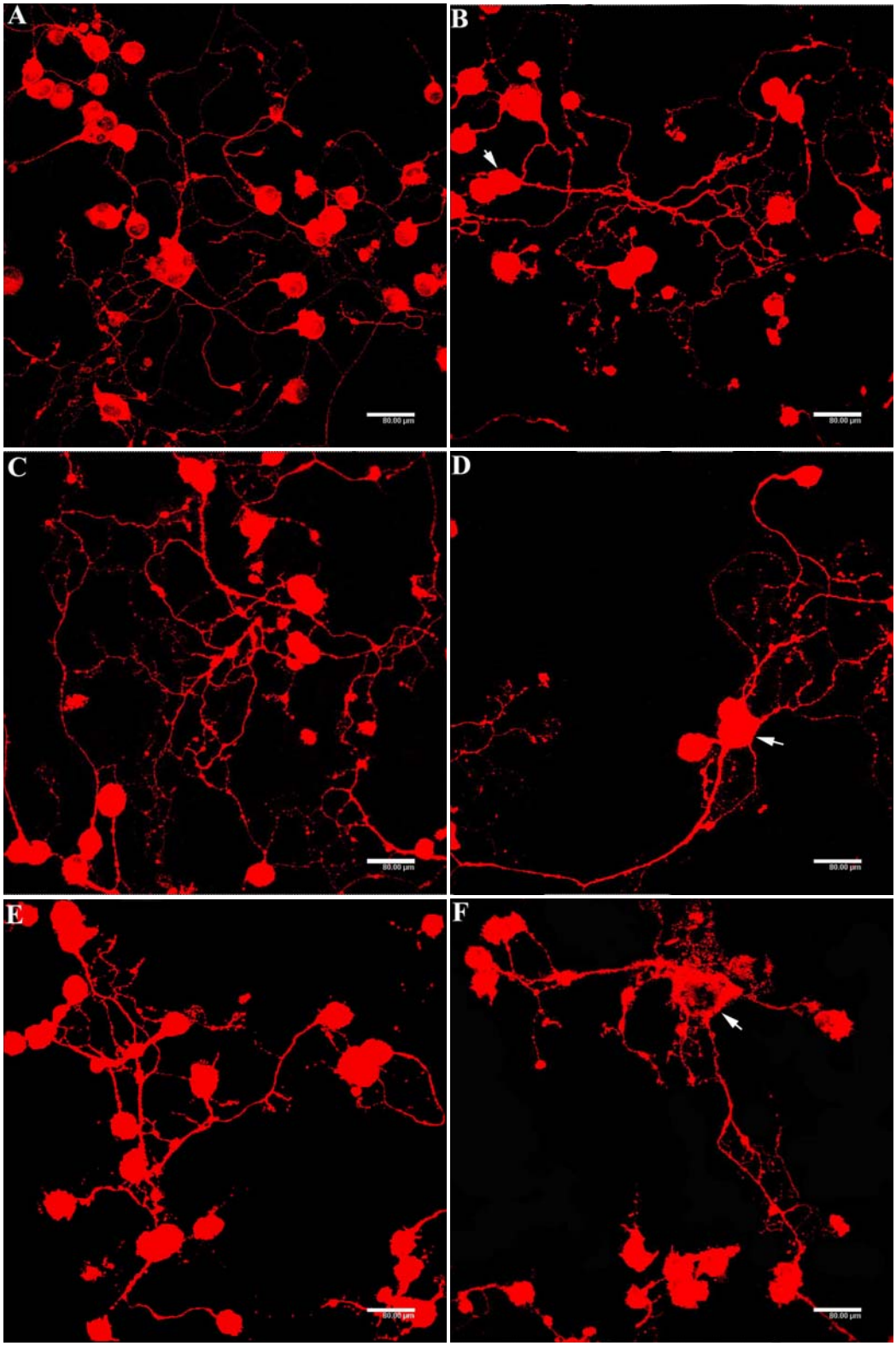

Figure 3-20. Confocal microscopy images of differentiated NG108-15 cells taken after 7-days incubation with 1-LBL **(A-B)**, 5-LBL **(C-D)**, and 10-LBL **(E-F)** nanotube films in serum-free medium. Images B, D, and F show single cells (indicated by arrowheads) with strong differentiation. All scale bars are 80 μm.

These neurites are seen to extend over long distances on the surface averaging 200-500 μm in length and reaching up to 700 μm or more in maximum length in some cases. Cell-to-cell contacts via the formation of neuronal synaptic contacts are also noticed in Figure 3-20. Single individual cells by themselves can illustrate maximum differentiation as shown in Figure 3-20(B, D, F) for cells indicated with arrowheads. These cells are seen extending one or two main neurites over long distances. From these main neurites extends many neuronal processes that are also seen spreading into many other branches as can be seen particularly in the cell shown in Figure 3-20B on the 1-LBL nanotube film. The cell shown in Figure 3-20(F) is noticed to undergo some morphological developments upon differentiation on the surface of 10-LBL nanotube film. This cell appears flat with irregular non-round shape with large area. It is also seen to extend many processes from its membrane. This cell seems to have reached high level of differentiation as compared to other cells adhered to the surface of 1-LBL, and 5-LBL films which appeared round with smaller size as shown in Figures 3-20(B) and (D), respectively.

Better observations of the morphological changes induced in the NG108-15 cells upon differentiation on the nanotube films were obtained using scanning electron microscopy. Cells were differentiated on the nanotube substrates and fixed after 7-days incubation with the nanotube films. Seen from Figure 3-21, the SEM images show well-differentiated cells on the surface of 1-LBL (Figure 3-21A,B), 5-LBL (Figure 3-21C,D), and 10-LBL (Figure 3-21E,F) nanotube films. Long elongated neurites are seen extended and branched on the surface of all the used substrates. Following a single neurite along the surface, we notice that it exhibits many junction points along its length where it emerges into two new neurites and many branches. The newly emerged neurites are also

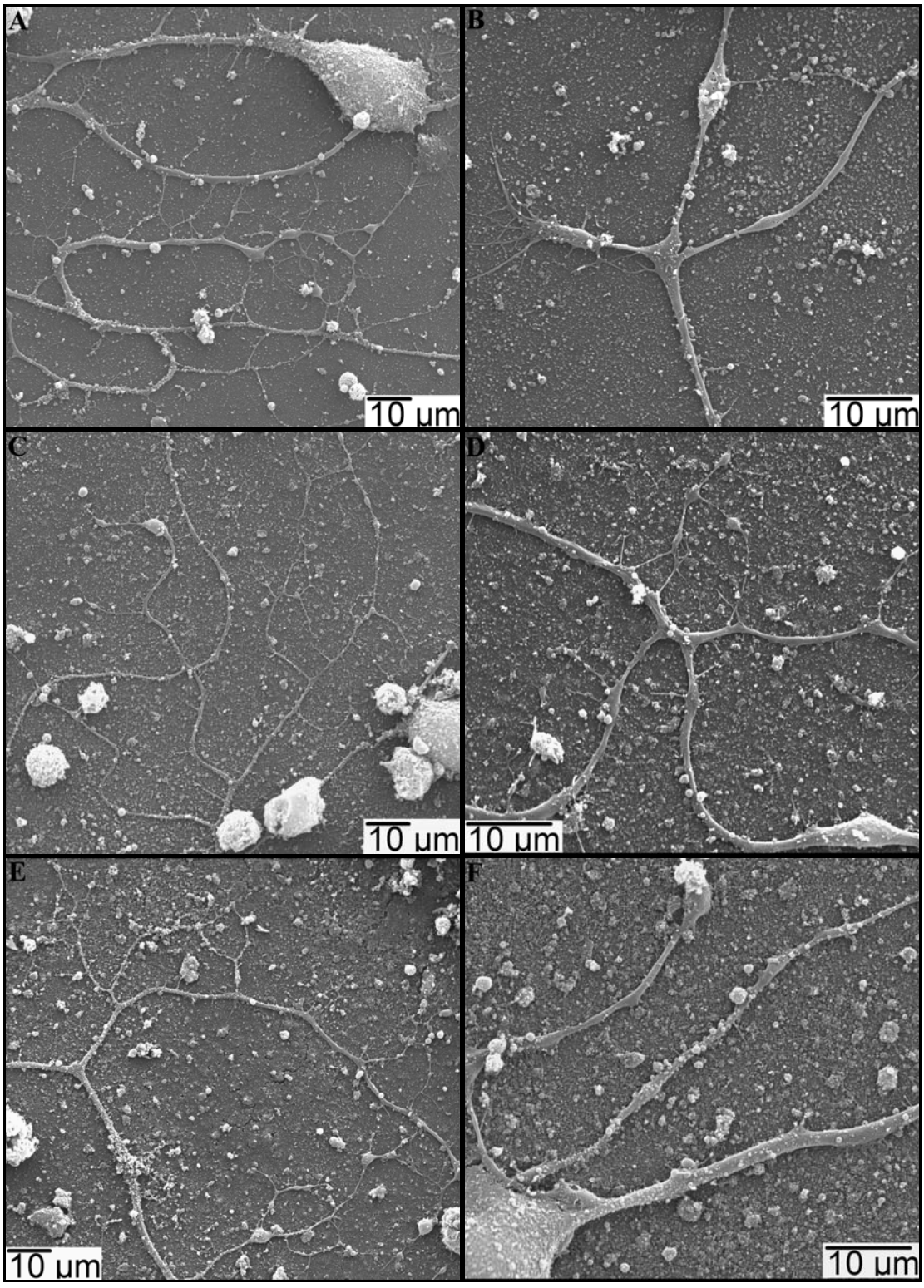

Figure 3-21. Scanning electron microscopy images of differentiated NG108-15 cells taken after 7-days incubation with 1-LBL (A-B), 5-LBL (C-D), and 10-LBL (E-F) nanotube films in serum-free medium. Images A, C, and E show many neurites and branches generated by differentiated cells forming neuronal network on the surface of the nanotube films. Images B, D, and F are high magnification images of individual differentiated cells.

seen to create another generation of neurites that branch into another generation of neuronal processes or terminate at another cell. A closer look at the extended neurites shows their interaction with the surface of the nanotube films by attaching to it and by extending small spinelike processes that terminate at the surface as can be seen in the high magnification images shown in Figure 3-21 (B, D, F). To better illustrate this, Figure 3-22 shows a single neurite on the surface of 10-LBL nanotube film. As can be seen, the neurite is terminated with many branches that appear extending along the surface. No nanotubes shadow is observed in this figure. This is resulting from a layer of culture medium components that covers the nanotubes especially after a long incubation for 7-days and despite the thorough rinsing of the substrates with buffer prior to cells fixation. This appears as a debris layer that prevents the direct observation of the nanotubes on the surface. A shadow of the nanotubes could only be seen at locations where this debris layer is stripped or cracked on the same sample as seen in Figure 3-23. Careful examination of Figure 3-22 reveals that some of the branches extend though the substrate surface. The assembled nanotube LBL composite consists of mainly alternating layers of PAA polyelectrolyte and modified nanotubes with the last deposited layer being a nanotube layer. It is predicted, thus, that the NG108-15 cells interact with the substrate surface by attaching neuronal processes to the assembled layer of positively charged polymer-coated nanotubes as PAA polyelectrolyte is known as a repellent to cell attachment [170]. A more convincing physiological evidence of cells contact with the nanotubes LBL composite will be presented later in this thesis.

The illustrated confocal (Figure 3-20) and SEM (Figure 3-21) images suggest that regardless of the number of assembled nanotube layers, the polymer-modified nanotube LBL films are permissive substrates for neurites elaboration and branching of NG108-15

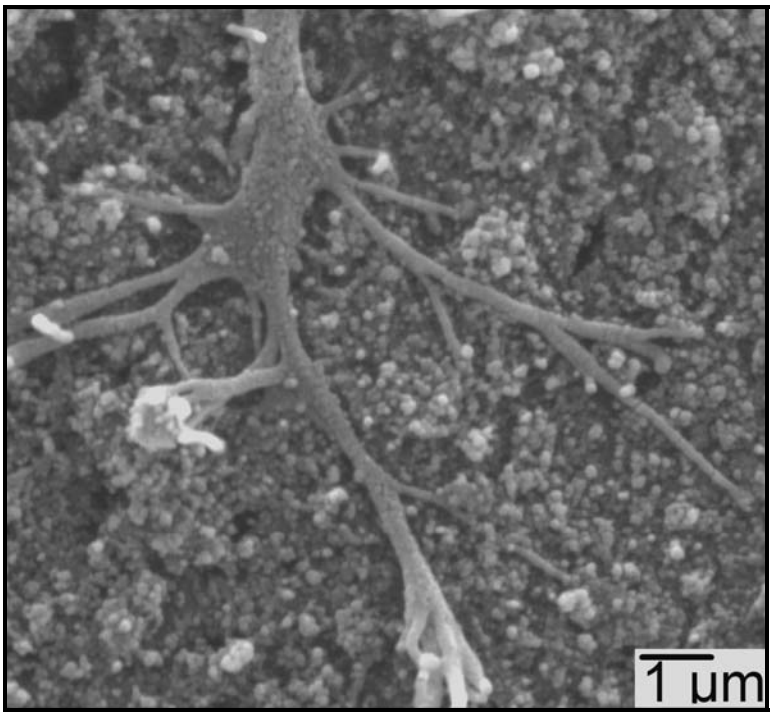

Figure 3-22. High magnification SEM image of differentiated neurite terminated with a number of branches that attach and extend through the 10-LBL nanotube substrate surface.

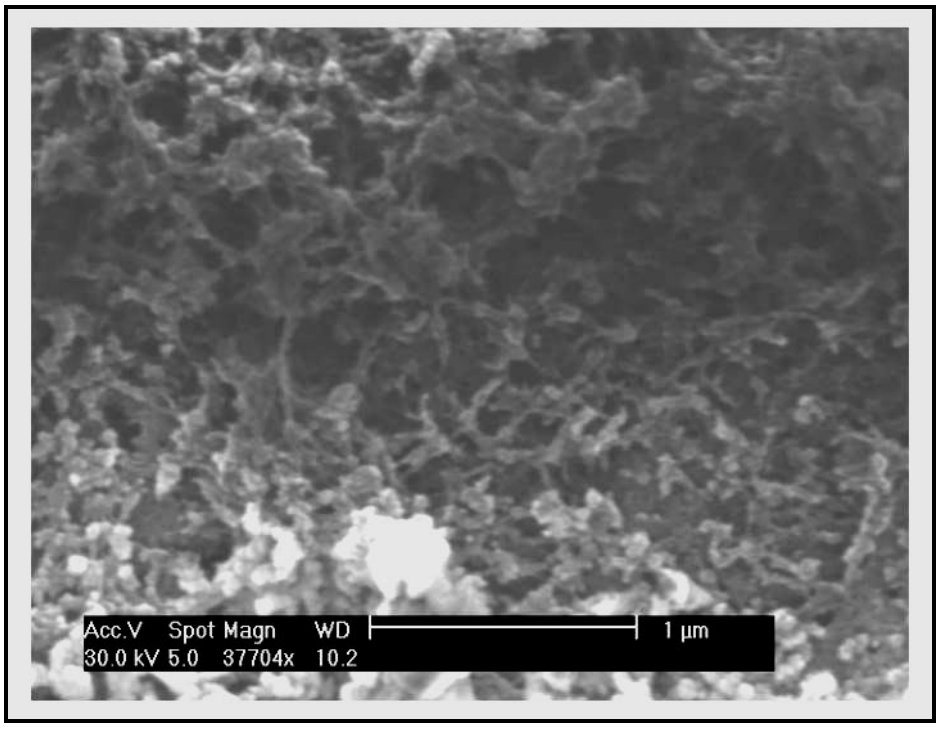

Figure 3-23. High resolution SEM image showing a shadow of nanotubes present behind the debris layer seen in Figure 3-22.

cells. Generally, the surface properties of the cell culture substrates play an essential role in determining the degree of cells differentiation [142,152-153]. The observed changes in the morphology of the neuron body of some NG108-15 cells, and their ability to extend many long neurites and branches on the nanotube substrates, all indicate good cells differentiation induced on the surface of all the used LBL films [168]. This is indicative of good interaction between the NG108-15 cells and the surface of the nanotube films.

To further illustrate the relation between cells differentiation and the substrates surface, we have carefully examined the neuronal elaboration of the NG108-15 cells as a function of surface properties of 1-LBL, 5-LBL, and 10-LBL nanotube films. As a control, cells were differentiated separately on the surface of a standard culture dish under the same experimental conditions to those of nanotube substrates in which the same number of cells was seeded in all cases. The used culture dish is negatively charged according to the source (Falcon culture dish, Fisher catalog no. 08-772F) and studying the differentiation of the cells on its surface gives good insights in comparison to cells differentiation on the surface of the positively charged polymer-coated nanotube LBL films.

When examined the differentiation of the cells on the culture dish, we have noticed that the majority of cells extend single neurite from their membrane, as shown in Figure 3-24A. Only very small percentage of the cells was seen to extend two neurites (%20) and three neuritis (%10). Cells differentiated on the nanotube LBL films, however, showed a wider distribution of neurites elaborate branching. Cells with single neurite were seen to dominate the majority of the examined cells on all the three LBL substrates with more cells percentage noticed on the surface of 10-LBL as opposed to the 5-LBL

and 1-LBL films (see Figure 3-24A). The overall percentage of cells extending one or two neurites was seen to be less for cells on the nanotube substrates than it is for cells on the culture dish. Additionally, the percentage of cells extending three neurites was quite higher on the nanotube LBL films than on surface of the culture dish. None of the examined cells were seen to branch into more than three neurites on the culture dish substrate. However, cells on the nanotube substrates were seen to extend up to six neurites and even seven in some cases. The overall average number of elaborated neurites per neuron was seen to be higher (statistically significant as determined from one-way ANOVA analysis) for cells attached to the nanotube LBL films than on culture dish, as can be seen from Figure 3-24B.

While most of the cells extending one and two neurites were those examined on the surface of 5-LBL and 10-LBL films, a higher percentage of cells extending three neurites and more was seen on the surface of 1-LBL film compared to the 5-LBL and 10-LBL nanotube films, as noticed from Figure 3-24A. More cells were seen to branch into five and six neurites when attached to the surface of 1-LBL film than to the surface of 5-LBL and 10-LBL films. The average number of elaborated neurites per neuron was seen to be slightly higher on the 1-LBL nanotube film than on 5-LBL and 10-LBL films, as shown in Figure 3-24B. Although this difference in the neurites number is quite small between the three nanotube substrates, it might indicate a slight dependence of the neurites elaboration on the number of assembled nanotube LBL films.

When measured the maximum neurite length, it was seen that NG108-15 cells have the potential to extend long processes on the surface of all the used substrates. Figure 3-25 shows the maximum neurite length measured from individual cells and averaged over a number of studied cells on the surface of the culture dish and nanotube films. The

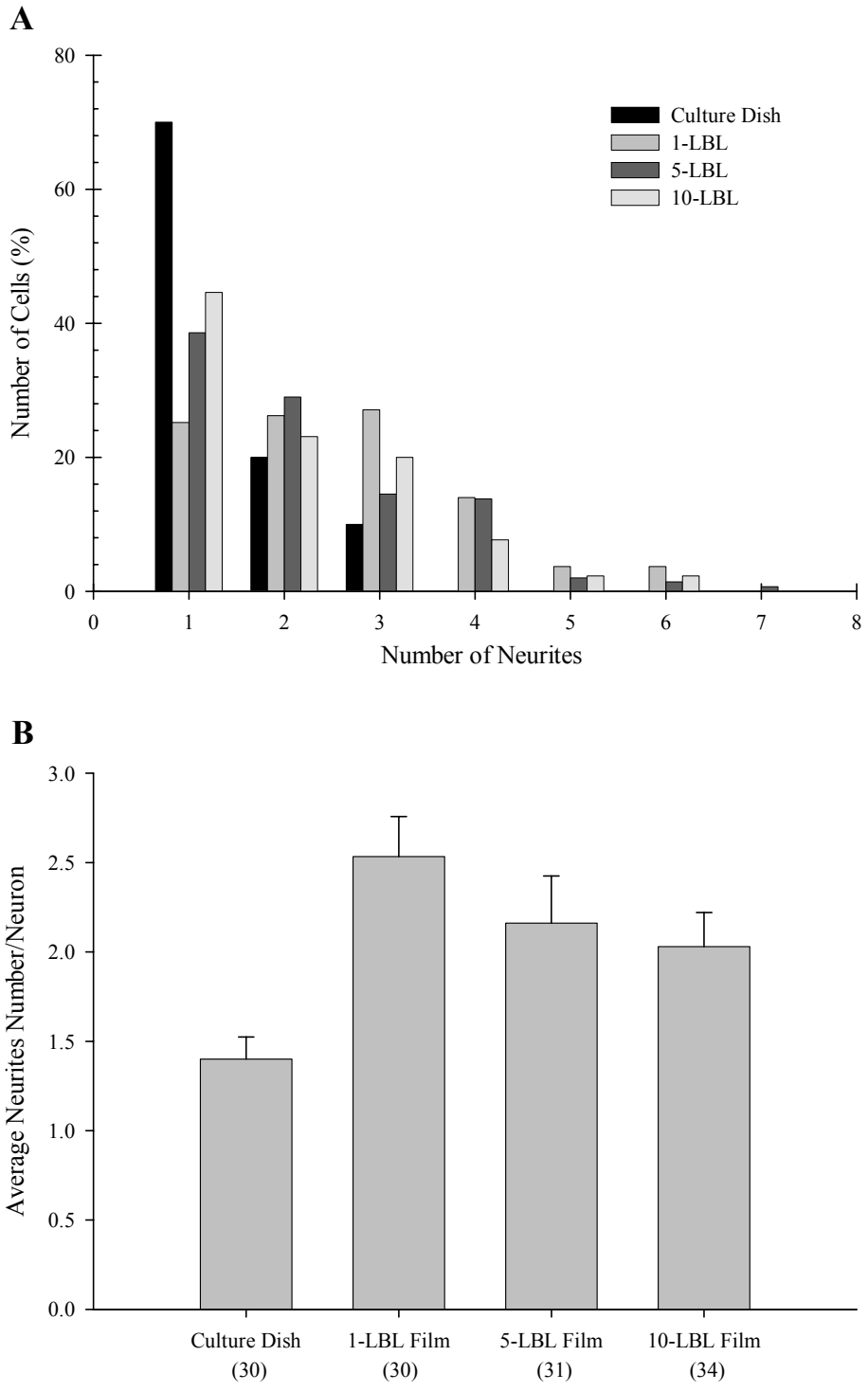

Figure 3-24. (A) Distribution of the percentage of cells versus extended neurites number on the surface of the used substrates. **(B)** Average number of main neurites elaborated per neuron for differentiated NG108-15 cells on the surface of culture dish, 1-LBL, 5-LBL, and 10-LBL nanotube films. One-way ANOVA analysis was used in B to determine the statistical significance with respect to the control which was the culture dish (p<0.0003 and significance level was 0.01). Error bars in B represent SEM in the measurements in each case. The numbers shown in parenthesis indicate the number of cells counted in each case.

average of the longest neurite elaborated from the cells on the culture dish surface was approximately 155 μm. This value was higher (statistically significant as determined from one-way ANOVA analysis) on the nanotube substrates where it ranged between 258 μm and 265 μm, with no observed significant difference in the length between the three nanotube films. The longest neurite measured on the surface of the culture dish was only 400 μm in length and only a very small number (%4) of the examined cells were seen to extend such long neurites. In comparison, neurites branching on the surface of the nanotube films were seen to extend over longer distances (500-700 μm) and reached up to 700 μm in maximum length (in some cases).

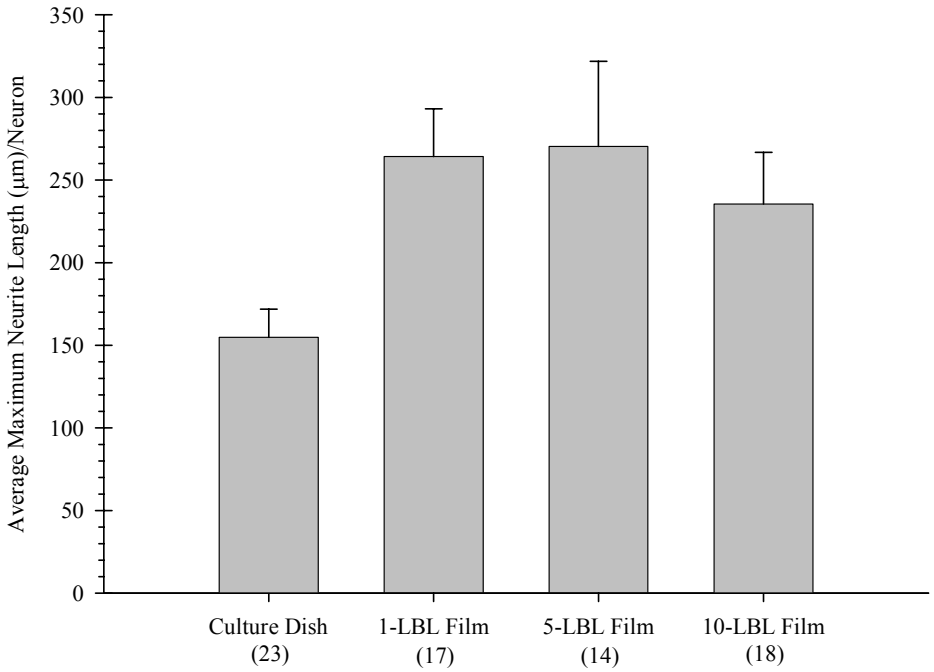

Figure 3-25. Average of longest neurite length per neuron for differentiated NG108-15 cells on culture dish, 1-LBL, 5-LBL, and 10-LBL nanotube Films. The length was measured using ImageJ software and was converted from pixels to μm units using the images scale bar as a standard. In each case, the maximum neurite length for each cell was measured and averaged over a number of cells (indicated in parenthesis). One-way ANOVA analysis was used to determine the statistical significance with respect to the control which was the culture dish ($p<0.025$ and significance level was 0.05). Error bars in B represent SEM in the measurements in each case.

Both the number of neurites and their length are used here as a measure of the degree of NG108-15 cells differentiation, where the higher the neurites number and the longer the neurites, the better the degree of differentiation is [168]. Results from both Figures 3-24 and 3-25 indicated that the overall differentiation of NG108-15 cells is more enhanced when the cells are attached to the surface of the polymer-modified nanotube layer-by-layer films than to the surface of the culture dish. This is concluded from observing higher neurites outgrowth and longer processes on the surface of 1-, 5-, and 10-LBL films compared to the culture dish. The main difference between the nature of both surfaces, the culture dish surface and the nanotube films surface, is in the net charge present on the surface. We correlate this difference in surface charge to the observed findings. Coating the substrates with the positively charged polymer/nanotube composites seems to induce better cells differentiation by promoting more neurites outgrowth and elaboration. It is believed that this is generated from more surface interaction between the positively charged polymer-coated nanotubes and the negatively charged phosphate groups existing within the membrane of NG108-15 cells. On the other hand, the negatively charged culture dish was seen to support the growth and differentiation of the cells but to a lesser degree than the nanotube substrates which is attributed to less favorable electrostatic interactions between the negatively charged dish surface and the membrane of the cells. This suggests strongly the effect of surface charge on the differentiation of NG108-15 cells and favors the use of modified nanotube based substrates, as good permissive substrates for neuronal growth and differentiation, over the use of typical culture dishes. Our observations agree well with previously reported results [152-153]. Surface charge of culture substrates usually plays an integral role in determining the degree of cells interaction with the substrate surface. Manipulating the surface charge of multi-walled

carbon nanotube (MWNTs) films was seen before to control the neurite outgrowth of Hippocampal culture cells [153]. Better neurites outgrowth characterized by the presence of more elaborate neuronal processes and longer neurites length was observed on the surface of positively charged MWNTs as opposed to the surface of negatively charged or neutral MWNTs substrates [153].

Although we have noticed no significant difference in the average maximum neurites length between the three prepared 1-, 5-, and 10-LBL nanotube films, it was noticed that neurite branching occurs at slightly higher number on the surface of 1-LBL nanotube film as compared to, mainly, the 10-LBL film (Figure 3-24). This observed difference in the neurite branching is attributed here to the topographical properties of the nanotube films. We have seen before that as the number of assembled nanotube films increases, both the thickness and the absorbance of the films increase (Figures 3-9 and 3-10). This was directly attributed to the increase in the amount of nanotube loading onto the surface as more films are deposited [159]. This is believed to induce some roughness into the surface which we have seen from the scanning electron micrographs compared before between 1-LBL and 10-LBL films (see Figure 3-8). Thus a 10-LBL film is expected to have more surface roughness than the 5-LBL film which also has more surface roughness than the 1-LBL film. This increase in the surface roughness with the increase in the number of assembled films is proposed as a factor explaining the observed decrease in degree of neuronal branching with the increase in the number of LBL films (Figure 3-24). This is suggestive of NG108-15 neuronal outgrowth preference to smoother surfaces rather than to rough surfaces. Previous studies have indicated the role played by surface topography on the degree of neurites branching, where smoother surfaces were seen to be more promotive to neuronal outgrowth than rough surfaces [151]. Moreover, it is also

possible that the higher nanotube loading (higher thickness) on the substrate surface is causing the loss of the cellular autocrine factors. These factors are usually produced by cells for self-stimulation of differentiation or for stimulating the differentiation of other neighboring cells. It is probable that such factors are being absorbed by the multilayers of polyelectrolytes and polymer/nanotubes on the surface of the rather thick 10-LBL film as compared to the 1-LBL film. As such, less stimulation of cell differentiation is expected on the 10-LBL film which might explain the low degree of cell differentiation on this substrate compared to mainly the 1-LBL film.

These surface properties including the charge, the roughness, and the thickness of the nanotube composite film, are considered here to contribute to the process of NG108-15 neuronal differentiation and neurites outgrowth. All the three LBL films were seen to be very effective and permissive substrates for neuronal differentiation to a degree that exceeds that of a typical negatively charged culture dish. Our results suggest that such layer-by-layer films, based on polymer-modified nanotubes, can be engineered to optimal structural properties for maximal neurites attachment and differentiation.

Free-Standing Structures of Nanotubes as Supporting Materials of Neuronal Differentiation of NG108-15 Cells

The observations obtained so far on the growth and differentiation of NG108-15 cells on the polymer modified nanotube LBL films strongly suggest the biocompatibility of such structures and demonstrate their permissive nature as cell culture substrates supporting the long term viability, growth and differentiation of NG108-15 cells. These observations are very important and essential for the further utilization of nanotube based

structures in biomedical applications. Being non-biodegradable materials and owing to their high strength (can reach up to 1000 GPa in Young's modulus which is 60 times or more stronger than that of bones), surface-modified single-walled carbon nanotubes can be very good base-materials and reinforcing structures of prostheses and can even by themselves be used as external implants for treatments of bodily injuries such as neuronal injuries, brain injuries, spinal cord injuries, or hip injuries.

In order to demonstrate such a possible application of nanotubes, we investigated, for the first time, the durability of modified single-walled carbon nanotube freestanding structures as supporting materials of neuronal differentiation of NG108-15 cells. To form a freestanding structure of the nanotube composites, a freestanding LBL film was first prepared by etching a 36-LBL film of nanotubes from the surface of glass substrate using %5 hydrofluoric acid and then rolling it into a small elongated nanotube structure. Figure 3-26A shows a scanning electron microscopic image of such nanotube fibrous structure of approximately 20-30 μm diameter. Such a structure consists of a large number of modified nanotubes that are seen to randomly contact with each other on the surface forming net-like arrangements as illustrated in Figure 3-26B. This nanotube-based structure is predicted to have enhanced mechanical and electrical properties resulting from the dense contacts between nanotubes, which makes it attractive as extracellular implant and neuronal supporting material.

In order to resemble the implanting process, the formed freestanding nanotube structure was placed, unsupported, at the bottom of a typically used culture dish. Cells were seeded in the dish and allowed to differentiate for 7-days in serum-free medium. Scanning electron microscopy was used to observe the differentiation of the cells on top of this prepared nanotube freestanding structure as shown in Figure 3-27. As observed, a

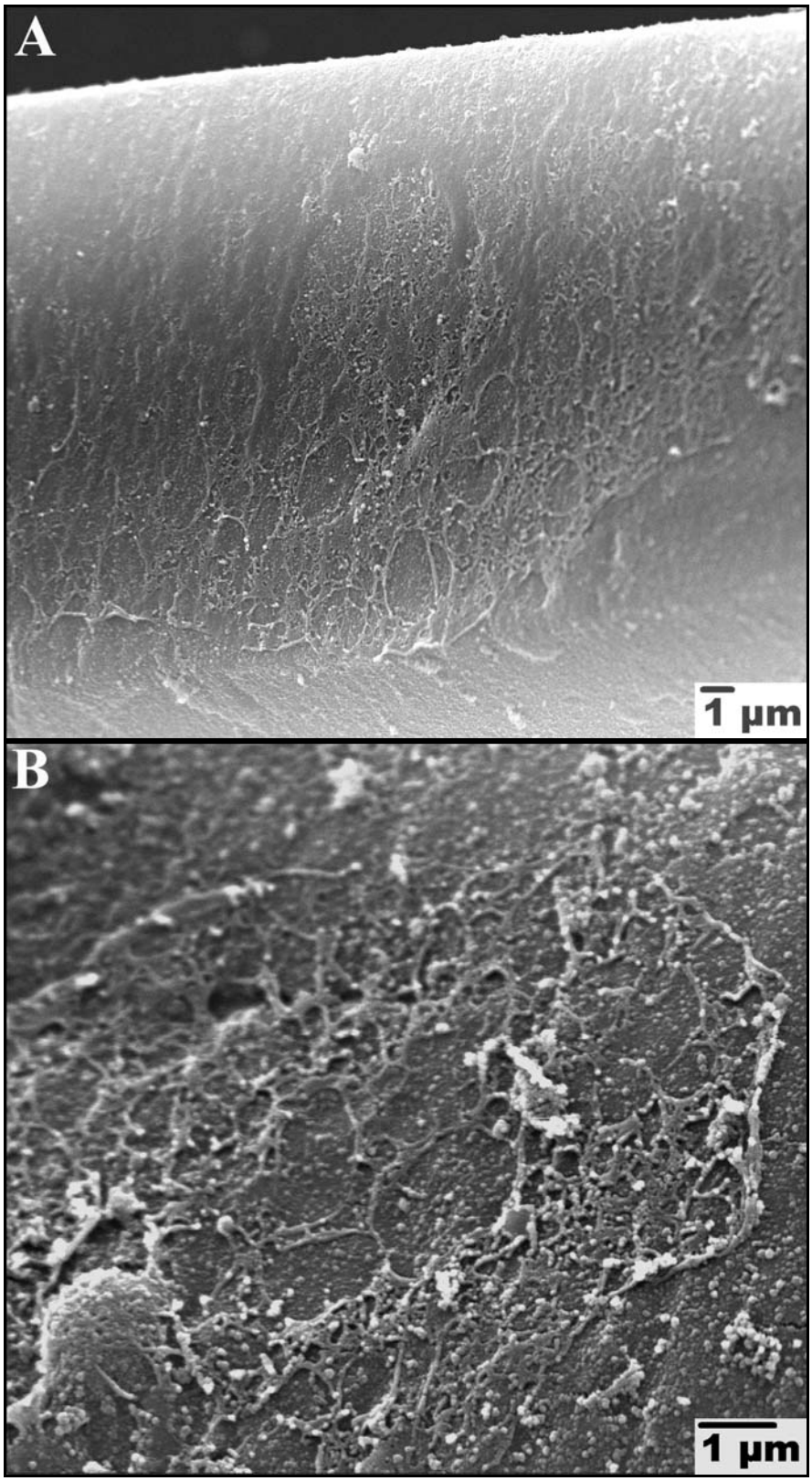

Figure 3-26. **(A)** Scanning electron micrograph of freestanding fibrous structure of single-walled carbon nanotubes. **(B)** Higher magnification SEM image of the surface of the structure shown in A showing the presence of nanotubes exposed on the surfaces

single cell is seen resting on top of the nanotube-based structure (Figure 3-27A). This cell is seen to extend one main neurite and few others along the surface. These neurites are seen to develop into many secondary neurites that branch in many directions on the surface as noticed in Figure 3-27B. Many neuronal processes are seen branching from these neurites and are seen buried into the supporting surface as better illustrated in Figure 3-28, and probably forming contacts with the nanotubes exposed on the surface (indicated by arrowheads in Figure 3-27B). One thing noticed mainly from Figure 3-27 is that the extension of neurites from cells almost follows the morphological shape and curvature of the surface of the nanotube-based structure. To investigate this further, a freestanding film of nanotubes was formed, rolled into the shape of small tube, and then stretched slightly to induce topographical elongated curves along the surface in the stretching direction, as can be seen from Figure 3-29. The morphological shape of such nanotube structure was seen to contribute to the cells differentiation. The cell shown in Figure 3-29 (indicated by red arrowhead) is seen anchored to the nanotube structure and is seen to extend three long neurites on the surface. Two of these neurites were seen extending along the direction of the stretched nanotube structure and were further seen to follow the surface curvatures induced by the stretching process.

The images shown in Figures 3-27, 3-28, and 3-29 strongly indicate the durability of the modified nanotube based freestanding structures as supporting platforms for NG108-15 cells. The positively charged polymer-wrapped nanotubes present on the surface of the freestanding structures illustrated in the figures are believed to form positively charged and hydrophobic contact area that facilitates the attachment of the cells. Moreover, these images indicated a strong differentiation of NG108-15 cells on the polymer-modified nanotube freestanding structures resulting from strong interaction

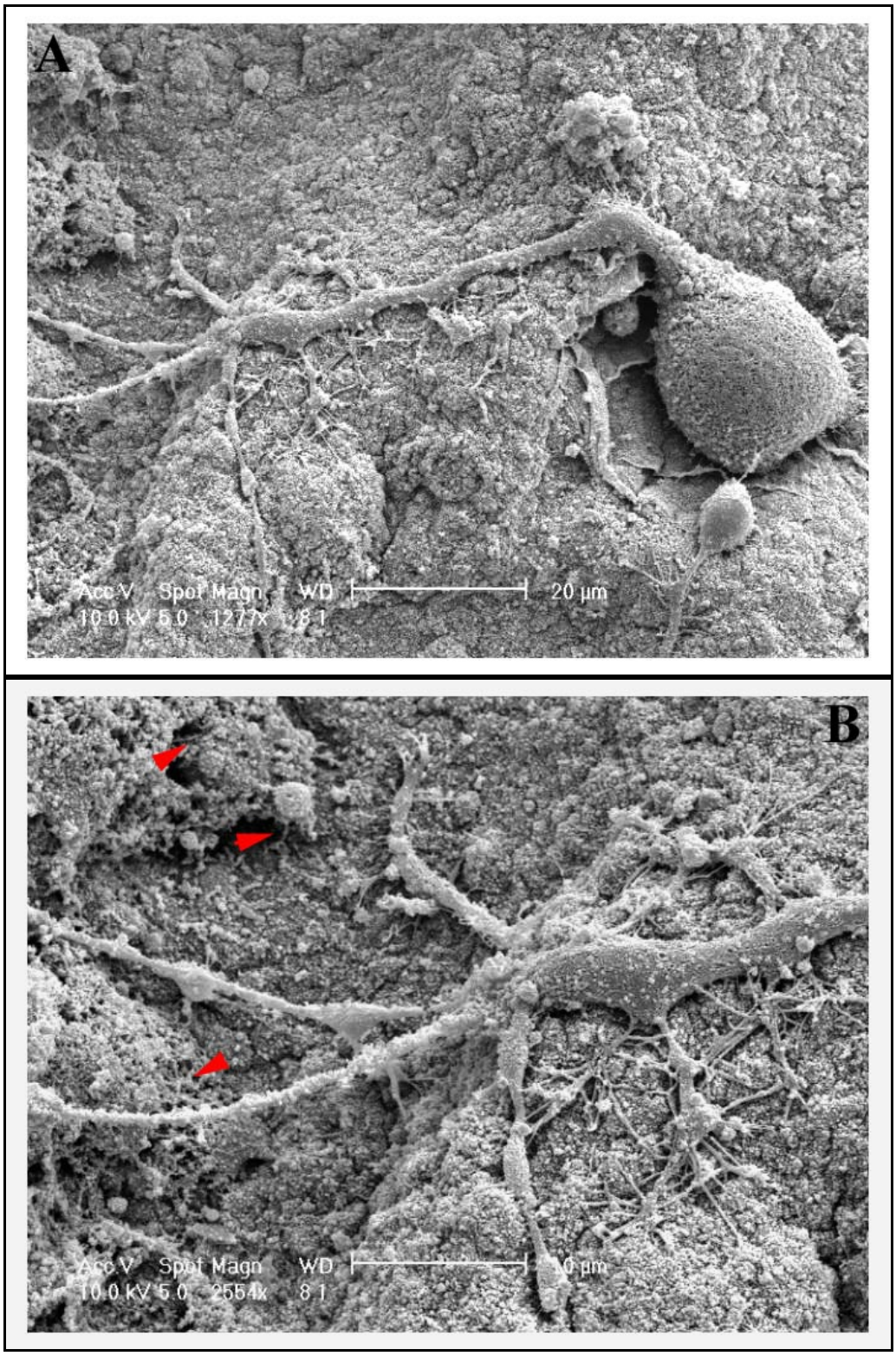

Figure 3-27. **(A)** Scanning electron micrograph of differentiated NG108-15 cell on the surface of freestanding structure of single-walled carbon nanotubes. **(B)** Higher magnification SEM image of the cell showing elaborated neurites and branches attaching to the surface of the nanotube structure. Arrowheads in B indicate the presence of exposed nanotubes on the surface. Scale bars: 20 µm in A and 10 µm in B.

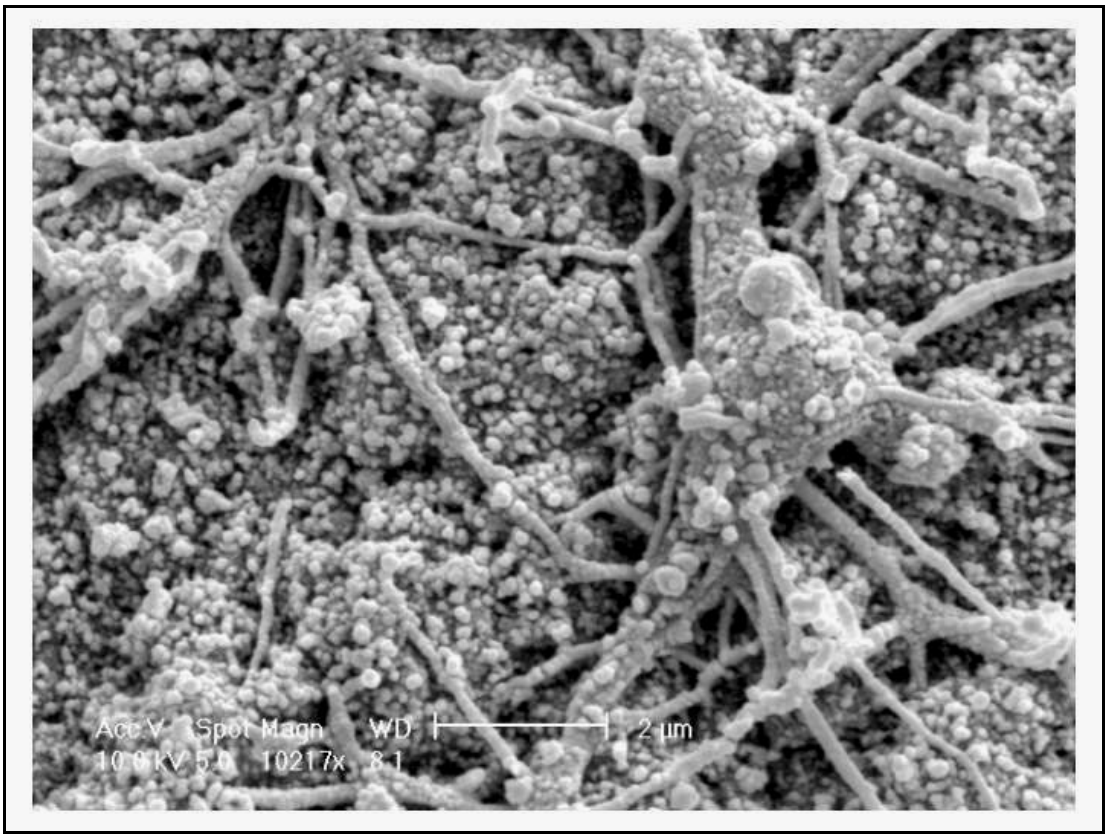

Figure 3-28. High-resolution SEM image showing enhanced differentiation of the cell shown in Figure 3-27. Scale bar: 2 μm.

between the cells and the surface. This interaction is essential requirement for nanotube-based structures to be used as external implants and neuronal repair devices. The dependence of the neurite outgrowth on the surface morphology is seen from the extension direction of the neurites that elongate along the morphology of the surface. These results are quite impressive and demonstrate, essentially, the possible utilization of modified nanotube based structures not only as extracellular implants and prostheses, but also as supporting platforms to guide neurite outgrowth and branching. They also demonstrate the possible use of modified nanotube structures as scaffolds for neurites regeneration and as platforms for neuronal communication and repair following neuronal

related injuries. The formed nanotube-based structures do not lack the mechanical strength. On the contrary, they posses high strength that exceeds the requirements for such type of applications. The measured tensile strength of the above illustrated freestanding structure of polymer-modified nanotubes was found to be 50-70 MPa and can even be engineered for ultimate strength. This favors the use of nanotubes over other materials for such sort of applications.

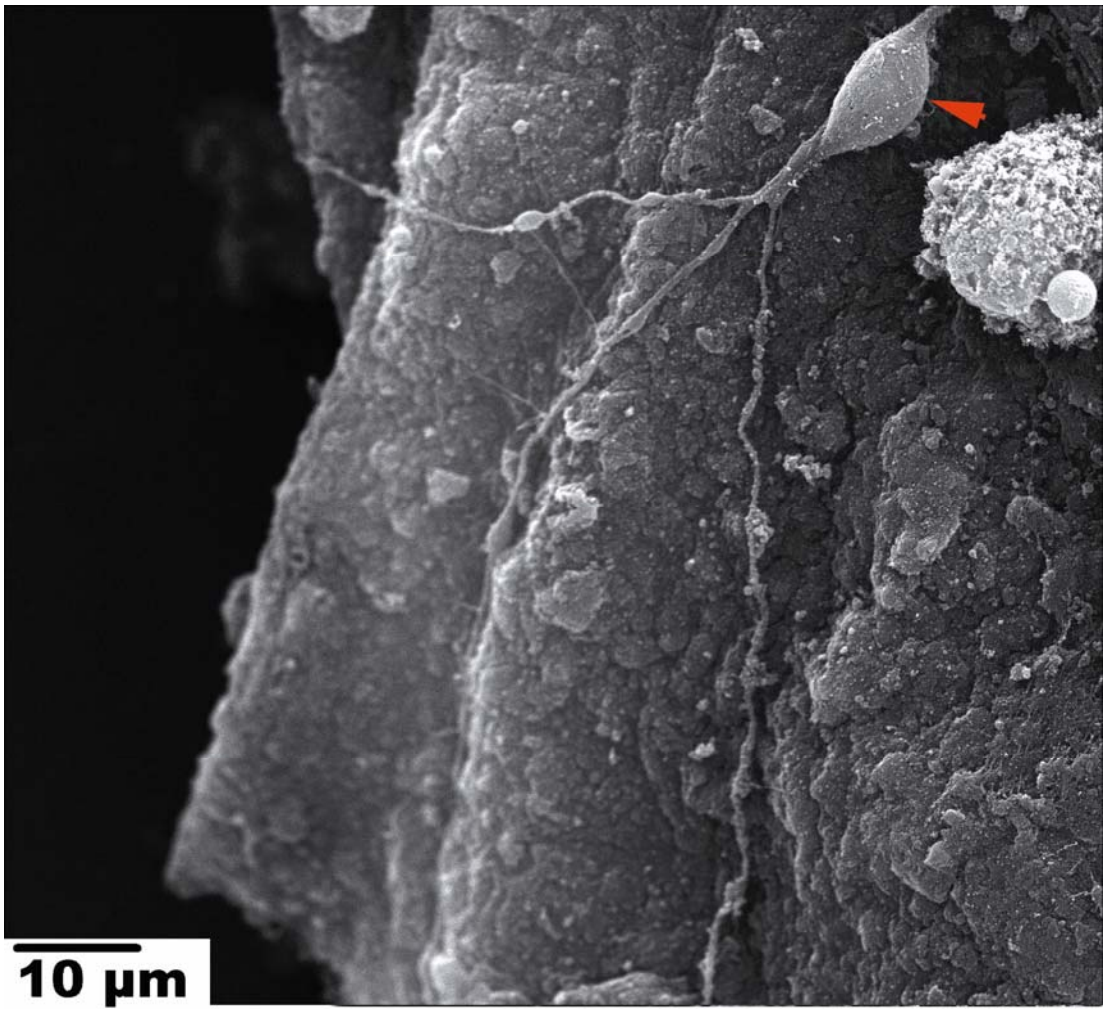

Figure 3-29. Scanning electron micrograph of differentiated NG108-15 cells (indicated with red arrowhead) extending long neurites along the existing morphological features of a stretched freestanding structure of nanotubes.

Stimulation of NG108-15 Hybrid Cells Using Conductive Nanotube Films

For nanotube-based structures, illustrated in the previous section, to be used as platforms for neuronal contacts, their ability to transduce and transmit neuronal signals is an essential requirement. This is demonstrated here, for the first time, where an actual communication between these man-made single-walled carbon nanotube materials and living cells was established. Utilizing the good electrical property of nanotubes, the conductivity of assembled modified nanotube LBL films was used to stimulate NG108-15 neuronal cells.

The layer-by-layer assembly affords the formation of conductive alternating layers of modified nanotubes and poly(acrylic acid) [172]. The inter-nanotube interactions within a single layer and between nanotubes in alternating layers, allows good contacts between nanotubes which are necessary for good transmission of electrical current. The conductivity of the assembled films is predicted to increase as more nanotube films are assembled due to the increase in the nanotube loading and consequently the increase in their contacts. To meet our goals, 30-LBL film of modified nanotubes (measured thickness of 316 nm) was prepared as a stimulation substrate. After annealing the assembled film at 100 ^{o}C for 1-hour, the conductivity of the film on glass substrate was 39.6 S.cm^{-1} at room temperature (Table 3-1). Annealing the nanotube LBL film at high temperatures is believed to increase the nanotube film conductivity [172,78]. This could be explained as a result of melting the amorphous carbon existing with the nanotubes which form resistive impurities to current conduction within the film. The conductivity of the assembled nanotubes film was seen to increase to 127 S.cm^{-1} (Table 3-1) for a film constructed on Indium-Tin Oxide (ITO) coated glass substrate. The measured

Table 3-1. Measured resistance and conductivity values of the substrates used in the electrophysiological measurements. The thickness of ITO coating as received from the source was 150 nm.

	Resistance	Conductivity
ITO Glass	15 Ω	444000 $S.cm^{-1}$
Nanotube Film on Glass	60-100 kΩ	39.6 $S.cm^{-1}$
Nanotube Film on ITO Surface	20-30 kΩ	127 $S.cm^{-1}$
Nanotube Film on Glass Inside Cells Chamber (Fig. 2-3 & 2-4)	25-35 kΩ	119 $S.cm^{-1}$

conductivity of the ITO substrates used in the study was 444000 $S.cm^{-1}$ (Table 3-1) and presumably the conductivity of the nanotube film is enhanced via the ITO conductivity when assembling the film on an ITO surface.

A special substrate design was used in order to, electrophysiologically, investigate the interface between the cells and the modified nanotube LBL film, as was shown in Figure 2-3. The nanotube LBL film was assembled on naked glass surface existing between two conductive ITO-coated surfaces. The ITO surfaces are used solely as conductive electrode-like surfaces where a constant potential difference can be applied and maintained across the nanotube LBL film via two silver wires that are connected directly to the ITO surfaces (see Figure 2-3). Cells were seeded and differentiated (in serum-free medium) for 5-7 days in a special chamber mounted on the substrate surface. In order to stimulate the cells exclusively via the conductive surface of the nanotube film only, the chamber was mounted on the nanotube LBL film assembled on the naked glass surface area. For maximum conduction through the substrate surface, the nanotube film was assembled in such a way to bridge the two ITO surfaces (see Figure 2-3). This configuration makes the whole substrate surface conductive with, however, different conductivity values at the different coated areas. In order to estimate the current conducted through this conductive surface, a simple model is suggested. The substrate

surface can be viewed as a number of resistors connected in series as sketched in Figure 3-30(inset). The resistance values of these resistors are as measured and illustrated in Table 3-1. The equivalent resistance value is 130030 Ω and is found by adding up the maximum resistance values (from Table 3-1) of the ITO surface, nanotube LBL film on ITO surface, and nanotube LBL film on glass surface in the arrangement shown in Figure 3-30-inset. This resistance is used to calculate the current values at different applied external voltages. The calculated current (on the order of nA) is predicted to be approximately the current passing through the substrate surface including the nanotube film.

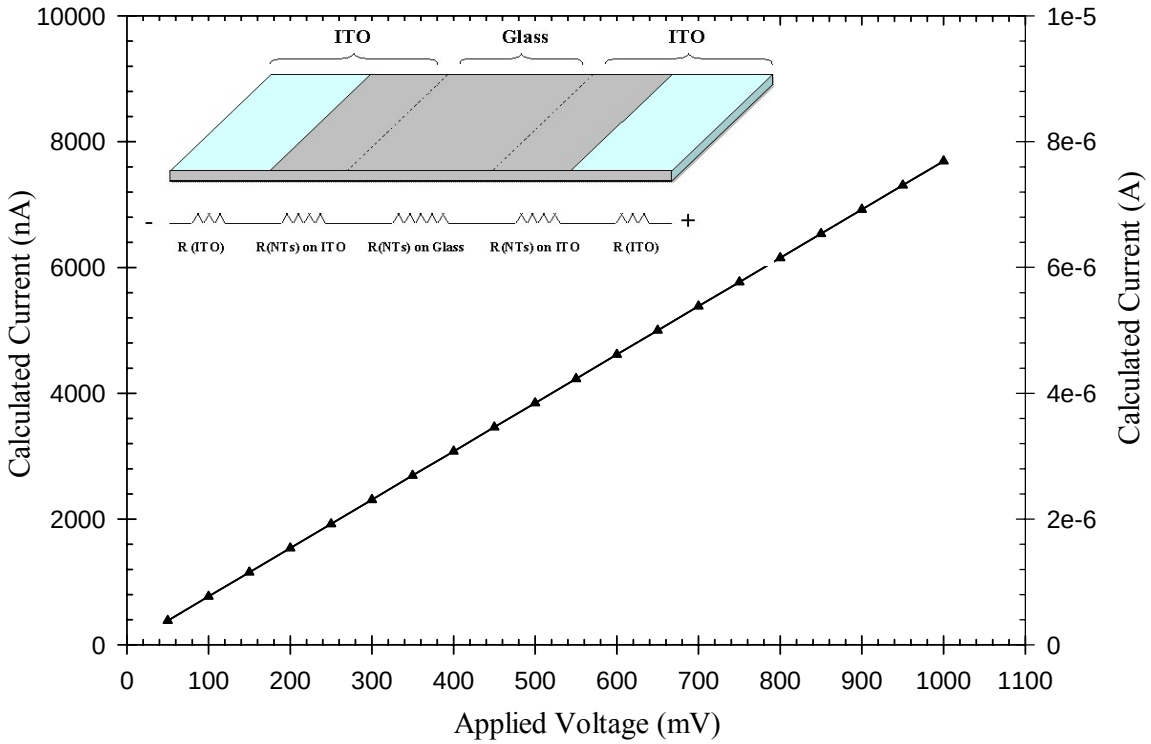

Figure 3-30. Calculated current that is predicted passing through the nanotube film and used to stimulate the NG108-15 cells. Calculations were based on assuming the various substrate coatings as resistors connected in series as shown in the inset. The equivalent resistance was 130030 Ω calculated by adding the maximum resistance values presented in the inset and shown in Table 3-1. The shaded gray area in the inset represents the assembled nanotube 30-LBL film.

The prepared conductive LBL film of the modified nanotubes was used to probe cells grown and differentiated on its surface. Electrophysiological measurements were conducted using the patch clamping technique. This technique, developed in 1976, is a well established and a proven method to register electrical activities taking place within the membrane of cells upon the excitation of that membrane [171]. The principle is based on forming a good seal between a patch of a cell membrane and a tip (1 μm diameter) of an extremely fine glass pipette that is in contact to an electrode (chloride silver) via conductive medium (usually KCl). A good contact, which holds the key to a successful recording of the membrane electrical activity, is usually achieved by applying brief suction to the pipette until a giga-seal is formed. This seal is characterized by the formation of resistance on the order of giga-ohm between the membrane and the electrode that no current can leak out of this seal. Currents flowing across the membrane can be then sensed using the electrode that transfers the signal to an amplifier and a recording system. A second electrode is typically connected to the amplifier and is immersed in the physiological medium as grounding electrode. The instant the pipette is impaled into the membrane and a contact is made, a potential value can be readily measured. This potential is the resting potential of the membrane resulting from the potential difference between the inside of the cell, which is naturally more negative, and the outside of the cell. For NG108-15 cells, this resting potential usually ranges from –35 mV to –65 mV and is mainly determined by the concentration of K^{+1} ions [173]. Any external electrical stimulation of the cells causes distortion of the ionic concentration across the cell membrane. This might lead to less negative membrane potential (membrane depolarization) causing the cell to elicit an action potential [142].

In our study, electrophysiological measurements were carried out in the whole cell

patch clamp configuration. In this configuration, the membrane patch is ruptured by the further application of suction into the pipette interior. This brings the pipette into direct contact with the cell interior with low resistance to current and diffusional flow. Measurements were carried out in the voltage clamp configuration where the potential difference between the cell and the pipette was held constant to -70 mV (which is close to the resting potential of the NG108-15 cells) by applying steady current through the pipette. This allowed the accurate detection of flowing currents through the whole cell membrane as a response to external stimulation.

Prior to stimulating the cells externally via conducting current through the nanotube film, their electrophysiological response was first examined through stimulation via the pipette electrode. Figure 3-31 shows representative current-voltage trace obtained from NG108-15 cells differentiated and attached on top of the assembled nanotube film. The top trace in the figure represents the current response of cells to a +20 mV voltage pulse step applied over 50 ms as shown in the bottom trace of the figure. At the instant the voltage is increased from its resting value at –70 mV to + 20 mV, a sharp spike is seen in the current trace indicating the current response, nearly 40 nA, of the cell to the sudden potential change. At the tail of this positive spike the current is seen to slightly rise then it remained steady over the 50 ms pulse period. This steady state is a result of no change occurring in the 20 mV voltage value over the 50 ms period. As the potential pulse is stepped down to –70 mV, a negative spike is seen followed by a negative tail current. This current behavior can be understood by imagining the cell membrane as a combination of a capacitor and a resistor connected together. Applying a voltage to the membrane causes an increase in its capacitance known as capacitive charging indicated by the observed positive current spike. When the applied voltage pulse is turned off, the

charged membrane starts to discharge through its resistance and the current response experiences a sharp decrease as indicated by the negative spike in the current trace shown in Figure 3-31. The observed positive rise in the current into a steady state is an indicative of some current activity taking place within the cell membrane which is most probably attributed to an outward current through the membrane. The opposite effect is seen when the voltage step is turned off where the current tail was seen to deflect down at the end of the negative spike tail (see Figure 3-31). This current-voltage trace strongly demonstrates the good response of the NG108-15 cells indicating that their membrane is electrically active and their current response is detectable. This was an essential step to establish before externally stimulating the cells via the conductive nanotube film.

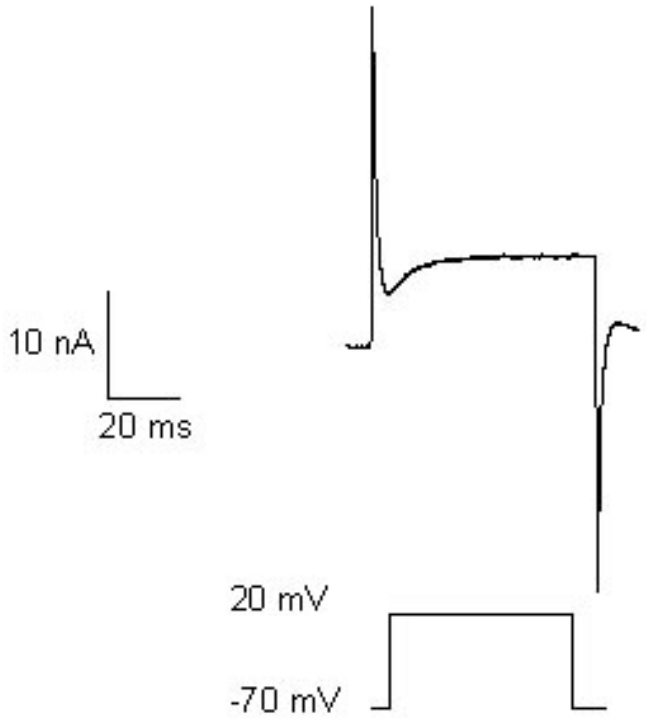

Figure 3-31. Representative current-voltage traces from NG108-15 cells differentiated on the surface of nanotube film in pipette electrode stimulation.

To demonstrate the possible stimulation of NG108-15 cells via solely the nanotube film, we probed cells adhered directly to the surface of the nanotube LBL film that is assembled on the naked glass surface (see Figure 2-3). For this purpose, an external potential was applied across the substrate holding the nanotube film in the arrangement discussed before (see Figure 2-3). This potential creates currents that are predicted to be stimulating the cells through the conductive nanotube film (Figure 3-30). Figure 3-32 shows three traces indicating current response of NG108-15 cells to various external potential values applied over 100 ms periods through the nanotube film. These currents were only measured from cells that exhibited induced differentiation, when viewed under the microscope, characterized by mainly the presence of long neurites extended from their membrane. The first noted observation from Figure 3-32 is the similar feature of the three traces to that trace shown in Figure 3-31. At three different applied voltage values namely 100, 500, and 1000 mV, an immediate sharp positive spike in the current trace is observed the instant the voltage is applied, which is an indicative of capacitive charging of the cells membrane. Discharging of the membrane capacitance is seen when the applied voltages are terminated as observed by the presence of the negative sharp spikes in the traces. These observations indicate that the cells are electrically active and respond to the electrical stimulation applied via the nanotube film.

Further examination of Figure 3-32 shows that the current traces at 500 mV and 1000 mV applied voltages exhibit slightly higher spikes than that at 100 mV. More interestingly, the current response at the tail of the positive spikes is seen to follow an up-rise that becomes more evident as the external voltage increases. This is clearly seen in the current signal of the 1000 mV applied voltage trace. These observations are considered as an evidence of the good electrical response of the cells to external

excitation through the nanotube film and indicate that more stimulation is established as higher voltage is applied. The obtained cells response is attributed to membrane activated channels. Stimulating the cell membrane via the nanotube film is believed to activate passive membrane channels that tend to leak current into the cell. This causes slight depolarization of the cell membrane as its potential becomes less negative. As a response, outward current channels, which are usually K^{+1} channels, get activated to hyperpolarize the cell as an attempt to restore the cell's natural equilibrium conditions bringing its potential to the resting value. These outward currents are detected by the penetrating pipette electrode and are believed to be causing the positive deflection in the current seen in Figure 3-32 near the tail of the positive spikes. The deflection is expected to be more evident at higher extrinsic voltages as more outward currents get activated and detected as was observed from the current-voltage trace at 1000 mV stimulating potential shown in Figure 3-32.

Activation of NG108-15 active membrane channels, which are usually Na^{+1} and Ca^{+2} channels, creates inward currents that induce strong depolarization (cell interior becomes less negative) of the cells. This maximal excitability of the cells leads to the firing of an action potential as a fast response of the cell to the strong depolarization. The occurrence of such action potential can be identified in the voltage response traces by noticing sudden increase in the potential (indicating strong depolarization) followed by long negative deflection in the voltage response over the stimulation period [173, 174]. In our case, the results do not indicate such membrane action potential even with high external stimulation. It is believed that the conductivity of the 30-LBL nanotube film is sufficient to electrically probe the cells to the threshold point necessary for generating action potentials. The estimated current conducted through the nanotube film inside the cells

chamber far exceeds the current values reported before to establish action potential within NG108-15 cells [166-167, 174]. Strong cells differentiation is crucial to cells excitability [142,173]. It is suggested that the absence of action potential here is related to the possibility that the cells did not exhibit the degree of differentiation to the point required for firing an action potential [174]. Possibly, the cells probed in our measurements were immature enough where the neuroblastomas did not completely develop into neurons. Nevertheless, It is of no major concern to us this absence of action potential in our nanotubes/cells interacting system since our main goal was achieved. That is mainly demonstrated from the observations of the possible stimulation of the cells via utilizing the conductivity of the nanotube LBL film which illustrates the electrical coupling between these cells and the modified single-walled carbon nanotubes as Figure 3-32 showed.

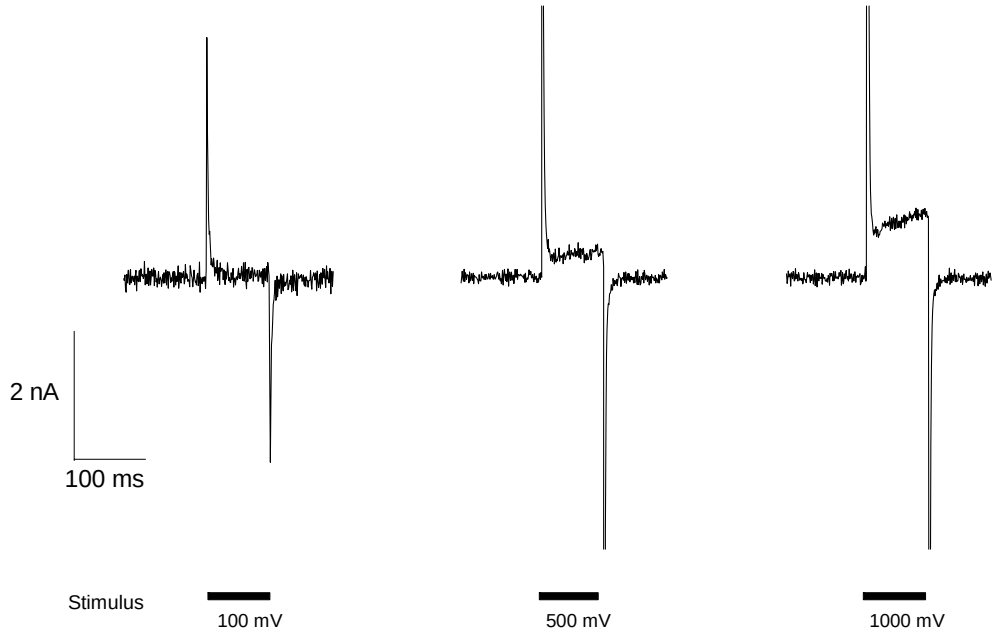

Figure 3-32. Traces indicating the current response of NG108-15 cells to three different external potential values, namely 100, 500, and 1000 mV. The voltages were applied across the nanotube LBL film over 100 ms time periods. At least 17 cells were probed for the obtained results.

To verify that the above-illustrated stimulation of cells is resulting from actual electrical coupling between the modified nanotube assembled LBL film and the NG108-15 cells adhered to it, electrophysiological measurements were also conducted on cells not directly in contact with the nanotube film. These cells were grown and differentiated on the surface of naked glass and were in contact with the nanotube film via the electrophysiological medium only. This was achieved by utilizing the substrate design that was illustrated in Figure 2-4. The cell chamber was mounted on the substrate surface in such a way that half of the chamber located on the assembled nanotube film whereas the other half located on the treated naked glass surface. Only those cells adhered to the glass surface and not in contact with the nanotube film were used as control cells. Stimulation of those cells was established only through the medium. The application of external potential across the nanotube film creates electrical current through the nanotube film and into the conductive electrophysiological medium to the cells stimulating their membrane. The electrical response from these cells was compared to that of cells stimulated directly through the nanotube film.

We first studied the cells electrical activity in the absence of external voltage applied through the nanotube film but via the application of various voltage pulses through the patch clamp pipette and measuring the corresponding current responses. The IV-characteristics of cells adhered to glass and those adhered to nanotube film is shown in Figure 3-33. For accurate current measurements, only cells that showed at least 75 MΩ membrane input resistance were used for the measurements. Both groups of cells, those adhered to the glass surface and those adhered to the nanotube film surface, with relatively similar input resistances (indicated in the figure), expressed interesting electrical response. For both groups of cells, the IV-curves were seen crossing the

voltage axis at around –70 mV which corresponds to the adjusted membrane resting potential with zero current response at this point (Figure 3-33). No difference in the current behavior below this point was noticed. As the voltage is varied above its steady value of –70 mV, the inside of the cell becomes less negative causing the depolarization of the membrane. Outward currents are thus detected explaining the increase in the current response to the increase in the voltage (Figure 3-33). The measured current values were seen higher for cells adhered to the nanotube surface than for cells on glass which was mainly evident at high voltage values in the 20-100 mV range. Higher current responses are expected to result from more induced cells stimulation. This seems to be the case here where cells adhered to the surface of the modified naotube LBL film are seen to exhibit more electrical response than those adhered to the glass surface. Similar observations were also obtained when the cells were stimulated externally via the application of various voltages across the substrate as shown in Figure 3-34. The measured outward current response to the extrinsic voltage was seen to increase as the voltage increased. Greater current values were measured from cells adhered to the nanotube film than from cell attached to the glass surface, indicating better cells stimulation through the direct coupling with the nanotube film rather than through the conductive medium.

Figures 3-33 and 3-34 presented evidence on the difference in the electrical response between cells attached to the surface of the nanotube LBL film and those attached to the glass surface. Both in the absence and presence of external voltage stimulation through the substrate, results showed that higher current response is detected from cells when they are grown on the nanotube film surface than when they are grown on the glass surface (Figure 3-33). These results propose that cells are healthier and exhibit better electrical

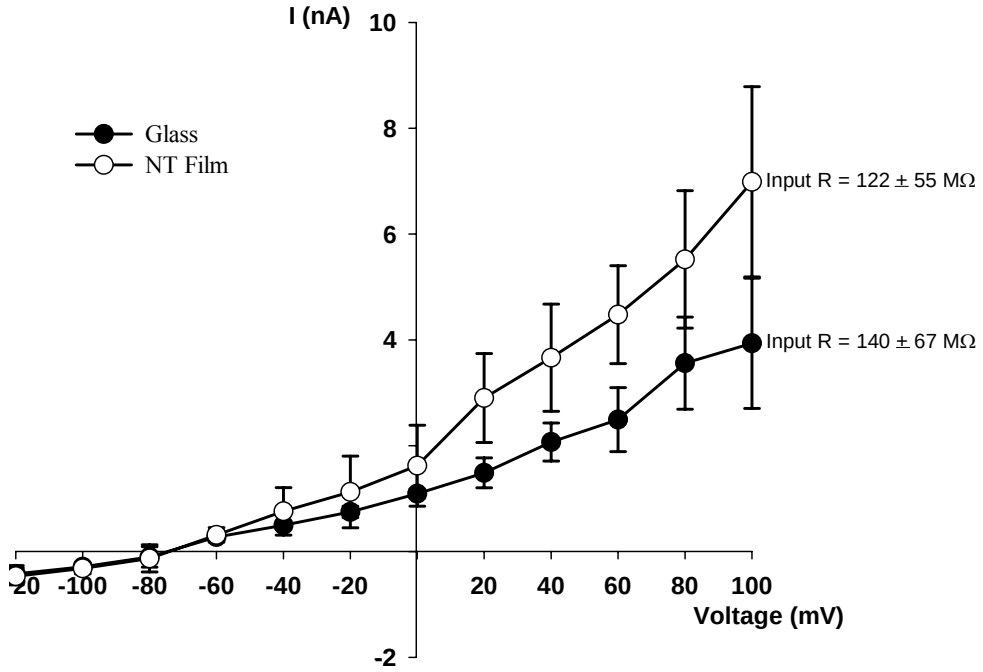

Figure 3-33. IV-characteristics of NG108-15 cells when stimulated intrinsically through the patch clamp pipette on the surface of glass and nanotube film. At least 17 cells were probed for the obtained results.

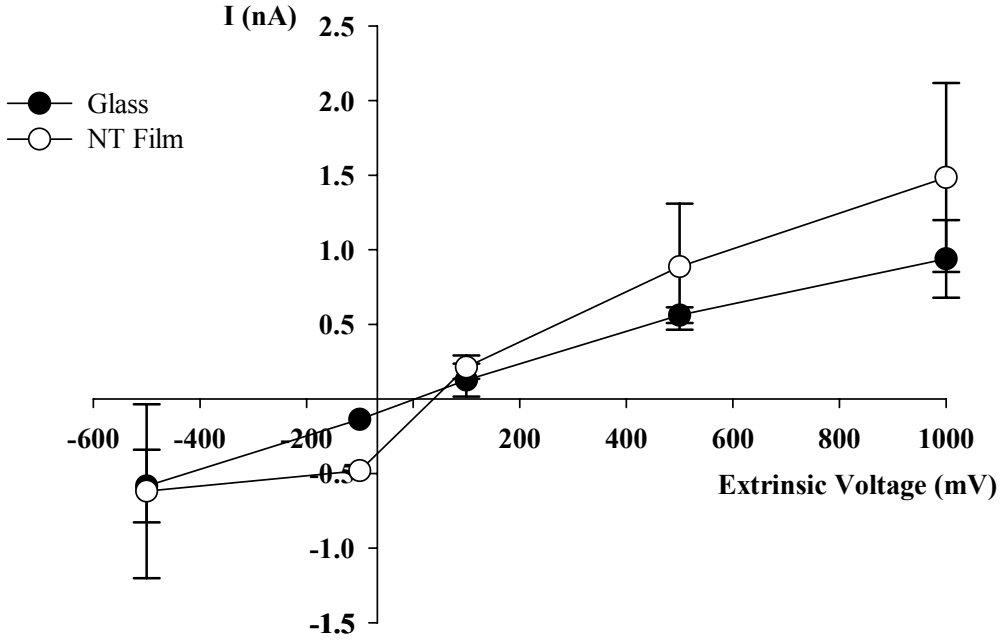

Figure 3-34. IV-curve comparison of NG108-15 cells stimulated externally on the surface of glass and nanotube film. At least 17 cells were probed for the obtained results.

excitability when grown on the surface of the nanotube based substrate than on glass only. The fact that more stimulation of cells is established when cells are excited externally via the nanotube film rather than the conductive medium (Figure 3-34) suggests that the observed cells electrical response to the externally applied voltage is an actual response to stimulation via electric conduction through the nanotube film. Better cells excitability and stimulation via the conductive layers of modified nanotube film can be attributed to better cells differentiation which is crucial for higher membrane excitability [142]. We have observed before, from Figures 3-24 and 3-25, that cells attached to the surface of modified nanotube LBL films exhibit better differentiation than cells plated on culture dish [175]. It is believed that this leads to the development of more neuron-like cells with more active membrane channels when adhered to the nanotube LBL film. Therefore, those cells are expected to show more electrical activity and excitability when stimulated externally through the conductive nanotube LBL film, as we have seen.

Our electrophysiological findings propose, for the first time, a possible electrical coupling between the polymer-modified nanotubes and NG108-15 cells. Conducting electrical signals between nanotubes and the cells can be proven important for synaptic formation between these neuronal cells or between these cells and other type of cells such as muscle cells on the surface of modified nanotube platforms [176]. We have demonstrated before the possibility of using modified nanotube freestanding structures as reinforcing materials to support and guide neurite outgrowth making them potential candidates as extracellular implants. The fact that these structures possess good electrical conductivity adds a great advantage to their use for the desired applications. Employing modified nanotube-based structures as mechano-devices for treatments of neuronal

related injuries requires that these devices be capable of conducting neuronal signals after the implanting process. Our results show promising future for potential utilization of such modified single-walled carbon nanotube layer-by-layer based structures in biomedical applications.

CHAPTER IV

FINAL REMARKS

Conclusions

Understanding the nature of interfacing inorganic materials, such as single-walled carbon nanotubes, with living cells and tissues is very crucial for the successful utilization of these materials in biological and biomedical applications. This study aimed, ultimately, at presenting a scientific demonstration of the possible utilization of the mechanical and electrical properties of single-walled carbon nanotubes in constructing high quality novel structures that can be useful as supporting and stimulating materials for neuronal growth and networking of the neuronal model cells NG108-15 culture line.

Achieving the intended goals of this study depended exclusively on obtaining stable suspensions of nanotubes in aqueous solution. This was achieved by engineering a designated hydrophobic poly(N-cetyl-4-vinylpyridinium bromide-*co*-N-ethyl-4-vinylpyridinium bromide-*co*-4-vinylpyridine) polymer whose hydrophobic and positively charged hydrophilic structural makeup served our purpose well in both dispersing and stabilizing the nanotubes and at the same time forming suitable platform for cells attachment. The first part of the study was dedicated to characterizing the polymer-modified nanotubes. Many techniques such as high-resolution transmission electron

microscopy (HRTEM), atomic force microscopy (AFM), Raman spectroscopy, and UV/Vis/NIR absorption spectroscopy have proven very powerful in gaining valuable insights about the polymer/nanotube system. Results from these techniques have led us to conclude that the stability of nanotubes and their dispersion depends on the way the polymer attaches to the nanotube surface. HRTEM showed that the polymer forms a uniform layer around the nanotube surface. The size of this coating was also determined by HRTEM supported by AFM. Absorption measurements indicated that the electronic structure of the nanotubes was preserved after the modification as identified by observing no changes in the spectral features of the absorption bands of transitions between van Hove singularities. Raman spectroscopy gave further valuable insights about the mode of polymer interaction with the nanotubes. An upshift in the spectral positions of the radial breathing modes and the tangential G-band of nanotubes was noticed after the incorporation of the polymer with the nanotubes. A narrowing in the G-band spectral width, which is an indicative of nanotubes debundling, was also noticed in the polymer/nanotubes Raman spectrum. All these microscopic and spectroscopic observations combined had led us to conclude that the polymer attaches to the nanotubes in a non-covalent manner where its hydrophobic groups wrap strongly around the nanotubes in elongated fashion separating nanotubes bundles whereas the hydrophilic groups of the polymer remain on the surface exposing the nanotubes to the aqueous hydrophilic medium [54].

Obtaining stable dispersion of nanotubes facilitated the further processing of nanotubes. Layer-by-layer assembly was adopted in the present study to construct composites of polymer modified nanotube thin films and freestanding structures. Raman signature of single-walled carbon nanotubes was still observable after the incorporation

of the modified nanotubes into forms of thin film structures. This study has yet proven the advantageous usefulness and effectiveness of the layer-by-layer assembly in designing nanotube structures with controlled mechanical and electrical properties and at the same preserving their identity.

The issue of single-walled carbon nanotubes biocompatibility and impact on living systems is an extremely important issue to be addressed and has found very limited research effort in literature [175]. One of the integral goals of this study was to address this subject utilizing mainly the two powerful confocal and scanning electron microscopic techniques. One of the major findings of this research work was our observation of that more than %94 of NG108-15 hybrid cells were seen to remain viable on the surface of the modified nanotube LBL films even after 10-days incubation. The cells were also seen to exhibit their natural processes of division, proliferation, and differentiation on the surface of various nanotube films of different roughness and thickness. These results directed us to the important conclusion that the polymer-modified single-walled carbon nanotubes and their assembled LBL structures are biocompatible and support the long-term viability and survival of the neuronal NG108-15 hybrid cells. Additionally, these nanotube based LBL films can be used as permissive substrates for cell culture and neuronal growth [175].

This study confirmed the role played by culture substrates surface properties in determining the degree of cells differentiation. Neuronal NG108-15 cells were seen to exhibit more induced differentiation, characterized by more neuronal branching and longer neurites length, on the surface of the positively charged 1-, 5-, and 10-LBL films compared to their differentiation on the surface of negatively charged culture dish. This concludes that substrates coated with LBL layers of the positively charged

polymer/nanotube composites can be used as more favorable substrates for cell culture over commonly used negatively charged culture dishes. The presence of the positively charged coating, imparted by the dispersing polymer, on the surface of the nanotubes was concluded to play the major role in promoting better neuronal outgrowth and elaboration on the nanotube films. Surface roughness and the thickness of the assembled LBL films were also proposed to induce slight effect on the process of neurites branching. Cells adhered to a smooth surface, presented by the 1-LBL film, were seen to exhibit more neuronal elaboration than cells adhered to a film with a rough surface and a thick coating (approximately 250-300 nm thickness), presented by the 10-LBL film. These results propose the possibility of constructing structural composites of modified single-walled carbon nanotubes with optimized surface properties for maximal neuronal growth and differentiation.

This study presented, for the first time, the possible utilization of freestanding structures of modified single-walled carbon nanotube as supporting platforms for neuronal growth. NG108-15 cells were seen to attach freely to the surface of the freestanding structure. They were also seen to exhibit induced differentiation characterized by extending long neurites that branch into many neuronal processes that were seen anchored to the surface of the formed nanotube structure. Surface features and morphological texture induced by stretching the nanotube freestanding structure were seen to guide neurites elaboration and outgrowth [175]. Such formed freestanding structures of modified single-walled carbon nanotubes possess high mechanical strength (70 MPa tensile strength) that makes them attractive as reinforcing structures. The flexibility, non-biodegradability, inertness, and durability of single-walled carbon nanotubes all add extra advantages to such materials over other currently used materials.

Based on our observations, nanotube-based nanodevices can soon be engineered with optimized mechanical and functional properties to be used as useful devices in tissue engineering and as external implants and prostheses. Furthermore, such devices can be used as platforms for neurites regeneration and repair following neuronal related injuries such as spinal cord injuries or brain injuries.

One very important possible application of single-walled carbon nanotube based structures was demonstrated in the last part of this study. Layer-by-layer assembled films of polymer-modified single-walled carbon nanotubes were demonstrated, for the first time, as conductive substrates for neuronal stimulation [177]. In the voltage patch clamp configuration, electrical response from NG108-15 neuronal cells was measured as a function of externally applied voltage through the nanotube films. Such stimulation was seen to partially depolarize the cells and activate outward currents through the cells membrane. Better cells differentiation on the nanotube film was concluded to contribute to better cell membrane excitability. More current response was observed from cells stimulated directly through the nanotube film than from cells adhered to glass surface and stimulated through the conductive physiological medium [177]. These observations indicated strongly an established electrical communication between the modified single-walled carbon nanotubes and living NG108-15 neuronal cells. Interfacing nanotubes with neurons can be very essential for neuronal circuitry analysis. Our results indicate a great promise of nanotubes to be incorporated into the design of nanodevices with maximized electrical properties and high sensitivity to be used as stimulating and sensing devices of neuronal signals. Moreover, such devices can be used to promote neuronal communication and establish synaptic contacts between neurons.

We believe that the results obtained from this study had weakened the boundaries

between inorganic materials and living organisms. It holds a promising scientific work for a promising future of single-walled carbon nanotubes. The output of the study is considered very important and very essential for further utilization of nanotubes and their corresponding structures in biomedical and biological applications.

Future Aspects

Based on the present study follows many possible future studies that will utilize the present system or similar ones for various biological and biomedical applications. To further address the issue of single-walled carbon nanotubes biocompatibility and toxicity, the viability of cells can be examined following their growth and differentiation on the surface of nanotube structures. This could provide insights about the health impacts and the long-term effect of nanotube-based implants on cells and tissues after such implants are removed from the body. Moreover, methods such as thermal annealing (at elevated temperatures) can be applied to eliminate the polymer monolayer coating on the nanotubes following their processing into multilayers of LBL films. Such composites can be then incubated with the cells and the growth and differentiation of cells can be examined to give direct information on the biocompatibility of single-walled carbon nanotubes in direct interface with the living cells.

One important future aspect of the present study is the investigation of single-walled carbon nanotubes as sensing materials of neuronal signaling. Utilizing their good electrical conductivity, single-walled carbon nanotubes can be used as based materials in transistor devices to sense the neuronal and synaptic contact signals. Such devices can be

useful in sensing signals from tumor infected brains which can help the early detection of cancerous cells in the brain. Single-walled carbon nanotubes can also be used as infrastructures of actuators that can be used to convert electrical energy into mechanical energy. This can be useful in fabricating artificial muscles based on nanotubes.

In the future, devices based on single-walled carbon nanotubes can be utilized as extracellular implants, prostheses, and orthopedic devices. For example, layer-by-layer assembly can be utilized to deposit and arrange single-walled carbon nanotubes in a specific pattern to form structural matrices that can be used to control the neuronal outgrowth and regeneration, which is very essential for treatments after neuronal injuries. It can also be possible soon to fabricate nanodevices based on single-walled carbon nanotubes with novel mechanical, electrical, and functional properties that can be used for various biological and biomedical applications, in general. Studies similar to the present one can be conducted on a wide range of culture cells including real neurons, cancer cells, and human cells. *In-vivo* investigations of modified biocompatible single-walled nanotubes/cells interactions represent another important route. In the long term, all these potential studies will help uncover some secrets of the functioning mechanism controlling living systems and can provide scientific protocols for injuries treatment and diseases cure.

REFERENCES

1. H. W. Kroto, J. R. Heath, S. C. O'Brein, R. F. Curl, r. E. Smalley. "C60: Buckminsterfullerene." Nature, Vol. 318, 162, 1985.

2. S. Iijima. "Helical Microtubules of Graphitic Carbon." Nature, Vol. 354, 56, 1991.

3. S. Iijima, T. Ichihashi. "Single-Shell Carbon Nanotubes of 1-nm Diameter." Nature, Vol. 363, 603, 1993.

4. D. S. Bethune, C. H. Kiang, M. S. De Vries, G. Gorman, R. Savoy, J. Vazquez, R. Beyers. "Cobalt-Catalysed Growth of Carbon Nanotubes with Single-Atomic-Layer Walls." Nature, Vol. 363, 605, 1993.

5. D. L. Roger, S. R. Goode, E. E. Mercer. Chemistry: Principles and Practice. Saunders College Publishing, Orlando, Florida, 1993.

6. **(A)** R. Saito, G. Dresselhaus, M. S. Dresselhaus. Physical Properties of Carbon Nanotubes. Imperial College Press, London, 1998; **(B)** M. S. Dresselhaus, G. Dresselhaus, P. C. Eklund. Science of Fullerenes and Carbon Nanotubes. Academic Press, Inc., San Diego, California, 1996.

7. P. C. Eklund, J. M. Holden, R. A. Jishi. "Vibrational Modes of Carbon Nanotubes; Spectroscopy and Theory." Carbon, Vol. 33, 959, 1995.

8. J. W. Mintmire, C. T. White. "Electronic and Structural Properties of Carbon Nanotubes." Carbon, Vol. 33, 893, 1995.

9. N. Hamada, S. Sawada, A. Oshiyama. "New One Dimensional Conductors: Graphitic Microtubules." Physical Review Letters, Vol. 68, 1579, 1992.

10. R. Saito, M. Fujita, G. Dresselhaus, M. S. Dresselhaus. "Electronic Structure of Chiral Graphene Tubules." Applied Physics Letter, Vol. 60, 2204, 1992.

11. J. W. Mintmire, B. I. Dunlap, C. T. White. "Are Fullerene Tubules Metallic." Physical Review Letters, Vol. 68, 631, 1992.

12. S. Reich, C. Thomsen. "Chirality Dependence of the Density-of-States Singularities in Carbon Nanotubes." Physical Review B, Vol. 62, 4273, 2000.

13. J. Wildoer, L. Venema, A. Rinzler, R. Smalley, C. Dekker. "Electronic Structure of Atomically Resolved Carbon Nanotubes." Nature, Vol. 391, 59, 1998.

14. M. S. Dresselhaus, G. Dresselhaus, R. Saito. "Physics of Carbon Nanotube." Carbon, Vol. 33, 883, 1995.

15. M. S. Dresselhaus, G. Dresselhaus, R. Saito. "Carbon Fibers Based on C60 and their Symmetry." Physical Review B, Vol. 45, 6234, 1992.

16. A. Thess, P. Nikolaev, H. Dai, P. Petit, J. Robert, C. Xu, Y. Lee, S. Kim, A. Rinzler, D. Colbert, G. Scuseria, D. Tomanek, J. fischer, R. Smalley. Science, Vol. 273, 483, 1996.

17. C. Journet, W. Maser, P. Bernier, A. Loiseau, M. Delachapelle, S. Lefrant, P. Deniard, R. Lee, J. Fischer. Nature, Vol. 388, 756, 1997.

18. J. H. Hafner, M. J. Bronikkowski, B. R. Azamian, P. Nikolaev, A. G. Rinzler, D. T. Colbert, K. A. Smith, R. E. Smalley. "Catalytic Growth of Single-Wall Carbon Nanotubes from Metal Particles." Chemical Physics Letters, Vol. 296, 195, 1998.

19. P. Nikolaev, M. Bronikowski, R. Bradley, F. Rohmund, D. Colbert, K. Smith, R. Smalley. "Gas-Phase Catalytic Growth of Single-Walled Carbon Nanotubes from Carbon Monoxide." Chemical Physics Letters, Vol. 313, 91, 1999.

20. M. Endo, K. Takeuchi, K. Kobori, K. Takahashi, H. Kroto, A. Sarkar. "Pyrolytic Carbon Nanotubes from Vapor-Grown Carbon Fibers." Carbon, Vol. 33, 873, 1995.

21. E. Dujardin, T. W. Ebbesen, A. Krishnan, M. J. Treacy. "Purification of Single-Shell Nanotubes." Advanced Materials, Vol. 10, 611, 1998.

22. L. Vaccarini, C. Goze, R. Aznar, V. Micholet, P. Bernier. "Purification Procedure of Carbon Nanotubes." Synthetic Metals, Vol. 103, 2492, 1999.

23. A. C. Dillon, T. Gennett, K. M. Jones, J. L. Alleman, P. A. Parilla, M. J. Heben. "A Simple and Complete Purification of Single-Walled Carbon Nanotube Materials." Advanced Materials, Vol. 11, 1354, 1999.

24. J. Chen, M. A. Hamon, H. Hu, Y. Chen, A. M. Rao, P. C. Eklund, R. C. Haddon. "Solution Properties of Single-Walled Carbon Nanotubes." Science, Vol. 282, 95, 1998.

25. A. Kukovecz, C. Kramberger, M. Holzinger, H. Kuzmany, J. Schalko, M.

Mannsberger, A. Hirsch. "On the Stacking Behavior of Functionalized Single-Wall Carbon Nanotubes." Journal of Physical Chemistry B, Vol. 106, 6374, 2002.

26. H. Peng, L. B. Alemany, J. L. Margrave, V. N. Khabashesku. "Sidewall Carboxylic Acid Functionalization of Single-Walled Carbon Nanotubes." Journal of the American Chemical, Vol. 125, 15174, 2003.

27. H. Hu, B. Zhao, M. E. Itkis, R. C. Haddon. "Nitric Acid Purification of Single-Walled Carbon Nanotubes." Journal of Physical Chemistry B, Vol. 107, 13838, 2003.

28. J. Liu, A. G. Rinzler, H. Dai, J. H. Hafner, R. K. Bradley, P. J. Boul, A. Lu, T. Iverson, K. Shelimov, C. B. Huffman, F. R. Macias, Y. S. Shon, T. R. Lee, D. T. Colbert, R. E. Smalley. "Fullerene Pipes." Science, Vol. 280, 1253, 1998.

29. K. Tohji, H. Takahashi, Y. Shinoda, N. Shimizu, B. Jeyadevan, I. Matsuoka, Y. Saito, A. Kasuya, S. Ito, Y. Nishina. "Purification Procedure for Single-Walled Nanotubes." Journal of Physical Chemistry B, Vol. 101, 1974, 1997.

30. J. Moon, K. An, Y. Lee, Y. Park, D. Bae, G. Park. "High-Yield Purification Process of Singlewalled Carbon Nanotubes." Journal of Physical Chemistry B, Vol. 105, 5677, 2001.

31. J. L. Zimmerman, R. K. Bradley, C. B. Huffman, R. H. Hauge, J. L. Margrave. "Gas-Phase Purification of Single-Walled Carbon Nanotubes." Chemistry of Materials, Vol. 12,, 1361, 2000.

32. C. A. Furtado, U. J. Kim, H. R. Gutierrez, L. Pan, E. C. Dickey, P. C. Eklund. "Debundling and Dissolution of Single-Walled Carbon Nanotubes in Amide Solvents." Journal of the American Chemical Society, Vol. 126, 6095, 2004.

33. J. Chen, A. M. Rao, S. Lyuksyutov, M. E. Itkis, M. A. Hamon, H. Hu, R. W. Cohn, P. C. Eklund, D. T. Colbert, R. E. Smalley, R. C. Haddon. "Dissolution of Full-Length Single-Walled Carbon Nanotubes." Journal of Physical Chemistry B, Vol. 105, 2525, 2001.

34. L. Zhang, V. U. Kiny, H. Peng, J. Zhu, Rui F. Lobo, J. L. Margrave, V. N. Khabashesku. "Sidewall Functionalization of Single-Walled Carbon Nanotubes with Hydroxyl Group-Terminated Moieties." Chemistry of Materials, Vol. 16, 2055, 2004.

35. C. A. Dyke, J. M. Tour. "Unbundled and Highly Functionalized Carbon Nanotubes from Aqueous Reactions." Nano Letters, Vol. 3, 1215, 2003.

36. C. A. Dyke, J. M. Tour. "Solvent-Free Functionalization of Carbon Nanotubes." Journal of the American Chemical Society, Vol. 125, 1156, 2003.

37. S. Qin, D. Qin, W. T. Ford, J. E. Herrera, D. E. Resasco, S. M. Bachilo, B. Weisman. "Solubilization and purification of Single-Wall Carbon Nanotubes in Water by In-Situ Radical Polymerization of Sodium 4-Styrenesulfonate." Macromolecules, Vol. 37, 3965, 2004.

38. H. Hu, B. Zhao, M. A. Hamon, K. Kamaras, M. E. Itkis, R. C. Haddon. "Sidewall Functionalization of Single-Walled Carbon Nanotubes by Addition of Dichlorocarbene." Journal of the American Chemical Society, Vol. 125, 14893, 2003.

39. J. L. Bahr and J. M. Tour. "Covalent Chemistry of Single-Walled Carbon Nanotubes." Journal of Materials Chemistry, Vol. 12, 1952, 2002.

40. S. Niyogi, M. A. Hamon, H. Hu, B. Zhao, P. Bhowmik, R. Sen, M. E. Itkis, R. C. Hadon. "Chemistry of Single-Walled Carbon Nanotubes." Accounts of Chemical Research, Vol. 35, 1105, 2002.

41. M. S. Strano, V. C. Moore, M. K. Miller, M. J. Allen, E. H. Haroz, C. Kittrell, R. H. Hauge, R. E. Smalley. "The Role of Surfactant Adsorption during Ultrasonication in the Dispersion of Single-Walled Carbon Nanotubes." Journal of Nanoscience and Nanotechnology, Vol. 3, 81, 2003.

42. V. C. Moore, M. S. Strano, E. H. Haroz, R. H. Hauge, R. E. Smalley. "Individually Suspended Single-Walled Carbon Nanotubes in Various Surfactants." Nano Letters, Vol. 3, 1379, 2003.

43. J. Chen, H. Liu, W. Weimer, M. D. Halls, D. H. Waldeck, G. C. Walker. "Noncovalent Engineering of Carbon Nanotube Surfaces by Rigid, Functional Conjugates Polymers." Journal of the American Chemical Society, Vol. 124, 9034, 2002.

44. A. Star, Y. Liu, K. Grant, L. Ridvan, J. Stoddart, D. Steuerman, M. R. Diehl, A. Boukai, J. R. Heath. "Noncovalent Side-Wall Functionalization of Single-Walled Carbon Nanotubes." Macromolecules, Vol. 36, 553, 2003.

45. B. Tang, H. Xu. "Preparation, Alignment, and Optical Properties of Soluble Poly(Phenylacetylene)-Wrapped Carbon Nanotubes." Macromolecules, Vol. 32, 2569, 1999.

46. M. J. O'Connell, P. Boul, L. M. Ericson, C. Huffman, Y. Wang, E. Haroz, C. Kuper, J. Tour, K. D. Ausman, R. E. Smalley. "Reversible Water-Solubilization of Single-Walled Carbon Nanotubes by Polymer Wrapping." Chemical Physics Letters, Vol. 342, 265, 2001.

47. A. Star, J. F. Stoddart, D. Steuerman, M. Diehl, a. Boukai, E. W. Wong, X. Yang, S. Chung, H. Choi, J. R. Heath. "Preparation and Properties of Polymer-Wrapped Single-Walled Carbon Nanotubes." Angew. Chem. Int. Ed., Vol. 40,

1721, 2001.

48. A. B. Dalton, C. Stephan, J. N. Coleman, B. McCarthy, P. M. Ajayan, S. Lefrant, P. Bernier, W. J. Blau, H. J. Byrne. "Selective Interaction of a Semiconjugated Organic Polymer with Single-Wall Nanotubes." Journal of Physical Chemistry B, Vol. 104, 10012, 2000.

49. A. Carrillo, J. A. Swartz, J. M. Gamba, R. S. Kane, N. Chakrapani, B. Wei, P. M. Ajayan. "Noncovalent Functionalization of Graphite and Carbon Nanotubes with Polymer Multilayers and Gold Nanoparticles." Nano Letters, Vol. 3, 1437, 2003.

50. R. S. Cohen, Y. Kalisman, E. Roth, R. Rozen. "Generic Approach for Dispersing Single-Walled Carbon Nanotubes: The Strength of a Weak Interaction." Langmuir, Vol. 20, 6085, 2004.

51. M. Chapelle, C. Stephan, T. P. Nguyen, S. Lefrant, C. Journet, P. Bernier, E. Munoz, A. Benito, W. K. Maser, M. T. Martinez, G. F. Fuente, T. Guillard, G. Flamant, L. Alvarez, D. Laplaze. "Raman Characterization of Single-Walled Carbon Nanotubes and PMMA-Nanotubes Composites." Synthetic Metals, Vol. 103, 2510, 1999.

52. C. Stephan, T. P. Nguyen, M. Chapelle, S. Lefrant, C. Journet, P. Bernier. "Characterization of Single-Walled Carbon Nanotubes-PMMA Composites." Synthetic Metals, Vol. 108, 139, 2000.

53. A. Hirsch. "Functionalization of Single-Walled Carbon Nanotubes." Angew. Chem. Int. Ed., Vol. 41, 1853, 2002.

54. **(A)** V. A. Sinani, M. K. Gheith, A. A. Yaroslavov, A. A. Rakhnyanskaya, A. A. Memedov, J. P. Wicksted, N. A. Kotov. "Aqueous Dispersions of Single- and Multi-Walled Carbon Nanotubes with Designed Amphiphilic Cations." Accepted in Journal of the American Chemical Society; **(B)** Muhammed K. Gheith, Vladimir A. Sinani, Alexander A. Yaroslavov, Anna A. Rakhnyanskaya, Arif A. Mamedov, James. P. Wicksted, Nicholas A. Kotov. "Amphiphilic Polyelectrolytes Solubilize Carbon Nanotubes in Aqueous Dispersions." Bulletin of the American Physical Society March Meeting, Vol. 49(No.1, Part A), Page 246, Palais des Congres de Montreal, Montreal, Quebec, Canada, March 22nd-26th, 2004.

55. R. Saito, T. Takeya, T. Kimura, G. Dresselhaus, M. S. Dresselhaus. "Raman Intensity of Single Wall Carbon Nanotubes." Physical Review B, Vol. 57, 4145, 1998.

56. H. Kuzmany, W. Plank, M. Hulman, C. Kramberger, A. Gruneis, T. Pichler, H. Petrlik, H. Kataura, Y. Achiba. "Determination of SWCNT Diamaters from the Raman Response of the Radial Breathing Mode." The European Physical

Journal B, Vol. 22, 307, 2001.

57. A. Kukovecz, C. Kramberger, V. Geogakilas, M. Prato, H. Kuzmany. "A Detailed Raman Study on Thin Single-Wall Carbon Nanotubes Prepared by the HiPCO Process." The European Physical Journal B, Vol. 28, 223, 2002.

58. Z. Yu, L. E. Brus. "(n,m) Structural Assignments and Chirality Dependence in Single-Wall Carbon Nanotube Raman Scattering." Journal of Physical Chemistry B, Vol. 105, 6831, 2001.

59. M. S. Strano, S. K. Doorn, E. H. Haroz, C. Kittrell, R. H. Hauge, R. E. Smalley. "Assignment of (n,m) Raman and Optical Features of Metallic Single-Walled Carbon Nanotubes." Nano Letters, Vol. 3, 1091, 2003.

60. M. S. Dresselhaus, G. Dresselhaus, A. Jorio, A. G. Souza Filho, R. Saito. "Raman Spectroscopy on Isolated Single Wall Carbon Nanotubes." Carbon, Vol. 40, 2043, 2002.

61. J.-L. Sauvajol, E. Anglaret, S. Rols, L. Alvarez. "Phonons in Single Wall Carbon Nanotubes Bundles." Carbon, Vol. 40, 1697, 2002.

62. A. M. Roa, E. Richter, S. Bandow, B. Chase, P. Eklund, K. Williams, S. Fang, K. Subbaswamy, M. Menon, A. Thess, R. Smalley, G. Dresselhaus, M. Dresselhaus. "Diameter-Selective Raman Scattering from Vibrational Modes in Carbon Nanotubes." Science, Vol. 275, 187, 1997.

63. D. A. Heller, P. W. Barone, J. P. Swanson, R. M. Mayrhofer, M. S. Strano. "Using Raman Spectroscopy to Elucidate the Aggregation State of Single-Walled Carbon Nanotubes." Journal of Physical Chemistry B, Vol. 108, 6905, 2004.

64. G. G. Samsonidze, S. G. Chou, A. P. Santos, V. W. Brar, G. Dresselhaus, M. S. Dresselhaus, A. Selbst, A. K. Swan, M. S. Unlu, B. B. Goldberg, D. Chattopadhyay, S. N. Kim, F. Papadimitrakopoulos. "Quantitive Evaluation of the Octadecylmine-Assisted Separation of Semiconducting and Metallic Single-wall Carbon Nanotubes by Resonance Raman Spectroscopy." Applied Physics Letters, Vol. 85, 1006, 2004.

65. S. M. Bachilo, M. S. Strano, C. Kittrell, R. H. Hauge, R. E. Smalley, R. B. Weisman. "Structure-Assigned Optical Spectra of Single-Walled Carbon Nanotubes." Science, Vol. 298, 2361, 2002.

66. L. Alvarez, R. Rols, E. Anglaret, J. Sauvajol, E. Munoz, W. Maser, A. Benito, M. Martinez, G. Fuente. "Diameter Dependence of Raman Intensities for Single-Wall Carbon Nanotube." Physical Review B, Vol. 63, 153401, 2001.

67. A. Jorio, R. Saito, J. Hafner, C. M. Lieber, M. Hunter, T. McClure, G.

Dresselhaus, M. S. Dresselhaus. "Structural (n,m) Determination of Isolated Single-Wall Carbon Nanotubes by Resonant Raman Scattering." Physical Review Letters, Vol. 86, 1118, 2001.

68. M. A. Pimenta, A. Jorio, S. M. Brown, A. Filho, G. Dresselhaus, J. Hafner, C. M. Lieber, R. Saito, M. S. Dresselhaus. "Diameter Dependence of the Raman D-Band in Isolated Single-Wall Carbon Nanotubes." Physical Review B, Vol. 64, 041401, 2001.

69. M. J. Mattews, M. A. Pimenta, G. Dresselhaus, M. S. Dresselhaus, M. Endo. "Origin of Dispersive Effects of the Raman D Band in Carbon Materials." Physical Review B, Vol. 59, R6585, 1999.

70. M. S. Strano, C. a. Dyke, M. L. Usrey, P. W. Barone, M. J. Allen, H. Shan, C. Kittrell, R. H. Hauge, J. M. Tour, R. E. Smalley. "Electronic Structure Control of Single-Walled Carbon Nanotube Functionalization." Science, Vol. 301, 1519, 2003.

71. R. H. Baughman, a. A. Zakhidov, W. a. Heer. "Carbon Nanotubes-the Route Toward Applications." Science, Vol. 297, 787, 2002.

72. E. W. Wong, P. E. Sheehan, C. M. Lieber. "Nanobeam Mechanics: Elasticity, Strength, and Toughness of Nanorods and Nanotubes." Science, Vol. 277, 1971, 1997.

73. V. N. Popov, V. E. Doren, M. Balkanski. "Elastic Properties of Single Walled Carbon Nanotubes." Physical Review B, Vol. 61, 3078, 2000.

74. R. A. Serway. Physics for Scientists and Engineers, 3rd Edition. Saunders College Publishing, Orlando, Florida, 1990.

75. M. Yu, B. S. Files, S. Arepalli, R. S. Ruoff. "Tensile Loading of Ropes of Single Wall Carbon Nanotubes and their Mechanical Properties." Physical Review Letters, Vol. 84, 5552, 2000.

76. A. A. Memedov, N. A. Kotov, M. Prato, D. M. Guldi, J. P. Wicksted, a. Hirsch. "Molecular Design of Strong Single-Wall Carbon Nanotube/Polyelectrolyte Multilayer Composites." Nature Materials, Vol. 1, 190, 2002.

77. W. Zhou, J. Vavro, C. Guthy, K. I. Winey, J. E. Fischer, L. M. Ericson, S. Ramesh, R. Saini, V. A. Davis, C. Kittrell, M. Pasquali, R. H. Hauge, R. E. Smalley. "Single Wall Carbon Nanotube Fibers Extruded from Super-Acid Suspensions: Preferred Orientation, Electrical, and Thermal Transport." Journal of Applied Physics, Vol. 95, 649, 2004.

78. M. Kozlov, R. Capps, V. Ebron, V. Seker, W. Sampson, K. Martin, L. Grigsby, D. Novitski, W. Alvarado, S. Abramov, J. Ferraris, R. Baughman. "Polymer-

Free Carbon Nanotube Fibers." Abstracts of Papers, 60th American Chemical Society Southwest Regional Meeting, September 29th – October 2nd, Fort Worth, Texas, 2004.

79. S. J. Tans, M. H. Devoret, H. Dai, A. Thess, R. E. Smalley, L. J. Greerligs, C. Dekker. "Individual Single-Wall Carbon Nanotubes as Quantum Wires." Nature, Vol. 386, 474, 1997.

80. S. J. Tans, A. M. Verschueren, C. Dekker. "Room-Temperature Transistor Based on a Single Carbon Nanotubes." Nature, Vol. 393, 49, 1998.

81. T. Rueckes, K. Kim, E. Joselevich, G. Tseng, C. Cheung, C. Lieber. "Carbon Nantube-Based Nonvolatile Random Access Memory for Molecular Computing." Science 289, 94, 2000.

82. A. Javey, H. Kim, M. Brink, Q. Wang, A. Ural, J. Guo, P. Mcintyre, P. Mceuen, M. Lundstrom, H. Dai. "High-κ Dielectrics for Advanced Carbon-Nanotube Transistors and Logic Gates." Nature Materials, Vol. 1, 241, 2002.

83. R. H. Baughman, C. Cui, A. a. Zakhidov, Z. Iqbal, J. N. Barisci, G. M. Spinks, G. G. Wallace, A. Mazzoldi, D. D. Rossi, A. G. Rinzler, O. Jaschinski, S. Roth, M. Kertesz. "Carbon Nanotube Actuators." Science, Vol. 284, 1340, 1999.

84. C. Niu, E. K. Sichel, R. Hoch, D. Moy, H. Tennent. "High Power Electrochemical Capacitors Based on Carbon Nanotube Electrodes." Applied Physics Letters, Vol. 70, 1480, 1997.

85. R. Martel, T. Schmidt, H. R. Shea, T. Hertel, Ph. Avouris. "Single- and Multi-Wall Carbon Nanotube Field-Effect Transistors." Applied Physics Letters, Vol. 73, 2447, 1998.

86. P. Qi, O. Vermesh, M. Grecu, A. Javey, Q. Wang, H. Dai, S. Peng, K. J. Cho. "Toward Large Arrays of Multiplex Functionalized Carbon Nanotube Sensors for highly Sensitive and Selective Molecular Detection." Nano Letters, Vol. 3, 347, 2003.

87. H. Chang, J. D. Lee, S. M. Lee, Y. H. Lee. "Adsorption of NH_3 and NO_2 Molecules on Carbon Nanotubes." Applied Physics Letters, Vol. 79, 3863, 2001.

88. P. G. Collins, K. Bradley, M. Ishigami, A. Zettl. "Extreme Oxygen Sensitivity of Electronic Properties of Carbon Nanotubes." Science, Vol. 287, 1801, 2000.

89. K. H. An, S. Y. Jeong, H. R. Hwang, Y. H. Lee. "Enhanced Sensitivity of Gas Sensor Incorporating Single-Walled Carbon Nanotube-Polypyrrole Nanocomposites." Advanced Materials, Vol. 16, 1005, 2004.

90. J. Kong, N. R. Franklin, C. W. Zhou, M. G. Chapline, S. Peng. "Nanotube Molecular Wires as Chemical Sensors." Science, Vol. 287, 622, 2000.

91. J. Li, Y. Lu, Q. Ye, M. Cinke, J. Han, M. Meyyappan. "Carbon Nanotube Sensors for Gas and Organic Vapor Detection." Nano Letters, Vol. 3, 929, 2003.

92. Y. M. Wong, W. P. Kang, J. L. Davidson, A. Wisitsora, K. L. Soh. "A Novel Microelectronic Gas Sensor Utilizing Carbon Nanotubes for hydrogen Gas Detection. Sensors and Actuators B, Vol. 93, 327, 2003.

93. S. Chopra, K. McGuire, N. Gothard, A. M. Rao. "Selective Gas Detection Using a Carbon Nanotube Sensor." Applied Physics Letters, Vol. 83, 2280, 2003.

94. A. Star, T. Han, j. Gabriel, K. Bradley, G. Gruner. "Interaction of Aromatic Compounds with Carbon Nanotubes: Correlation to the Hammett Parameter of the Substituent and Measured Carbon Nanotube FET Response." Nano Letters, Vol. 3, 1421, 2003.

95. K. Bradley, J. Gabreil, A. Star, G. Gruner. "Short-Channel Effects in Contact-Passivated Nanotube Chemical Sensors." Applied Physics Letters, Vol. 83, 3821, 2003.

96. Y. Lu, J. Li, J. Han, H. Ng, C. Binder, C. Partridge, M. Meyyappan. "Room Temperature Methane Detection Using Palladium Loaded Single-Walled Carbon Nanotube Sensors." Chemical Physics Letters, Vol. 391, 344, 2004.

97. W. A. Heer, A. Chatelian, D. Ugarte. "A Carbon Nanotube Field-Emission electron Source." Science, Vol. 270, 1179, 1995.

98. A. G. Rinzler, J. H. Hafner, P. Nikolaev, L. Lou, S. G. Kim, D. Tomanek, P. Nordlander, D. T. Colbert, R. E. Smalley. "Unraveling Nanotubes: Field Emission from an Atomic Wire." Science, Vol. 269, 1550, 1995.

99. N. S. Lee, D. S. Chung, I. T. Han, J. H. Kang, Y. S. Choi, H. Y. Kim, S. H. Park, Y. W. Jin, W. K. Yi, M. J. Yun, J. E. Jung, C. J. Lee, J. H. You, S. H. Jo, C. G. Lee, J. M. Kim. "Application of Carbon Nanotubes to Field Emission Displays." Diamond and Related Materials, Vol. 10, 265, 2001.

100. Y. Saito, s. Uemura. "Field Emission from Carbon Nanotubes and its Application to Electron Sources." Carbon, Vol. 38, 169, 2000.

101. J. H. Hafner, C. L. Cheung, C. M. Leiber. "Direct Growth of Single-Walled Carbon Nanotube Scanning Probe Microscopy Tips." Journal of the American Chemical Society, Vol. 121, 9750, 1999.

102. V. Georgakilas, N. Tagmatarchis, D. Pantarotto, A. Pianco, J. P. Briand, M. Prato. "Amino Acid Functionalization of Water Soluble Carbon Nanotubes."

Chemical Communication, 3050, 2002.

103. S. Wang, E. Humphreys, S. Chung, D. Delduco, S. Lustig, H. Wang, K. Parker, N. Rizzo, S. Subramoney, Y. Chiang, A. Jagota. "Peptides with Selective Affinity for Carbon Nanotubes." Nature Materials, Vol. 2, 186, 2003.

104. G. Dieckmann, A. Dalton, P. Johnson, J. Razal, J. Chen, G. Giordano, E. Munoz, I. Musselman, R. Baughman, R. Draper. "Controlled Assembly of Carbon Nanotubes by Desugned Amphiphilic Peptide Helices." Journal of the American Chemical Society, Vol. 125, 1770, 2003.

105. V. Zorbas, A. Acevedo, A. Dalton, M. Yoshida, G. Dieckmann, R. Draper, R. Baughman, M. Yacaman, I. Musselman. "Preparation and Characterization of Individual Peptide-wrapped Single-Walled Carbon Nanotubes." Journal of the American Chemical Society, Vol. 126, 7222, 2004.

106. W. Huang, S. Taylor, K. Fu, Y. Lin, D. Zhang, T. Hanks, A. M. Roa, Y. Sun. "Attaching Proteins to Carbon Nanotubes via Diimide-Activated Amidation." Nano Letters, Vol. 2, 311, 2002.

107. M. Shim, N. Kam, R. Chen, Y. Li, H. Dai. "Functionalization of Carbon Nanotubes for Biocompatibility and Biomolecular Recognition." Nano Letters, Vol. 2, 285, 2002.

108. R. Chen, Y. Zhang, D. Wang, H. Dai. "Noncovalent Sidewall functionalization of Single-Walled carbon Nanotubes for Protein Immobilization." Journal of the American Chemical Society, Vol. 123, 3838, 2001.

109. M. Zheng, A. Jagota, E. D. Semke, B. A. Diner, R. S. Mclean, S. R. Lustig, R. E. Richardson, N. G. Tassi. "DNA-Assisted Dispersion and Separation of Carbon Nanotubes." Nature Materials, Vol. 2, 338, 2003.

110. M. Zheng, A. Jagota, M. S. Strano, A. P. Santos, P. Barone, S. G. Chou, B. A. Diner, M. S. Dresselhaus, R. S. Mclean, G. B. Onoa, G. G. Samsonidze, E. D. Semke, M. Usrey, D. J. Walls. "Structure-Based Carbon Nanotube Sorting by Sequence-Dependent DNA Assembly." Science, Vol. 302, 1545, 2003.

111. M. S. Strano, M. Zheng, A. Jagota, G. B. Onoa, D. A. Heller, P. W. Barone, M. L. Usrey. "Understanding the Nature of the DNA-Assisted Separation of Single-Walled Carbon Nanotubes Using Fluorescence and Raman Spectroscopy." Nano Letters, Vol. 4, 543, 2004.

112. A. Bianco, M. Prato. "Can Carbon Nanotubes be Considered Useful Tools for Biological Applications." Advanced Materials, Vol. 15, 1765, 2003.

113. H. Cai, X. Cao, Y. Jiang, P. He, Y. Fang. "Carbon Nanotube-Enhanced Electrochemical DNA Biosensor for DNA Hybridization Detection." Analytical

and Bioanalytical Chemistry, Vol. 375, 287, 2003.

114. Guo, P. Sadler, S. Tsang. "Immobilization and Visualization of DNA and Proteins on Carbon Nanotubes." Advanced Materials, Vol. 10, 701, 1998.

115. K. Besteman, J-O. Lee, F. G. Wiertz, H. A. Heering, C. Dekker. "Enzyme-Coated Carbon Nanotubes as Single-Molecule Biosensors." Nano Letters, Vol. 3, 727, 2003.

116. H. Xue, W. Sun, B. He, Z. Shen, "Single-Wall Carbon Nanotubes as Immobilization Materials for Glucose Biosensor." Synthetic Metals, Vol. 135-136, 831, 2003.

117. J. Davis, K. Coleman, B. Azamian, C. Bagshaw, M. Green. "Chemical and Biochemical Sensing with Modified Single Walled Carbon Nanotubes." Chemical European Journal, Vol. 9, 3732, 2003.

118. S. Sotiropoulou, N. A. Chaniotakis. "Carbon Nanotube Array-Based Biosensors." Analytical and Bioanalytical Chemistry, Vol. 375, 103, 2003.

119. A. Star, J. P. Gabriel, K. Bradly, G. Gruner. "Electronic Detection of Specific Protein binding Using Nanotube FET Devices." Nano Letters, Vol. 3, 459, 2003; R. Chen, Y. Zhang, D. Wang, H. Dai, Journal of the American Chemical Society, Vol. 123, 3838, 2003.

120. R. J. Chen, H. C. Choi, S. Bangsaruntip, E. Yenilmez, X. Tang, Q. Wang, Y. Chang, H. Dai. "An Investigation of the Mechanisms of Electronic Sensing of Protein Adsorption on Carbon Nanotube devices." Journal of the American Chemical Society, Vol. 126, 1563, 2004.

121. K. Bradley, M. Briman, A. Star, G. Gruner. "Charge Transfer from Adsorbed Proteins." Nano Letters, Vol. 4, 253, 2004.

122. J. Kong, H. Dai. "Full and Modulated Chemical Gating of Individual Carbon Nanotubes by Organic Amine Compounds. " Journal of Physical Chemistry B, Vol. 105, 2890, 2001.

123. S. S. Wong, E. Joselevich, A. T. Woolley, C. L. Cheung, C. M. Lieber. "Covalently Functionalized Nanotubes as Nanometer-Sized Probes in Chemistry and Biology." Nature, Vol. 394, 52, 1998.

124. D. B. Warheit, T. R. Webb, K. L. Reed, C. M. Sayes, V. Colvin. "Assessing the pulmonary Hazards and Health Risks of Nano(ultrafine)-Particles and Carbon Nanotubes: Lung Toxicity Studies in Rats and Relevance of these Findings for Humans." Abstracts of Papers, 227th ACS National Meeting, Anaheim, CA, USA, March 28-April 1, 2004.

125. V. L. Colvin, C. M. Sayes, K. D. Ausman, J. Fortner, D. Lyons. "Environmental Chemistry and Effects of Engineered Nanostructures." Abstracts of Papers, 227th ACS National Meeting, Anaheim, CA, USA, March 28-April 1, 2004.

126. C. M. Sayes, J. D. Fortner, W. Guo, D. Lyon, A. M. Boyd, K. D. Ausman, Y. J. Tao, B. Sitharaman, L. J. Wilson, J. B. Hughes, J. L. West, V. Colvin. "The Differential Cytotoxicity of Water-Soluable Fullerenes." Nano Letters, Vol 4, 1881, 2004.

127. D. Pantarotto, C. d. Partidos, J. Hoebeke, F. Brown, E. Kramer, J. P. Briand, S. Muller, M. Prato, A. Bianco. "Immunization with Peptide-Functionalized Carbon Nanotubes Enhances Virus-specific Neutralizing antibody Responses." Chemistry and Biology, Vol. 10, 961, 2003.

128. D. Pantarotto, J. Briand, M. Prato, A. Pianco. "Translocation of Bioactive Peptides Across Cell Membranes by Carbon Nanotubes." Chemical Communication, Vol. 1, 16, 2004.

129. N. Kam, T. C. Jessop, P. A. Wender, H. Dai. "Nanotube Molecular Transporters: Internalization of Carbon Nanotube-Protein Conjugates into Mammalian Cells." Journal of the American Chemical Society, Vol. 126, 6850, 2004.

130. C. Lam, J. T. James, R. McCluskey, R. L. Hunter. "Pulmonary Toxicity of Single-Wall carbon Nanotubes in Mice 7 and 90 Days After Intratracheal Instillation." Toxicological Sciences, Vol. 77, 126, 2004.

131. D. B. Warheit, B. R. Laurence, K. L. Reed, D. H. Roach, G. A. M. Reynolds, T. R. Webb. "Comparative Pulmonary Toxicity Assessment of Single-Wall Carbon Nanotubes in Rats." Toxicological Sciences, Vol. 77, 117, 2004.

132. R. Dagani. "Nanomaterials: Safe or Unsafe?" Chemical engineering News, Vol. 81(17), 30, 2003.

133. K. L. Dreher. "Health and Environmental Impact of Nanotechnology: Toxicological Assessment of Manufactured Nanoparticles." Toxicological Sciences, Vol. 77, 3, 2004.

134. V. L. Colvin. "The Potential Environmental Impact of Engineered Nanomaterials." Nature Biotechnology, Vol. 21, 1166, 2003.

135. V. A. Sinani, D. S. Koktysh, B. G. Yun, R. L. Matts, T. C. Pappas, M. Motamedi, S. N. Thomas, N. A. Kotov. "Collagen Coating Promotes Biocompatibility of Semiconductor Nanoparticles in Stratified LBL Films." Nano Letters, Vol. 3, 1177, 2003.

136. X. Gao, Y. Cui, R. M. Levenson, L. K. Chung, s. Nie. "In Vivo Cancer targeting and Imaging with Semiconductor Quantum Dots." Nature Biotechnology, Vol.

22, 969, 2004.

137. J. O. Winter, T. Y. Liu, B. A. Korgel, C. E. Schmidt. "Recognition Molecule Directed Interfacing Between Semiconductor Quantum Dots and Nerve Cells." Advanced Materials, Vol. 13, 1673, 2001.

138. M. E. Akerman, W. c. W. Chan, P. Laakkonen, S. N. Bhatia, e. Ruoslahti. "Nanocrystal Targeting in Vivo." Proceedings of the National Academy of Science, Vol. 99, 12617, 2002.

139. W. Chan, S. Nie. "Quantum Dot Bioconjugates for Ultrasensitive Nonisotopic Detection." Science, Vol. 281, 2016, 1998.

140. A. M. Derfus, W. Chan, S. N. Bhatia. "Intracellular Delivery of Quantum Dots for Live Cell Labeling and Organelle Tracking." Advanced Materials, Vol. 16, 961, 2004.

141. H. J. Morton. "A Survey of Commercially Available Tissue Culture Media." In Vitro, Vol. 6, 89, 1970.

142. B. Hamprecht. "Structural, Electrophysiological, Biochemical, and Pharmacological Properties of Neuroblastoma-Glioma Cell Hybrids in Cell Culture." International Review of Cytology, Vol. 49, 99, 1977.

143. B. Hamprecht, T. Glaser, G. Reiser, E. Bayer, F. Propst. "Culture and Characteristics of Hormone-Responsive Neuroblastoma x Glioma hybrid Cells." Methods in Enzymology, Vol. 109, 316, 1985.

144. K. N. Seidman, J. H. Barsuk, R. F. Johnson, J. A. Weyhermeyer. "Differentiation of NG108-15 Neuroblastoma Cells by Serum Starvation or Dimethyl Sulfoxide Results in Marked Differences in Angiotensin II receptor Subtype Expression." Journal of Neurochemistry, Vol. 66, 1011, 1996.

145. H. Ammer, R. Schulz. "Regulation of Stimulatory Adenylyl Cyclase Signaling During Forskolin-Induced Differentiation of Mouse Neuroblastoma x Rat Glioma (NG108-15) Cells." Neuroscience Letters, Vol. 230, 143, 1997.

146. C. L. Bergsbaken, S. L. Sommers, P. Y. Law. "Effect of Forskolin and Isobutylmethylxanthine on Delta-Opioid Receptor Activity in Neuroblastoma x Glioma NG108-15 Cells." Journal of Pharmacology and Experimental Therapeutics, Vol. 264, 1474, 1993.

147. A. Laurenza, E. M. Sutkowski, K. B. Seamon. "Forskolin: a Specific Stimulator of Adenylyl Cyclase or a Diterpene with Multiple Sites of Action." Trends Pharmacol. Science, Vol. 10, 442, 1989.

148. Y. Qin, J. Shi, W. Wu, X. Li, Z. Guo, D. Zhu. "Concise Route to Functionalized

Carbon Nanotubes." Journal of Physical Chemistry B, Vol. 107, 12899, 2003.

149. M. Holzinger, J. Abraham, P. Whelan, R. Graupner, L. Ley, F. Hennrich, M. Kappes, A. Hirsch. "Functionalization of Single-Walled Carbon Nanotubes with (R-)Oxycarbonyl Nitrenes." Journal of the American Chemical Society, Vol. 125, 8566, 2003.

150. F. Liang, a. Sadana, A. Peera, J. Chattopadhyay, Z. Gu, R. H. Hauge, W. E. Billups. "A Convenient Route to Functionalized Carbon Nanotubes." Nano Letters, Vol. 4, 1257, 2004.

151. J. H. Lustgarten, M. Proctor, R. I. Haroun, A. M. Avellino, A. A. Pindzola, M. Kliot. "Semipermeable Polymer Tubes Provide a Microenvironment for In Vivo Analysis of Dorsal Root Regeneration." Journal of Biomechanical Engineering, Vol. 113, 184, 1991.

152. M. P. Mattson, R. C. Haddon, A. M. Rao. "Molecular Functionalization of Carbon Nanotubes and Use as Substrates for Neuronal Growth." Journal of Molecular Neuroscience, Vol. 14, 175, 2000.

153. Hui Hu, Yingchun Ni, Vedrana Montana, Robert C. Haddon, and Vladimir Parpura, "Chemically Functionalized Carbon Nanotubes as Substrates for Neuronal Growth" Nano Letters **4** (3), 507 -511, 2004.

154. H. Kataura, Y. Kumazawa, Y. Maniwa, I. Umezu, S. Suzuki, Y. Ohtsuka, Y. Achiba. "Optical Properties of Single-Wall Carbon Nanotubes." Synthetic Metals, Vol. 103, 2555, 1999.

155. R. Jacquemin, S. Kazaoui, D. Yu, A. Hassanien, N. Minami, H. Kataura, Y. Achiba. "Doping Mechanism in Single-Wall Carbon Nanotubes Studied by Optical Absorption." Synthetic Metals, Vol. 115, 283, 2000.

156. B. Zhou, Y. Lin. H. Li, W. Huang, J. W. Connell, L. F. Allard, Y. P. Sun. "Absorptivity of Functionalized Single-Walled Carbon Nanotubes in Solution." Journal of Physical Chemistry B, Vol. , 2003.

157. F. Caruso. "Nanoengineering of Particle Surfaces." Advanced Materials, Vol. 13, 11, 2001.

158. N. A. Kotov, I. Dekany, J. H. Fendler. "." Journal of Physical Chemistry, Vol. 99, 13065, 1995.

159. G. Decher. "Fuzzy Nanoassemblies: Toward Layered Polymeric Multicomposites." Science, Vol. 277, 1232, 1997.

160. N. A. Kotov. "Ordered Layered Assemblies of Nanoparticles." Materials Research Society Bulletin, Vol. 26, 992, 2001.

161. J. Minna, D. Glazer, M. Nirenberg. "Genetic Dissection of Neuronal Properties Using Somatic Cell Hybrids." Nature New Biology, Vol. 235, 225, 1972.

162. T. Amino, B. Hamprecht, W. Kemper. "High Activity of Choline Acetyltransferase Induced in Neuroblastoma x Glia Hybrid Cells." Experimental Cell Research, Vol. 85, 399, 1974.

163. W. Klee, M. Nirenberg. "A Neuroblastoma x Glioma Hybrid Cell Line with Morphine Receptors." Proceedings of the National Academy of Science. USA, Vol. 71, 3474, 1974.

164. M. O'donnell, M. Villereal. "Membrane Potential and Sodium Flux in Neuroblastoma x Glioma Hybrid Cells: Effects of Amiloride and Serum." Journal of Cellular Physiology, Vol. 113, 405, 1982.

165. V. Kowtha, H. Bryant, J. Pancrazio, D. Stenger. "Influence of Extracellular Matrix Proteins on Membrane Potentials and Excitability in NG108-15 Cells." Neuroscience Letters, Vol. 246, 9, 1998.

166. J. Doebler. "Membrane Potential and Resistance Changes in NG108-15 Cells: An In Vitro Model to Study Membrane-Active Compounds." Toxicology Methods, Vol. 9, 35, 1999.

167. J. Doebler. "Electrophysiological Analysis of NG108-15 Cells in Vitro Model for Evaluating Antagonists of Membrane-Active Compounds." Toxicology Methods, Vol. 10, 239, 2000.

168. D. Schubert, S. Humhreys, f. Vitry, F. Jacob. "Induced Differentiation of a Neuroblastoma." Developmental Biology, Vol. 25, 514, 1971.

169. M. K. Gheith, V. A. Sinani, R. L. Matts, J. P. Wicksted, N. A. Kotov. "Layer-by-Layer Assembled Thin Films of Single Walled Carbon Nanotubes as Supporting Materials for Neuronal Growth." Abstracts, 60th Southwest Regional Meeting of the American Chemical Society, Fort Worth, Texas, United states, September 29th – October 4th, 2004, SEPT04-397.

170. S. Y. Yang, J. D. Mendelsohn, M. F. Rubner. "New Class of Ultrathin, Highly Cell-Adhesion-Resistant Polyelectrolyte Multilayers with Micropatterning Capabilities." Biomacromolecules, Vol. 4, 987, 2003.

171. E. Neher. "Ion Channels for Communication Between and Within Cells." Neuron, Vol. 8, 605, 1992.

172. M. F. Durstock, M. F. Rubner. "Dielectric Properties of Polyelectrolyte Multilayers." Langmuir, Vol. 17, 7865, 2001.

173. D. J. Aidley. The Physiology of Excitable Cells. 2nd Edition, Cambridge

University Press, Cambridge, 1978.

174. P. Nelson, W. Ruffner, M. Nirenberg. “Neuronal Tumor Cells With Excitable Membranes Grown in Vitro.” Biochemistry, Vol. 64, 1004, 1969.

175. M. K. Gheith, V. A. Sinani, R. L. Matts, J. P. Wicksted, N. A. Kotov. “Biocompatible Single-Walled Carbon Nanotube Structures as Supporting Platforms for Neuronal Growth and Differentiation.” In Preparation.

176. P. Nelson, C. Christian, M. Nirenberg. “Synaptic Formation Between Clonal Neuroblastoma x Glioma Hybrid Cells and Striated Muscle Cells.” Proceedings of the National Academy of Science, USA, Vol. 73, 123, 1976.

177. M. K. Gheith, T. C. Pappas, A. V. Liopo, V. A. Sinani, M. Motamedi, J. P. Wicksted, N. A. Kotov. “Single-Walled Carbon Nanotubes as Conductive Surfaces for Neuronal Stimulation of NG108-15 Hybrid Cells.” In Preparation.

VITA

MUHAMMED KHAMEIS GHEITH

Candidate for the Degree of

Doctor of Philosophy

Thesis: SINGLE-WALLED CARBON NANOTUBES AS SUPPORTING STRUCTURES AND STIMULATING MATERIALS FOR NG108-15 NEUROBLASTOMA-GLIOMA HYBRID CULTURE CELLS

Major Field: Photonics

Biographical:

Education:

Received Bachelor of Science degree in Physics from The University of Jordan, Amman, Jordan in June 1997. Received the Master of Science degree with honor in Physics from Middle East Technical University, Ankara-Turkey in December 1999. Completed the requirements for the Doctor of Philosophy degree at Oklahoma State University in December 2004.

Synergistic Activities:

-Member of the American Association for the Advancement of Science.
-Member of the American Physical Society.
-Member of the American Chemical Society.
-Member of the National Geographic Society.